Design, Verification and Validation of a Dynamic Model for an Intramuscular Autoinjector

Author
Ntokozo Magubane
MGBNTO003

Dissertation presented
in partial fulfilment of the requirements for an MSc in Biomedical Engineering by coursework and dissertation

Department of Human Biology
Division of Biomedical Engineering
University of Cape Town

Supervisors Names
Prof Sudesh Sivarasu
A/Prof Malebogo Ngoepe
2023

DECLARATION

1.I know that plagiarism is wrong. Plagiarism is to use another's work and pretend that it is one's own.
2.I have used the Harvard referencing convention for citation and referencing. Each contribution to, and quotation in, this dissertation from the work(s) of other people has been attributed, and has been cited and referenced. Any section taken from an internet source has been referenced to that source.
3.This dissertation is my own work, and is in my own words (except where I have attributed it to others).
4.I have not allowed, and will not allow, anyone to copy my work with the intention of passing it off as his or her own work.
5. I acknowledge that copying someone else's assignment or essay, or part of it, is wrong, and declare that this is my own work.

Signature Signed by candidate

ACKNOWLEDGEMENT

“Things really do work out for those who love Him and according to His purpose” - Romans 8:28

This is a dedication to my dad. Nkomose, you taught me to always to put my foot forward. Rest easy dad, I will continue to work hard and make you proud always. I would like to thank my mom for all her support, love and for consistently believing in me. I also, want to thank the rest of my family for their support and love. You all have made my journey a lot easier.

I want to express special gratitude to my supervisors, Prof Sudesh Sivarasu and A/Prof Malebogo Ngoepe. Thank you so much for your guidance, support, patience and for consistently believing in me. Most importantly, thank you for inspiring me.

I also want to thank Impulse biomedical for funding this research and for allowing me to use their facilities and equipment for testing. I want to thank the Roopam Dey, Gokul Nair, Giancarlo Beukes, Seth Thompson and the entire Impulse team for all their support and guidance throughout this journey. Last but not least, I would like to thank the University of Cape Town Centre of Material Engineering (CME) and the Hair and Skin Research (HSR) Lab for allowing me to use their equipment and facilities for testing.

ABSTRACT

The rising prevalence of autoimmune and chronic conditions is a concern worldwide , leading to a need for disease management therapies to aid medication adherence and compliance. Autoinjectors are prime medical devices used to inject antidotes and prophylactics into the intramuscular or subcutaneous layer. These devices are used in various autoimmune and chronic conditions to counteract opioid overdose and nerve gas poisoning . They are easy to use and often allow for self-administration of medication. Developing new injectable molecules for different diseases and reformation of first-generation pharmaceuticals has led to growing interest in making autoinjectors usable for different medications. The major challenge in this quest is the complexity of injecting highly viscous drugs in large volumes. This research aims to develop a dynamic model to describe the influence of drug viscosity and volume on the injection process and evaluate the sensitivity of medication fluid behaviour to variations in component dimensions of the autoinjector fluid delivery system.

Using mathematical modelling, the kinematic properties relating to the plunger motion were modelled and verified through physical testing. This model was optimised via evaluating sensitivity and measuring the results against the validation results. A Computational Fluid Dynamics (CFD) study was conducted to analyse the fluid behaviour of different viscous medications. This study allowed for the variation of fluid viscosity, medication volume, needle gauge and length. The computational model was then verified and validated using the American Standard of Mechanical Engineers Verification and Validation Standards (ASME V&V 40 and V&V20). This was accompanied by fluid characterisation of four medications, namely adrenaline, amikacin, Vaxigrip and insulin basaglar using a rheometer. The ZwickRoell universal tester measured the syringe force and plunger displacement to derive the pressure changes. These results were evaluated against the computational model.

According to the optimised mathematical model and validation results, the plunger displacement increases linearly when the plunger motion is initiated until a maximum displacement is reached. Separation flow was observed in the syringe for viscosities between 15 - 80 cP. This represents decreasing flow as pressure increases in the syringe for medications with a viscosity in this range. This phenomenon increases the chances of needle deformation and injection pain due to tissue damage. High-gauge needles are more effective for injecting lower volumes and low-viscosity medications, while low-gauge needles work best for injecting larger volumes or highly viscous medications.

The model risk is defined to be high according to the ASME guidelines. If the model results directly impact the autoinjector design without any further testing to inform the design process, an incorrect model would result in poor-performing autoinjectors that fail to deliver the desired dose of medication into the intramuscular layer at the required injection time. This research has proved that it’s possible to inject highly viscous drugs and large doses using an autoinjector if the right balance of injection force, injection time and needle dimensions is carefully selected to improve compliance and patient experience.

Table of Contents

LIST OF FIGURES

LIST OF TABLES

NOMENCLATURE

IM	-	Intramuscular
AAI	-	Adrenaline Autoinjector
SC	-	Subcutaneous
TNF	-	Tumour Necrosis Factor
RA	-	Rheumatoid Arthritis
PK	-	Pharmacokinetics
MS	-	Multiple Sclerosis
RRMS	-	Relapsing Remitting Multiple Sclerosis
PPMS	-	Primary Progressive Multiple Sclerosis
SPMS	-	Secondary Progressive Multiple Sclerosis
CIS	-	Clinically Isolated Syndrome
mAb	-	Monoclonal Antibodies
cP	-	Centipoise
AChE	-	Acetylcholinesterane
FDA	-	US Food and Drug Administration
ASME	-	American Society of Mechanical Engineers
V&V	-	Verification and Validation
CFD	-	Computational Fluid Dynamics
AUC	-	Area Under the Curve
CL	-	Drug Clearance
COU	-	Context Of Use
CAGR	-	Compound Annual Growth Rate
DMARD	-	Disease Modifying Antirheumatics
QOI	-	Question of Interest

LIST OF SYMBOLS

μ	Viscosity
k	Flow consistency index
n	Power law index
$\dot{\gamma}$	Shear rate
t_{inj}	Injection time
L	Length of the needle
R	Syringe barrel inner radius
r	Needle inner radius
x	Plunger displacement
$F_{plunger}$	Plunger force
$F_{friction}$	Frictional force
Cmax	Maximum drug concentration
Q	Flow rate
$P_{dynamic}$	Dynamic pressure

$F_{actuation}$	Actuation force
A	Area
ρ	Density
t	Time
u	Flow velocity
$\frac{\partial \rho}{\partial t}$	Time derivative
$\dot{\gamma}_{eff}$	Effective shear rate
$\dot{\gamma}_p$	Wall shear rate
$P_{air-gap}$	Pressure in the air gap
F_s	Static friction
F_{fr}	Frictional force
F_{fl}	Fluid resistance friction
m_p	Mass of the plunger
a_p	Acceleration of the plunger
$\frac{\partial (\rho u_x)}{\partial t}$	Change in velocity with respect to time
$\nabla(\rho u_x u)$	Convection momentum
$\frac{\partial \rho}{\partial x}$	Surface force
$\frac{\partial}{\partial x}\left[2\mu \frac{\partial u_x}{\partial x} + \lambda \nabla u\right]$	Diffusion term in the z-direction
ρg_x	Mass force
x_i	Preload
μ_s	Static coefficient of friction
F_N	Normal force
g	Gravitational acceleration
F_{vf}	Viscous friction
$\mu_{viscous}$	Viscous friction coefficient
$\frac{dx}{dt}$	Differential function of x representing the velocity
$\mu_{dynamic}$	Dynamic friction coefficient
ΔP	Change in pressure
f_d	Darcy frictional factor
P_{static}	Static pressure
P_{atm}	Atmospheric pressure
P_{tissue}	Tissue pressure
F_{fluid}	Fluid force
P_{total}	Total pressure
N	Normal force

CHAPTER 1: LITERATURE REVIEW

1.1 Overview

Autoinjectors are a prime therapy in rheumatology and autoimmunity. These devices are useful for rapidly administering antidotes and prophylactics in the intramuscular (IM) or subcutaneous (SC) layer. The use of autoinjectors is associated with improved patient compliance, ease of self-administration, dosage accuracy and reduced anxiety. Autoinjectors were first designed in the 1960s for the military industry (Vijayaraghavan, 2012). They were used to inject antidotes for nerve gas poison in chemical warfare. To date more that 20 pharmaceutical companies have developed over 80 autoinjectors (Roy et.al., 2021). Market research predicts an even bigger expansion of the autoinjector market due to the prevalence of autoimmune and chronic conditions, the development of molecules targeting different diseases and the reformations of first-generation pharmaceuticals. The incidence and prevalence of anaphylaxis is another major factor contributing to the growth of the autoinjector market.

Anaphylaxis is a rapid-onset, allergic reaction usually caused by food, medication and insect venoms (Brown et.al., 2006). Anaphylactic shocks are characterised by life-threatening hypertension, bronchospasm and upper airway constriction (Brown et.al, 2006). The shock is rapid and can start minutes to hours after exposure to the allergen. Anaphylaxis patients are prescribed adrenaline to use when exposed to an allergen. Adrenaline can be administered orally, subcutaneously and in the intramuscular layer. Oral administration is ineffective and subcutaneous administration takes up to 30 minutes to reach peak level (Simons et.al, 2001, 2014). Patients use adrenaline autoinjectors (AAIs)for intramuscular administration of adrenaline. epiPEN, Twinject, INTO1 and INTO2 are some of the prominent AAIs. The epiPEN jr is prescribed for patients with less than 30 kg of body weight. Autoinjectors are a primary adrenaline delivery system because they promote rapid medication administration and absorption. When anaphylaxis patients experience delayed adrenaline administration, they suffer from risks of hospitalization, hypoxic-ischemic encephalopathy and death (Sicherer, 2017).

Autoinjectors are a preferred therapy for multiple autoimmune and chronic conditions. In a study of 118 multiple sclerosis patients, 90% preferred autoinjectors over their previous injection method (Ziemssen et.al, 2015). High level of satisfactory indicated in this study was due to ease of use and reduced injection site pain. Diazepam autoinjectors inject 10 - 20 mg of diazepam to manage different types of seizures(Roy et.al., 2021). Diazepam is prescribed for managing anxiety, status epilepticus, severe recurrent convulsive seizures and repetitive acute seizures. Recent studies proved that intramuscular administration of diazepam via autoinjectors could provide rapid, accurate dosing and absorption (Silbergleit et.al, 2012, Lamson et.al, 2011, Gernett et.al, 2011). A study to compare the effectiveness of diazepam delivery system via a rectal gel and an intramuscular autoinjector concluded that IM administration results in more rapid and less variable drug absorptions than rectal delivery (Garnett et.al, 2011). Another study proved a 10 mg diazepam via an IM autoinjector equivalent to a 10 mg diazepam given via a conventional IM needle (Lehmann et.al., 2013).

The most common cause of migraines is the release of chemicals in the arteries surrounding the brain. This increases blood circulation and pressure leading to swollen walls in the blood vessels (Mahtab, 2021). Sumatriptan is one of the drugs prescribed for migraines. It is available as a nasal spray, oral tablet, rectal suppository, and subcutaneous injection (Roy, 2021). Subcutaneous injections of sumatriptan have been proven to provide the fastest relief (Adelman et.al, 2001; Loder, 2010). A study to evaluate the safety and effectiveness of a sumatriptan autoinjector reported a 93% headache response rate in 2 hours and 63% pain-free patients in 2 hours (Landy at.el, 2013). These patients were administered 6mg of sumatriptan during onset of a migraine attack and they were assessed 72 hours later.

More sumatriptan autoinjectors have been designed to accommodate lower dosages. Higher sumatriptan doses are associated with adverse events such as fainting, loss of bladder and bowel control and sleepiness. A study compared different doses of subcutaneous sumatriptan succinate and measured the dose-response relationship after an hour (Mathew et.al, 1992). The study measured efficiency as reducing of pain from severe or high to moderate or no pain. The efficacy measured at different dosages was 24%; 1 mg, 43%; 2 mg, 57%; 3 mg, 57%; 4 mg, 50%; 6 mg, 73%; and 8 mg, 80% (Mathew et.al, 1992). While large doses are the most effective, they result in devastating tropin-adverse events. A two-step, DFN-1 autoinjector was found to be effective in managing migraines at 3mg subcutaneous injections (Brand-Schieber et.al., 2016). In a human factor validation study, more than 50% of patients reported pain relief after a DFN- 1 injection (Brand-Schieber et.al., 2016).

Golimumab is a monoclonal antibody used as an immunosuppressive medication for tumour necrosis factor (TNF) (Xu et.al, 2015). Inflammation such as swelling of the sinuses due to a cold are good immune system responses. These responses can be counterproductive for rheumatoid arthritis (RA) or psoriasis arthritis patients. For these patients, the TNF responsible for inflammation start attacking organs and joints. Rheumatoid arthritis is a systemic autoimmune disease associated with inflammation of joints and extra-articular organs (Radu et.al, 2021). One approved therapy for RA is a subcutaneous golimumab autoinjector with a 50mg or 100mg dose (Simponi, 2013). A study comparing the tolerability of a single dose golimumab autoinjector delivered subcutaneously to a standard needle and syringe proved tolerability between the two methods (Xu et.al, 2015). The golimumab SC delivery provided no pharmacokinetic (PK) differences, no injection site reaction or infection (Xu et.al, 2015).

Status epilepticus is a neurological emergency that occurs when a seizure last longer or when multiple seizures occur in a short period. It is due to the failure of the body's response for seizure termination or the initiation of prolonged migraine (Trinka et.al, 2015). Midazolam is a benzodiazepine that act as anticonvulsant (Mandrioli et.al, 2008). It is a long-acting drug that works by relaxing the muscle, brain and nerves. Under the benzodiazepines, lorazepam and diazepam act as alternatives for status epilepticus patients. In earlier studies, it has been shown that paramedics use midazolam for status epilepticus reduces patients with repetitive seizures and admitted patients in ICU for refractory status (Alldredge et al., 2001). Prolonged use of midazolam and other benzodiazepines is prohibited due to the risk of inhibiting conscious memory and development of tolerance (Isojärvi et.al, 1998).

Organophosphorus compounds or nerve gases such as tabum, sarin and soman inhibit the enzyme acetylcholinesterase (AChE) (Vijayaraghavan, 2010). This prevents ACh's breaking down and escalates neurotransmission's duration and frequency . Adverse events include difficulty in breathing, bradycardia, tremors, respiratory paralysis and death (Ganesan, 2010). Exposure to these gases is always followed by decontamination, evacuation and drug treatment (Vijayaraghavan, 2010). Recommended drug treatment includes atropine, pralidoxime or multiple-drug combination of atropine, pralidoxime and diazepam. Atropine reverses muscuric symptoms while pralidoxime restores cholinesterase activity (Roy et.al, 2021). The MARK 1 nerve agent antidote is one of the earlier treatment regimens prescribed for nerve gas exposure. It consists of a pair of autoinjectors, one to administer 600 mg of 2-PAM Cl and the other to administer a 2 mg of atropine (Newmark, 2019). The most recent treatment for nerve gas poison is a double-chamber autoinjector with a 2.1 mg of atropine and 600 mg of 2-PAM Cl (Newmark, 2019). This double chamber kit is called the New Agent Antidote Kit (Naak).

Multiple sclerosis (MS) is an autoimmune disease that attacks the central nervous system by damaging the spinal cord and the brain. It affects about 2.3 million people worldwide with 140 cases per 100,000 in North America, 108 cases per 100,000 in Europe and 2.1 cases per 100,000 in sub-Saharan Africa (Doshi et.al, 2016 & Multiple Sclerosis International Federation. London: MSIF; 2013). Symptoms include inflammation of the optic nerve, tremors, Uhthoff's phenomenon characterised by body temperature fluctuation and Lhermitte's phenomenon, characterised by electric shock. There are multiple phenotypes of MS, with the most common types being Relapsing Remitting MS (RRMS), Primary Progressive MS (PPMS), Secondary Progressive MS (SPMS) and Clinically Isolated Syndrome (CIS) (Doshi et.al, 2016).The RebiSmart™ and the Betaconnect® are electronic subcutaneous autoinjectors used to administer interferon β-1a for treating MS (Lugaresi, 2013). In a study to analyse MS autoinjector preference; 39 Betaconnect® users, 36 RebiSmart™ users and 10 ExtaviPro users were interviewed (Limmroth et.al, 2017). 82% Betaconnect®, 67% RebiSmart™ and 60% ExtraviPro users were satisfied with their device (Limmroth et.al, 2017). Most patients preferred the Betaconnect® device for its ease of handling, low noise and pain-free injections.

Opioids are a class of drugs used for sedative and palliative care. They interact with the opioid receptors in the brain to reduce pain, soothe patients and create euphoria. Prolonged use, misuse or overdose of opioids is linked to opioid dependence and addiction. This leads to unconsciousness, respiratory problems and bradycardia. Naloxone is a short-acting drug used to reverse opioid overdose (Roy et.al, 2021). A 2 mg of naloxone hydrochloride injection is prescribed as an intramuscular or subcutaneous autoinjector (EVZIO) for treating opioid overdose (FDA, 2016). It is injected into the anterolateral part of the thigh by both adults and paediatric patients. Naloxone interacts with opioid receptors to reverse the effects of opioid overdose and misuse; and to restore normal respiration and heart rate.

Insulin is a hormone produced by the pancreas to regulate blood sugar level. Failure to produce this hormone or abnormal function of the hormone results in diabetes mellitus. Insulin therapy is one of the most common treatment regimens for diabetes. Insulin should be administered

subcutaneously using special syringes to permit accurate dosage and delivery via the correct path (Diadiun et.al, 2016). The Novo Nordisk autoinjector was developed in 1984 to deliver 1.5 ml and 3 ml of insulin subcutaneously (Roy et.al.,2021). Autoinjectors such as the NovePen4, INSUPen, ALLStar, Densupen and the Smartpen aim to deliver the correct insulin dosage into the subcutaneous layer (Diadiun et.al, 2016). Exenatide is prescribed as a supplementary therapy to treat diabetes 2. A study to prove the efficacy and tolerability of exenatide autoinjector concluded that exenatide is associated with a more significant reduction of HbA1c and favorable gastrointestinal AE profile and hence more tolerable (Wysham et.al., 2018).

Amikacin is an aminoglycoside used in the treatment of bacterial infections. It binds to prokaryotic ribosomes to inhibit bacterial protein synthesis(Sagent pharmaceuticals, 2018). A study to prove the tolerability and safety of amikacin autoinjectors reported changes in biochemical and haematological stress-produced responses in rats, pigs and rabbits (Vijayaraghavan et.al, 2014). The study proved intraperitoneal injections of amikacin by an autoinjector to be well tolerable by rats. Lower doses were tolerable in rabbits with significant changes when injecting higher doses equivalent to the dose given to humans (Vijayaraghavan et.al, 2014). While autoinjectors are already used for multiple applications, their favourability promotes the development of more of these devices to deliver other traditional and natural drugs for other disease applications.

1.2 Influence Of Rheological Properties On The Injection Process

Rheology is the study of the flow and deformation of materials. It is characterised by elasticity and viscosity. The design of autoinjector devices requires an understanding of the flow or rheological properties of the fluid during the injection process. Wall shear stresses resulting from fluid velocity, wall thickness and induced pressure changes are important rheological properties in understanding the rapid injection of different drugs. A tolerable level of dynamic pressure is required to inject a solution into the correct layer in the body (Cilurzo et.al, 2011). The concentration of the medication injected is critical as it affects injection forces. Injection of highly concentrated or large molecules leads to high injection forces due to high viscosities (Krayukhina et.al, 2020). Molecules at higher concentrations tend to attract one another to form clusters. These clusters cause solutions to become viscous leading to increased viscosity.

Insulin is a large molecule weighing 5.8 kDa (Fry, 2014). Humira is a molecule used to treat rheumatoid arthritis and it is 25 times bigger than the size of insulin. The high concentration of drugs such as insulin and humira results in challenges during design and manufacturing of suitable autoinjectors. Monoclonal antibodies (mAb) are proteins developed to act like the natural antibodies that the body produces to fight infections. Common mAbs include emicizumab (administered subcutaneously), palivizumab (administered intramuscularly), infliximab (administered intravenously) and retuximab (administered on any route) (Manis, 2022). Injecting mAbs is challenging due to high viscosity and often large doses prescribed for patients. High-viscosity drugs need to handle high pressures whilst exposing patients to minimal impact. This means less pain, discomfort and the ability to actuate autoinjector using smaller forces. The development of long-acting injectable medications has contributed to the increase in high viscous injectables. These medications require slow release into the bloodstream with viscosity ranging

from 100 – 1000 cP. They are used to treat mental illnesses such as bipolar. Considerations such as using large needles, higher spring forces or longer delivery times can be explored for the injection of these drugs. However, these considerations are linked to increased injection site pain, decreased usability and device malfunction.

Autoinjector designers often have to assess and weigh device requirements such as:

- The possible volume that can be injected by a device considering the required dosage as per the patient's prescription;
- The manageable viscosity results in tolerable injection forces and dynamic pressures.
- Adequate concentration to achieve the required efficacy, bioavailability, and pharmacokinetic properties.
- Combat devices requiring low actuation forces that deliver medications accurately to the correct layer with minimal or no injection pain.

Some injectable pharmaceuticals exhibit non-Newtonian fluid characteristics with non-linear flow behaviour. This presents complex and non-predictable flow during injections. Dilatant or shear-thickening fluids demonstrate increased viscosity with increasing shear stress. Pseudoplastics or shear-thinning fluids demonstrate decreased viscosity with increased stress. Concentrated protein-based pharmaceuticals present low injection forces due to shear-thinning behaviour (Allmendiger et.al, 2014). Studies have linked shear-thinning injectables with viscous resistance and increased pain perception (Fry, 2014). Device changes such as thin-walled needles, needle-free systems, dampers and constant force springs have been explored to reduce the effects of shear-thinning injectables.

The power law or Ostwald de Waele's equation estimates the shear dependency of a solution as follows:

$$\mu = k\dot{\gamma}^{n-1} \qquad 1.2$$

Where μ is the viscosity, k is the flow consistency index and n is the power law index. The wall's total shear stress is contingent to the shear behaviour and the power law index. If the power law index is less than 1, the power law equation estimates decrease in effective viscosity with increasing shear stress, hence shear-thinning. If the power law index equals 1, the equation estimates constant viscosity and hence Newtonian fluid. If the power law index is greater than 1, the equation estimates increased effective viscosity with increased shear rate, hence shear-thickening.

1.3 Key Industrial Performance Characteristics Of An Autoinjector

The key performance characteristics of an autoinjector are injection time, needle insertion depth, injection force and pharmacokinetics related to the medication application. These parameters affect patient experience, device performance and medication adherence. Patient experience is the sum of patient-rated comfort, pain perception, usability and, occurrence and severity of adverse events.

1.3.1 Injection site, Needle length and Pain Perception

Parental medications are administered into the intramuscular, subcutaneous, intradermal or intravenous layer. Intramuscular injections are used when medication is to be injected into the muscle tissue. This method is preferred because of the presence of multiple blood vessels in muscles which induces faster medication absorption. Common muscles for intramuscular injections are the deltoid muscle in the shoulder, the vastus lateralis muscle in the thigh, the ventrogluteal muscle in the hip and the Dorsogluteal muscle in the buttocks. Intramuscular injections in the deltoid muscle are administered midway between the acromion and the deltoid tuberosity as shown in Figure 1 below. This injection site has a drug volume limitation due to its surface area. Only medications (e.g. vaccines) required in small volumes can be injected in the deltoid muscle (Mallet et.al, 1996).

Patients prefer thigh or abdomen injections because of the ease to self-inject in these sites (Stauffer et.al, 2018).The vastus lateralis muscle becomes a better option for self-administration as it is easier to self-inject medication into the thigh, than in the shoulder. This injection site is located by breaking down the thigh into three equal part and injecting into the middle segment. This can be located a hand away from the greater trochanter of the femur as shown in Figure 1 below. The ventrogluteal muscle is considered the safest injection site due to its depth and minimal presence of major nerves and blood vessels. It is located by placing the hand in pronation on the hip and creating a triangle between the three fingers in the posterior position and two fingers in the anterior position. This is located in the gluteus Medius muscle as shown in Figure 1 below. Studies have shown contradicting information as to whether this site is considered the most common due to the ease of accessibility or for safety reasons (Kirk, 2018).

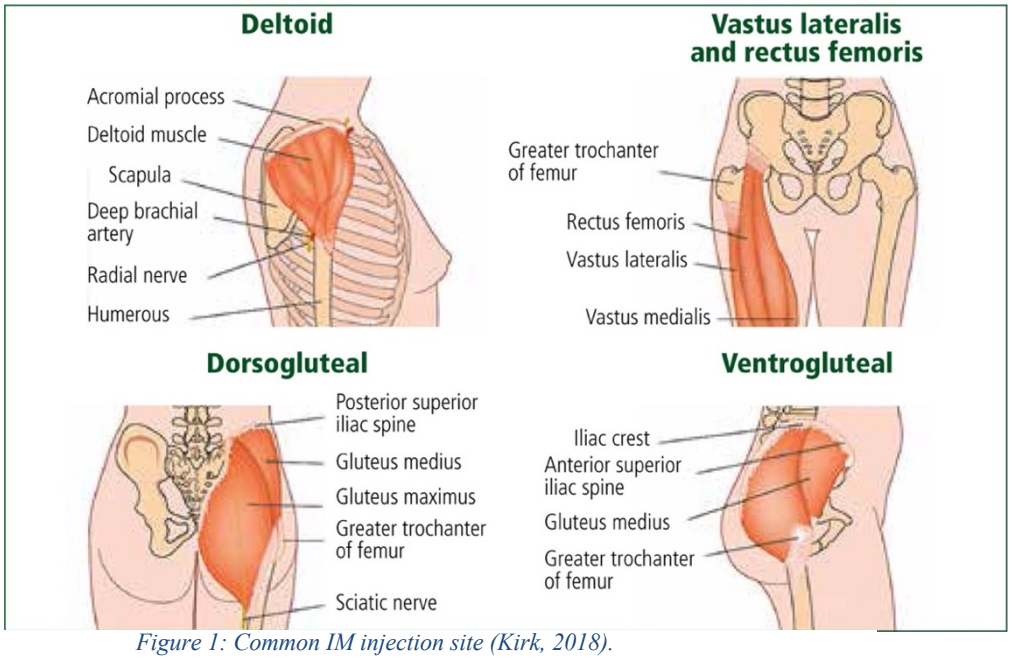

Figure 1: Common IM injection site (Kirk, 2018).

In a study to evaluate the suitability of the ventrogluteal site for IM injections in infants, it was found that muscle thickness of the ventrogluteal and anterolateral muscle is the same (Atay et.al, 2017). This thickness was larger than that of the deltoid muscle. Another study to evaluate the

suitability of ventrogluteal site in children generated interconnected results. This study reported differences in muscle thickness for different age groups and low muscle and subcutaneous thickness in the deltoid muscle compared to the anterolateral and ventrogluteal sites (Gunes et.al, 2016).Contradicting results are presented when comparing the occurrence and severity of side effects in the different injection sites. A study reported more systematic reactions in the anterolateral site compared to the deltoid and ventrogluteal site when administering vaccines in children (Cook et.al, 2003). However, early studies reported injuries, irritation, pain, bleeding and sciatic nerve damage due to ventrogluteal IM injection (Beyea et.al, 1996; Wilson et.al, 1996 & Farley et.al, 1986).

Subcutaneous administration is the injection of medication into the fatty layer underneath the skin. It is ideal for medication that require steady absorption of medication over time. Subcutaneous injections are less intrusive and are associated with high compliance compared to other administration modes (Jackisch et.al, 2016). Intravenous infusions are time-consuming and require patients to be in the hospital for hours to days at a time. This administration method has the highest bioavailability.

Injectability is the study of simple administration of accurate doses of medication. It depends on procedure ergonomics, pain perception, occurrence and severity of adverse events or tolerability. Drug delivery systems associated with high occurrence of adverse events affect medication compliance and adherence. Studies indicate that adherence to oral medication is poor due to the occurrence and severity of adverse events (Hepp et.al, 2015 & Lipton et.al, 2015).

A study reported 23 side effects (Stauffer et.al, 2018).16 related to the use of autoinjectors and 7 to prefilled syringe (Stauffer et.al, 2018). Some of the side effects, such as pain in the injection site, are caused by incorrect use of the autoinjector. Injecting in incorrect angles, failure to actuate device and injecting prematurely are common device usability challenges.

Skin-to-Muscle depth impacts medication delivery into the subcutaneous or intramuscular layer. This makes it exceptionally important to use the correct needle size for each patient. Needle size and injection depth have been inconsistently determined due to the differences in the skin-to-muscle depth and the tissue compression during intramuscular injections. Shorter needles have been recommended in literature, although there are concerns for injecting in thicker tissue layers. Smaller needles sizes have been further linked to comfort during injections (Hirsch et.al, 2012). Another study recommends needles with diameter ranges, 6-8 mm and thin walls for better patient experience and comfort in subcutaneous injections (Watt et.al, 2019).

Pain perception has been linked with the injection of high-viscosity drugs. High viscosity leads to drug aggregation and dispersion and this induces high force and hence injection pain. Autoinjector manufacturers exploring manufacturing of high-viscosity autoinjectors have recommended using regulators or torsion springs to limit and control high injection forces (Badkar et.al, 2021). The difficulty controlling and limiting spring forces makes alternatives such as compressed gas and electrochemical motors better actuation devices for autoinjectors. Other considerations aimed at

enabling high-viscosity autoinjectors are short needles, thin-wall or ultra-thin needles and tapered needles (Badkar et.al, 2021).

One-visit, randomised trial to investigate pain associated with subcutaneous administration of antiglycaemic medication in diabetes 1 and 2 patients had patients receive 5 injections in the thigh and 12 injections in the abdomen at different speeds and volumes (Heise et.al, 2014). Large volumes and faster injection speeds were linked to higher pain perception when compared to injecting lower volumes or slower speeds (Heise et.al, 2014). More patients preferred abdomen injections compared to injections in the thigh due to the severity of injection pain in the thigh. The abdomen has thicker muscle layers and is hence associated with less pain. Injection speeds 450$\mu l/s$, 300$\mu l/s$ and 150$\mu l/s$ and injection volumes 400,800,1200 and 1600 μl were used in this study.

Contradicting results have been presented on the influence of injection speed on pain perception. One study concluded that there is no difference in pain perception in patients who injected 1000 $\mu l/s$ or those who injected 100 $\mu l/s$ of lidocaine in the dorsum of the hand (Krause et.al, 1994). Another study concluded higher pain severity in patients that received the same dose of subcutaneous lidocaine in the arm at 200 $\mu l/s$ compared to 33 $\mu l/s$ (Scarfone et.al, 1998). Another study proved similar results to Scarfone et.al, 1998. In this study, faster injections (200 $\mu l/s$) resulted in severe pain compared to slower injections (Chan et.al,2001).

1.3.2 Forces Related To The Plunger Motion

Forces such as glide force, break loose force and activation force influence the performance of an autoinjector. The glide force is required to sustain plunger motion after overcoming static friction. The break loose force is required to move the plunger from its initial position. The relationship between the glide force and the break loose force must be so that the total force is sufficient to inject the medication with minimal effort; however not too low to induce sudden plunger motion. The magnitude of these forces is related to the usability of a drug-delivery device and provides guidance on injectability. Break loose and glide forces are usually calculated for prefilled syringes and then replaced by activation force for autoinjectors. It is however important to determine glide and break loose forces for autoinjectors too, to capture details related to injectability.

Studies have shown different results when determining the plunger force and displacement relationship. In the presence of an actuator, the plunger force decreases during needle insertion which creates high frictional forces. Once the plunger is released; friction decreases causing the plunger force to increase. This trend is shown in Figure 2 below as result of a study to develop an injection time model. This study used an autoinjector with either a 25 - or 27-gauge needle to inject mAbs with viscosity ranges 5.9 – 12.9 mPas (Thueer et.al, 2018). Another study reported an increase in plunger force when the plunger is displaced during the injection process shown in Figure 3 below (Wilkins et.al, 2012). In this study the decrease in plunger force due to increasedinternal friction was not captured. This might be linked to the consideration of a 2.5mm air bubble that was not considered in the previous study. Air gaps increase the pressure inside the plunger. Hence this pressure along with the fluid pressure could overcome friction and

increase plunger force. The other reason for the difference between the two models is the fluid characterisation. Wilkins et.al used constant viscosity while Thueer et.al used a viscosity model dependent on drug concentration and temperature.

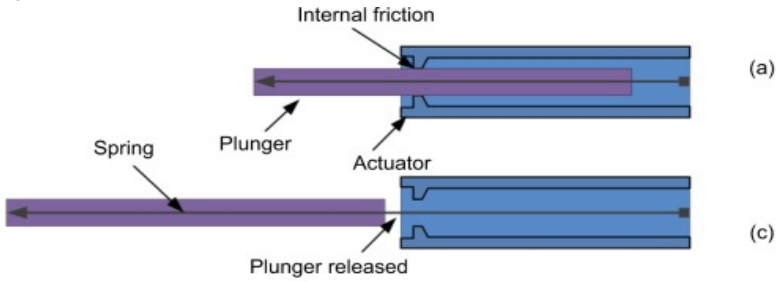

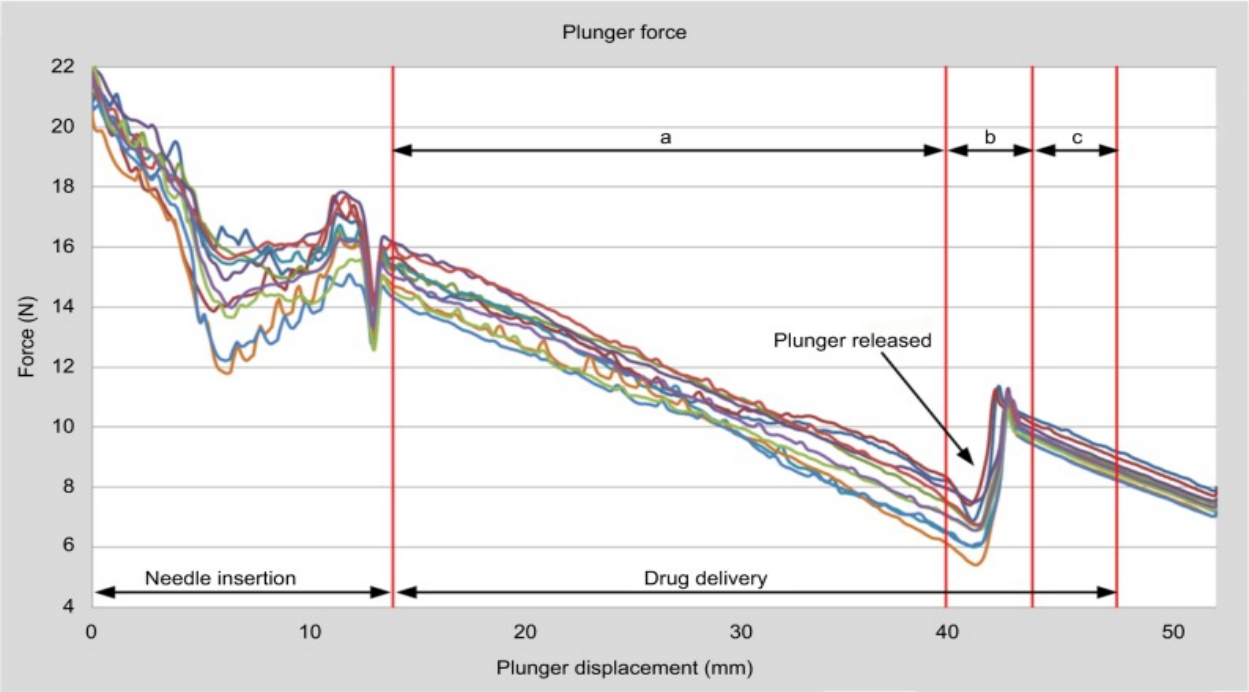

Figure 2: Plunger force vs Plunger displacement (Thueer et.al, 2018).a) Upon plunger release, b) Reduction in friction force and c) Increased plunger force

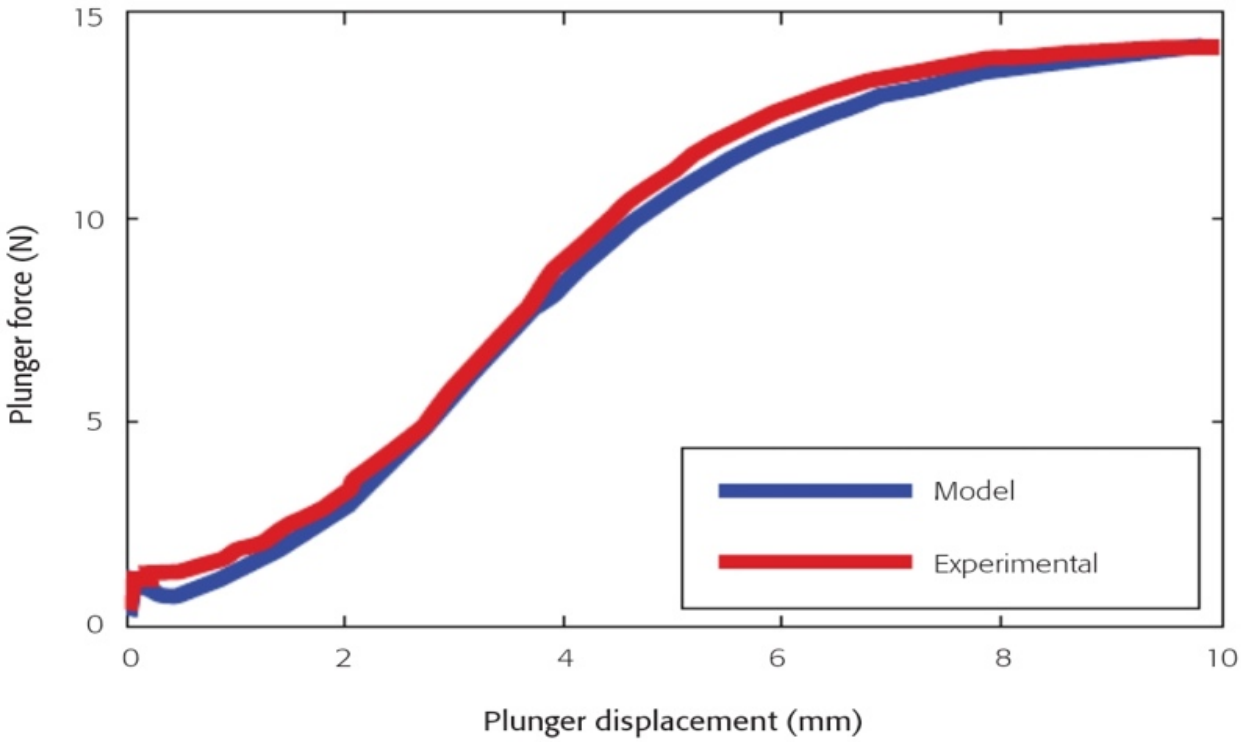

Figure 3: Plunger force vs plunger displacement (Wilkins et.al, 2012).

The most common configuration of a spring-driven autoinjector is shown in Figure 4 below. It includes a driving rod that speeds up to induce spring compression. The rod strikes the plunger inducing compression of the air gap. This process is called actuation and increases the pressure in the syringe rapidly. The frictional force and pressure in the syringe cause acceleration of the syringe. The syringe motion is ceased by a mechanical stop such as a stopper or rubber. The driving rod and the plunger continue to accelerate to inject the medication via the needle into the injection site.

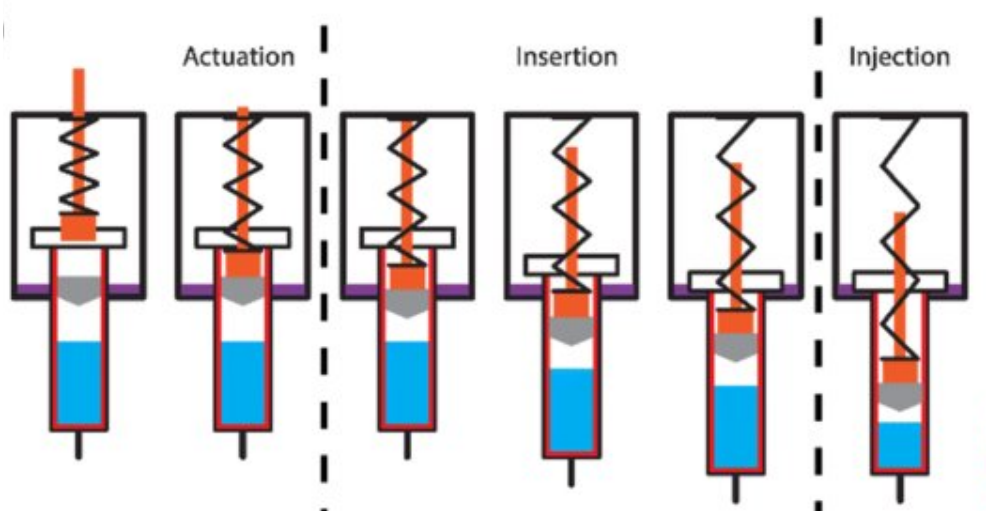

Figure 4: Configuration and processes involved during the injection for a spring-driven autoinjector (Zhong et.al, 2018)

In a study to develop a dynamic model for an autoinjector, the plunger motion was associated with the rod-plunger force. At equilibrium, this force is the sum of the frictional force in the rod housing, F_M and the spring force F_{spring} as shown in Figure 5 below (Zhong et.al, 2018). To move the plunger, the sum of the rod-plunger force and the force due to the atmospheric pressure must be higher than the frictional force between the spring and syringe; and the air gap pressure (Zhong et.al, 2018).

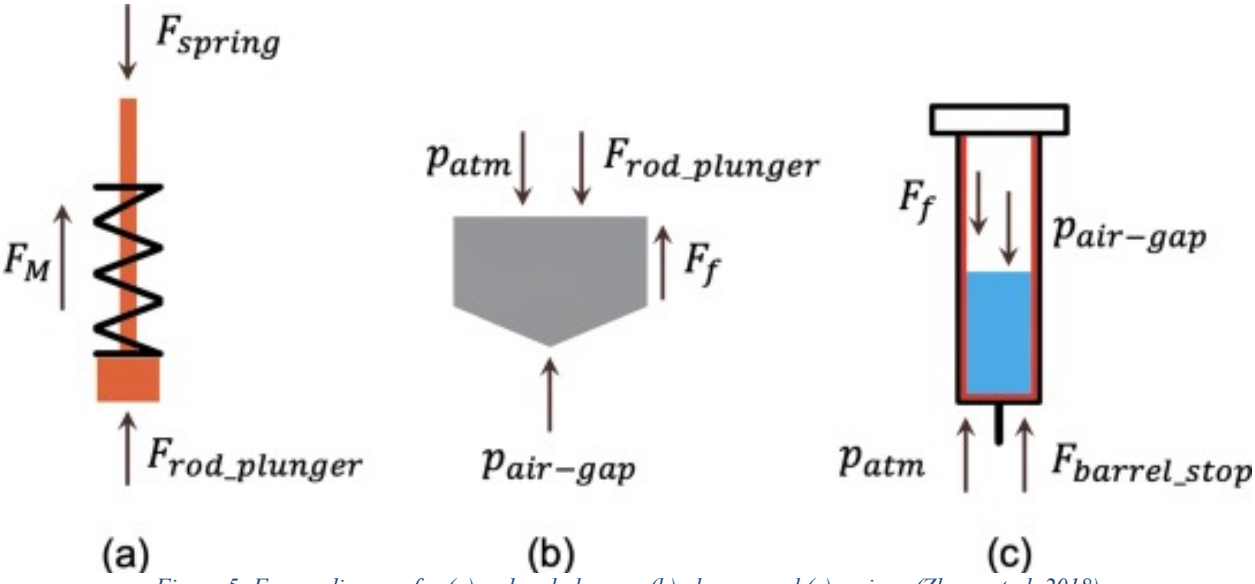

Figure 5: Forces diagram for (a) rod and plunger, (b) plunger and (c) syringe (Zhong et.al, 2018)

1.3.3 Injection Time

Injection time is the time taken to complete injection of a full dose of medication. This parameter is critical to ensure rapid intramuscular injections. Factors such as formulation viscosity, drug volume, needle length and injection force affect injection time. Autoinjectors with stronger needles have shorter injection time (Veilleux et.al,2018). These autoinjectors are however linked to increased chances of device failure, solution cavitation, protein aggregation and fractured

syringes. Most autoinjector tests report maximum injection times of either 15s,10s, 5s and the highest injection time reported is 17s (Hu et.al, 2019). For conditions such as anaphylaxis, this measurement could be the reason for the survival or death of a patient post an allergic shock. In a study to evaluate the performance of two autoinjectors; the Aimovig was rated the best-performing device with an injection time of 0.26 - 0.46s compared to 0.75 - 1.53s for the Emgality (Dou et.al, 2020).

Injection time can be measured experimentally using machines such as the ZwickRoell and Instron. These machines allow for compression tests on autoinjectors and prefilled syringes. Injection time can be determined theoretically via calculations or mathematical modelling. Mathematical modelling and SIMULINK can be used to determine injection time by modelling autoinjector components as a system of differential equations as in Wilkins et.al, 2012. Equations of motion can be used to deduce injection time as in Rathore et al., 2011. Application of Newton's 2^{nd} Law to sum the static forces influencing the injection can also be used to determine injection time as in Ajaghari et al., 2016. These static forces are due to the pressure drop in the needle defined by the Hagen- Poiseuille equation, static and dynamic pressure losses and the friction between the syringe and the stopper.

1.4 Comparison Of Autoinjectors To Other Delivery Systems

1.4.1 Usability

Usability is an important user requirement that autoinjector manufacturers need to get right. It describes how easy it is to actuate, hold and inject using the autoinjector with minimal or no training. Multiple studies reported the high usability of autoinjectors compared to other delivery systems. A study comparing a prefilled syringe and an autoinjector reported that 94% of the users rated the autoinjector as easy to use after first exposure and 92% confirmed complete dose injections (Stauffer et.al, 2018). In this study 120 or 240 mg of galcanezumab was injected subcutaneously using a prefilled syringe and autoinjector once a month for a year, and patients were interviewed for device preference or usability.

Another study concluded that patients and caregivers can safely use ixekizumab autoinjectors regardless of training (Duffin et.al, 2016). This study combined 49 patients and their caregivers who were either rheumatoid arthritis, psoriasis, psoriatic arthritis and Systematic Lupus Erythematosus (SLE) patients and their caregivers. Participants injected 160 mg once and 80 mg of ixekizumab biweekly subcutaneously for 12 weeks. Out of a group of 17 trained and 32 untrained device users, 2 injection failures were reported (Duffin et.al, 2016). Failed injections were associated with the patient state. The first failed injection was from a 73-year-old patient with multiple comorbidities, hence taking other medications known to affect cognitive functions. The other patient confirmed their understanding of training, however failed to actuate the device.

Device preference is dependent on usability. In a human factor study to analyse and contrast the performance and preference of three autoinjectors (zembrace SymTouch – two-step autoinjector shown in Figure 6 below; Sumavel DosePro – Three-step , disposable autoinjector shown in

Figure 7 below and Imitrex STATdose – multistep, reloadable autoinjector shown in Figure 8 below) patients preferred the device with the highest usability (Andre at.al, 2017). This study combined 54 patients who conducted two simulated subcutaneous injections of sumatriptan using each device. 88.9% of the patients preferred the two-step autoinjector, while 13% preferred the three-step disposable and only 1.9% preferred the multistep reloadable (Andre at.al, 2017). Although reloadable, the STATdose autoinjector was less preferred due to the multistep to be followed when injecting. A study to analyse the performance of two pen injectors (one disposable and the other reusable) for recombinant human growth hormone (rhGM) concluded that there is no statistical difference in the usability of a disposable vs a reusable autoinjector (Hey-Hadavi et.al, 2010).

Figure 6: Two-step, disposable autoinjector - Zembrace SymTouch (Andre at.al, 2017).

Figure 7:Three-step, single-use auotinjector - Sumavel DosePro (Andre at.al, 2017)

Figure 8: Multistep, reloadable autoinjector (Andre at.al, 2017).

Another usability and patient experience study of four adrenaline autoinjectors concluded that user-centred design significantly impacts preference (Guerlain et.al, 2010).In this study 48 participants performed untrained simulated injections using the TwinJect, EpiPen, INT01, and INT02 autoinjectors shown in Figure 9 below. Patients who completed correct injections after following all written instructions were recorded as 46% INTO1, 27% INTO2, 12% EpiPen and 0% TwinJect (Guerlain et.al, 2010). The INTO1 recorded the highest usability and this is associated with device features such as the Light- emitting diodes for visuals and sound-prompt system that guides users during the injection. However, this study's results are biased as half the users were experienced autoinjector users. The risk of patients rating familiar autoinjectors as highly usable is high.

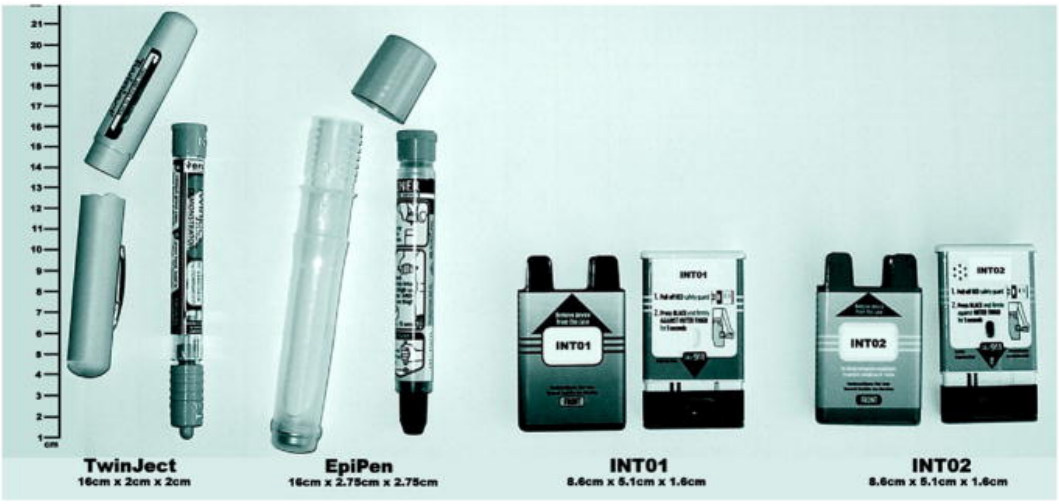

Figure 9: TwinJect, EpiPen, INT01 and INT02 adrenaline autoinjectors (Guerlain et.al, 2010)

1.4.2 Pharmacokinetics

Pharmacokinetics defines the interaction of the human body and the medication taken by the patient from drug absorption to elimination. It involves the process of absorption, distribution, metabolism, and excretion. Absorption is the transportation of medication from administration to the systematic circulation. It depends on the rate and concentration of the drug. Different administration methods e.g., intramuscular, oral, intrathecal, intravenous, inhaled, rectal, transdermal, buccal have different absorption rates. Bioavailability measures the drug present in the systematic circulation compared to the drug administered. It is affected by medication chemistry and administration method. Intravenous administration is defined as the best administration method as it results in 100% drug bioavailability (Starkey et.al, 2015). Early studies of injection site showed that IM diazepam absorption is irregular and results in lower plasma level compared to oral administration (Gamble et.al.,1975; Hillestad et.al., 1974; Kanto, 1974, 1975; Magnessun et.al, 1979).

Calculating the area under the drug amount vs time curve (AUC) and the maximum drug concentration measured in the targeted organ, blood or cerebrospinal fluid (Cmax) are some of the techniques used to determine bioavailability. The AUC shown in Figure 10 describes the changes in plasma concentration over time.

Distribution is the dissemination of the drug in the body. It is a measure of diffusion and conversion of the drug. Patient physiology and biochemical properties of the drug are important contributors of drug distribution patterns. The ability of the drug to bind with proteins affects drug distribution. Drugs that are less likely to bind with proteins have higher plasma concentrations, therefore more effective in treating symptoms and diseases. Drugs are metabolised into successive compounds to induce excretion. The kidney is the popular organ for excretions, however some drugs are excreted by the gastrointestinal tract, skin or the lungs. Excretion is measured by capturing drug clearance (CL). This is the proportion of the speed of the excreted drug to the drug concentration in plasma. These givens an indication of the speed of the injection, hence the injection time

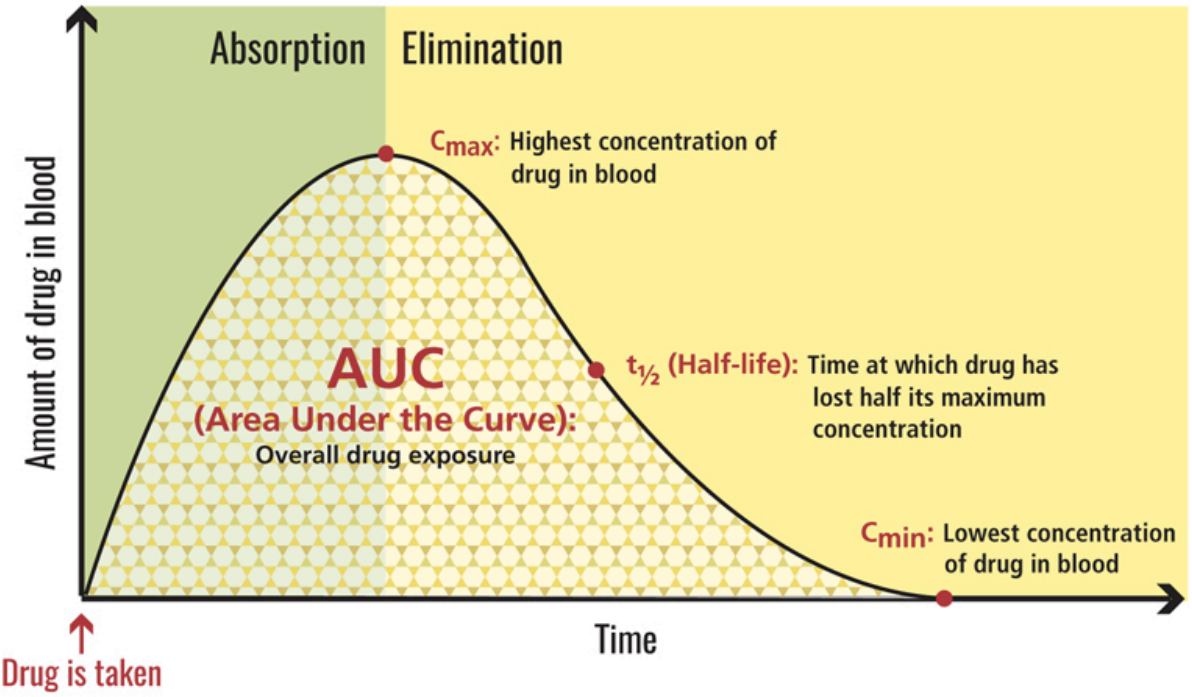

Figure 10:Amount of drug in blood over time (clinicalinfo. 2022).

Bioequivalence is the biochemical resemblance between two or more drugs. If two drugs discharge the same quantity of the effective ingredient at the same speed and quality, they are said to be bioequivalent. Bioequivalence study is required when drug formulation or route of administration of administration had been changed. This measure is useful for determining device performance by using different devices to deliver the same drug to the same site in the body. A study to compare the pharmacokinetics of a prefilled syringe and autoinjector reported a Cmax between 0.8 to 1.25 and 90% CL ratio for autoinjectors (Stauffer at.al, 2018). This study concluded that the is no significant concentration different between the two delivery systems regardless of the injection site (Stauffer et.al, 2018). Some autoinjectors do not meet bioequivalence criteria. This is linked to the injection depth of these autoinjectors (Hu et.al, 2019).

Bioavailability of administering biological drugs subcutaneously has been difficult to predict. Studies report a bioavailability between 24-100% (Tang et.al, 2004, Matucci et.al, 2018 & Ritcher

et.al, 2012). Subcutaneous injections of biologics are pharmacoeconomically admirable due to location, diffusion and convection. These processed need to occur from intermediary tissues, then directed to lymphatic capillaries and then finally to the blood vessels. This results in lower Cmax that takes longer to reach. Differences in injection time, needle gauge affect device performance and can affect Cmax and plasma concentration.

1.5 Existing Models

Different static, quasistatic, and dynamic models exist in the literature to describe the relationship of parameters like injection forces, injection time, and fluid characterization. In a study to determine the force, and injectability relationship for subcutaneous injections; it was determined that needle length, the thickness of the needle wall, and the inner diameter of the plunger and syringe are important dosing material characteristics (Watt et.al, 2019). These characteristics are linked to how well the dosing material can inject a solution. The injectability of the dosing material was used to predict injection force. The study concluded that an 80 N injection force is not manageable, and the recommended standard injection force is 20 N (Watt et.al, 2019).

Other models in the literature are developed to predict injection time. One such model represented time parameters as statistical elements modeled by distribution functions (Thueer et.al, 2018). The forces influencing injection time are the stopper friction, plunger force, and fluid force due to the pressure drop in the needle as shown in Figure 11 below.

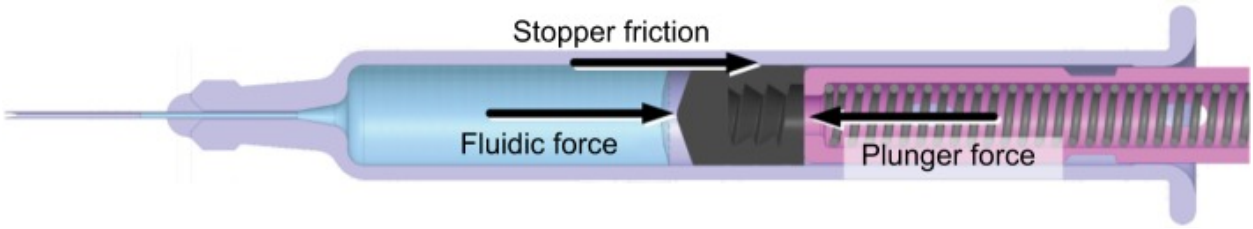

Figure 11: Force diagram showing forces that contribute to injection time variation (Thueer et.al, 2018)

Injection force is calculated using:

$$t_{inj} = f(\mu, L, x, R^4, \frac{1}{r^4}, \frac{1}{F_{plunger} - F_{friction}}) \qquad 3.4$$

Where t_{inj} is the injection time, μ is the viscosity of the medication, L is the length of the needle, R is the syringe barrel inner radius, r is the needle inner radius, x is the plunger displacement, $F_{plunger}$ is the plunger force and $F_{friction}$ is the frictional force.

Equilibrium of the forces in *Figure 11* above and *Equation 5.6* was used to determined injection time (Thueer et.al, 2018). Neglecting inertial terms and pressure losses between the syringe and the needle under assumptions of low masses and velocity increases the risks of accumulating errors in calculating injection time. This is a major limitation of this model.

Another mathematical model was developed to predict the key performance of an autoinjector. This study modelled each autoinjector component as a mathematical equation such that the

needle was represented by the Hagen-Poiseuille equation and inertial pressure losses; and the plunger modelled as a linear compliance (Wilkins et.al, 2012). This advanced the model to study the effects of shear stress during the injection process. It was concluded that large needles create high shear strain rate as shown in Figure 12 below (Wilkins et.al, 2012). Hence, inducing drug degradation and device failure. Shear stress is sensitive during actuation because the spring force induces compressive forces on air bubbles. This increases dynamic pressure inside the needle and drug velocity.

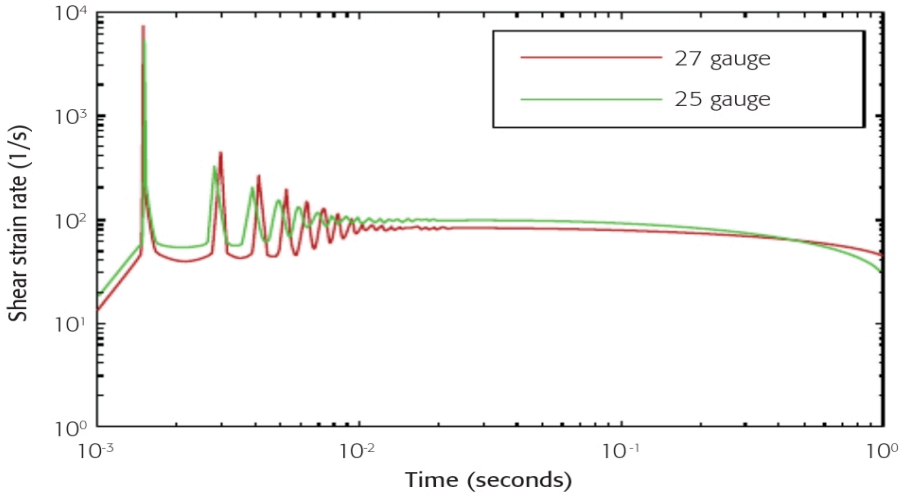

Figure 12: Shear stress vs time for a autoinjector with 25 or 27 gauge needle (Wilkins et.al, 2012)

Modelling air bubbles as part of the components of an autoinjector is a common approach in autoinjector modelling. A model to determine the dynamic properties of an autoinjector considered an air gap between the plunger and the medication. The air gap is due to syringe plugging and methods used for plunger insertion (Veilleux, 2019). The schematic showing the fluid flow and related forces in the autoinjector is shown in Figure 13 below.

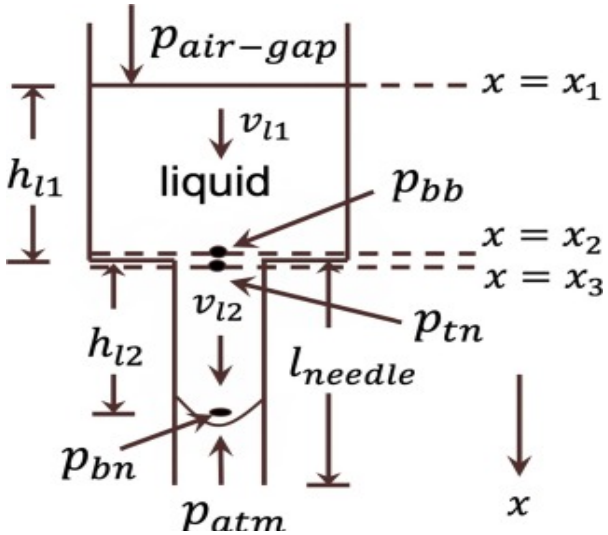

Figure 13: Schematic showing the flow and associated forces for an autoinjector (Zhong et.al, 2020)

The pressure inside an air gap, $P_{air-gap}$, induces the fluid flow at velocity v_{l1}. The air gap's presence requires using a heat transfer model to account for energy losses during thermal conversion between the liquid and air. The pressure difference between the syringe and the needle is accounted for using the Bernoulli equation, and this leads to a change in momentum as the fluid enters the needle. The model proves direct proportionality between drug solution's volume, viscosity, and injection time (Zhong et.al, 2020). Furthermore, Injection time is proven to be inversely proportional to the spring force (Zhong et.al, 2020). These results are consistent with Thueer et.al, 2018.

Injecting high viscosity fluids leads to high injection forces. Hence, there is a need to study the injection force – viscosity relationship further. A mathematical model was developed to correlate changes in injection force for Newtonian and Non-Newtonian models to viscosity measurements from cone rheometry (Allmendiger et.al, 2014). This study developed a viscosity–shear rate profile for monoclonal antibodies (mAbs) and commercial proteins (CPT 1 – CPT 10). Injection forces were measured on the Zwick machine and correlated with viscosity measurements from the rheometer. These results were compared to forces calculated using the Hagen-Poiseuille equation. All solutions exhibited an agreement between theoretical and practical results excluding CPT10 and CPT9. Both these products were reported to exhibit shear-thinning behavior. CPT10, CPT9 and mAb1 recorded lower injection forces than other solutions because of shear-thinning at peak shear rates. Figure 14 below shows the viscosity profile of (a) mAb1 AT 20°C, (b) CPT4 (commercial protein), (c) CPT10 (Commercial protein) and (d) mAb1 at 25°C. Viscosity remains constant for CPT 4 irrespective of the shear rate at all measured temperatures. This proves Newtonian behaviour. CPT10 and mAb1 showed shear dependency as viscosity decreases with increasing shear rate.

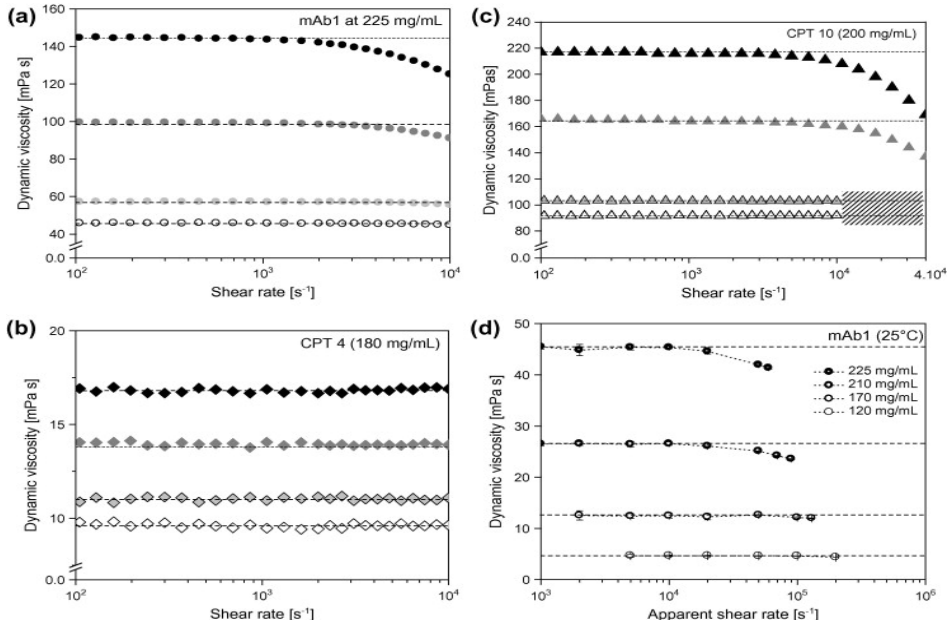

Figure 14: Dynamic viscosity vs shear rate for (a) mAb1 at 20°C, (b) CPT 4, (c) CPT 10 and (d) mAb1 at 25°C (Allhendiger et.al, 2014)

The model used average shear rate by considering non-linear shear stress variation at the needle diameter. Effective shear rate is calculated as:

$$\dot{\gamma}_{eff} = \frac{2Q}{\pi r_{needle}{}^3}\left(\frac{3n+1}{2n+1}\right) \qquad 1.7$$

Where Q is the flow rate, r_{needle} is the inner radius of the needle and n is the power law index. Another study used wall shear rate to calculate the injection forces of concentrated proteins (Fischer et.al, 2015). In this study, shear rate at the wall was calculated as:

$$\dot{\gamma}_p = \left(\frac{3n+1}{4n}\right)\frac{4Q}{\pi r_{needle}{}^3} \qquad 1.6$$

Shear rate at the wall is higher than effective shear rate and has a larger dependency on the power law index. The viscosity and shear rate relationship for the three proteins solutions is shown in Figure 15 below. mAB2 have lower viscosity and shear-thinning behavior is observed at higher viscosities than mAB1. mAB3 shows constant viscosity and hence Newtonian behavior. mAB1 and mAB2 injection forces were correctly predicted using maximum shear rate, however poorly estimated using effective shear rate.

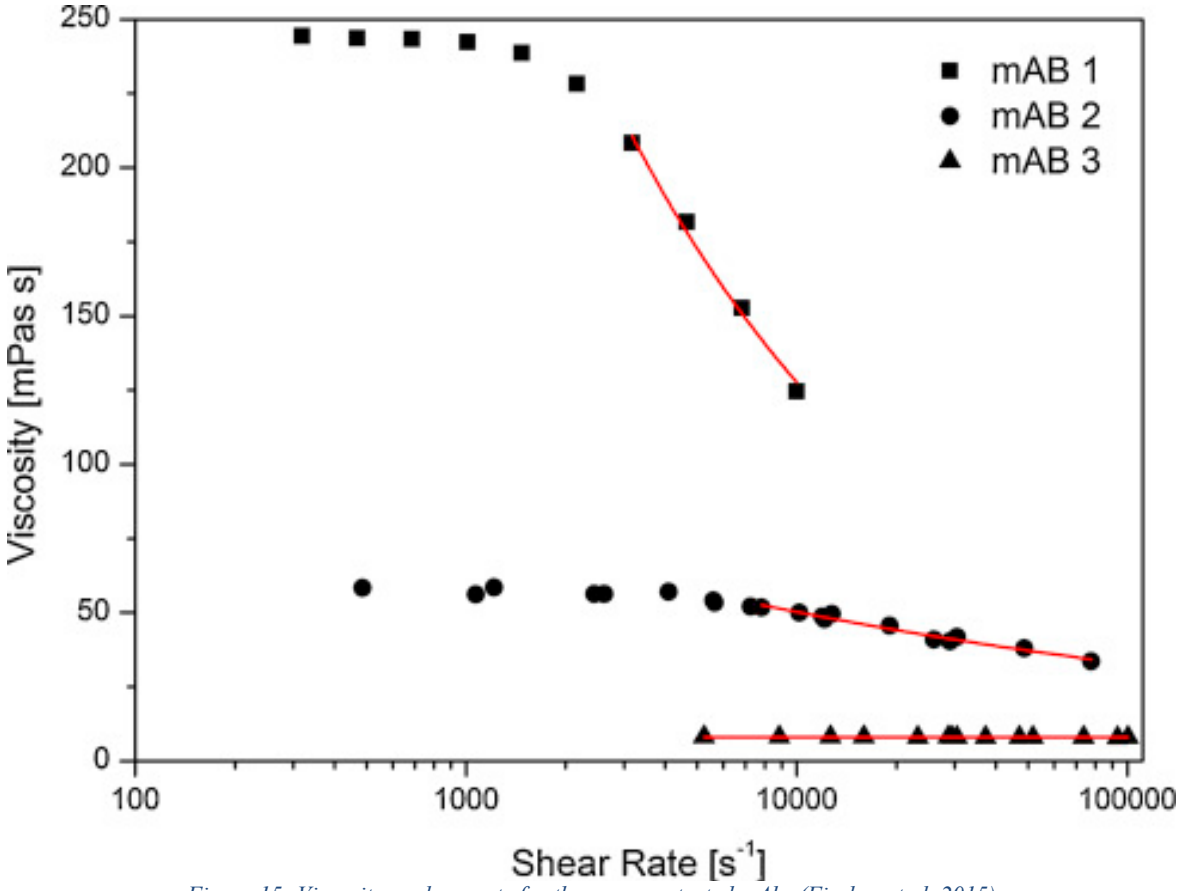

Figure 15: Viscosity vs shear rate for three concentrated mAbs (Fischer et.al, 2015)

A study to determine stress and pressure changes in autoinjectors captured syringe acceleration during needle insertion and deceleration when the injection depth is reached (Veilleux et.al, 2018). The pressure changes observed are shown in Figure 16 below. The pressure measurement on the injected liquid is initially atmospheric pressure. This pressure increases to at least 10 times due to the spring force forcing the plunger to move. Two other significant pressure changes are measured due to syringe acceleration and rebound. A quasi-static phase is reached immediately after the pressure drop is captured for syringe rebound. When an air gap is considered, the first pressure variation is due to the growth and implosion of the bubble. This creates a significant decrease in pressure resulting in lower peak pressures at syringe acceleration compared to when measured in the absence of an air gap. In the presence of an air gap, syringe acceleration occurs first followed by pressurisation. While no cavitation is observed, the pressure increases rapidly to at least 4 times than required pressure for correct rapid injection (Veilleux et.al, 2018). These two processes occur simultaneously in the absence of an air gap. Implosion of bubbles leads to cavitation, and this increases pressure 10 times the required pressure for high performing autoinjector (Veilleux et.al, 2018).

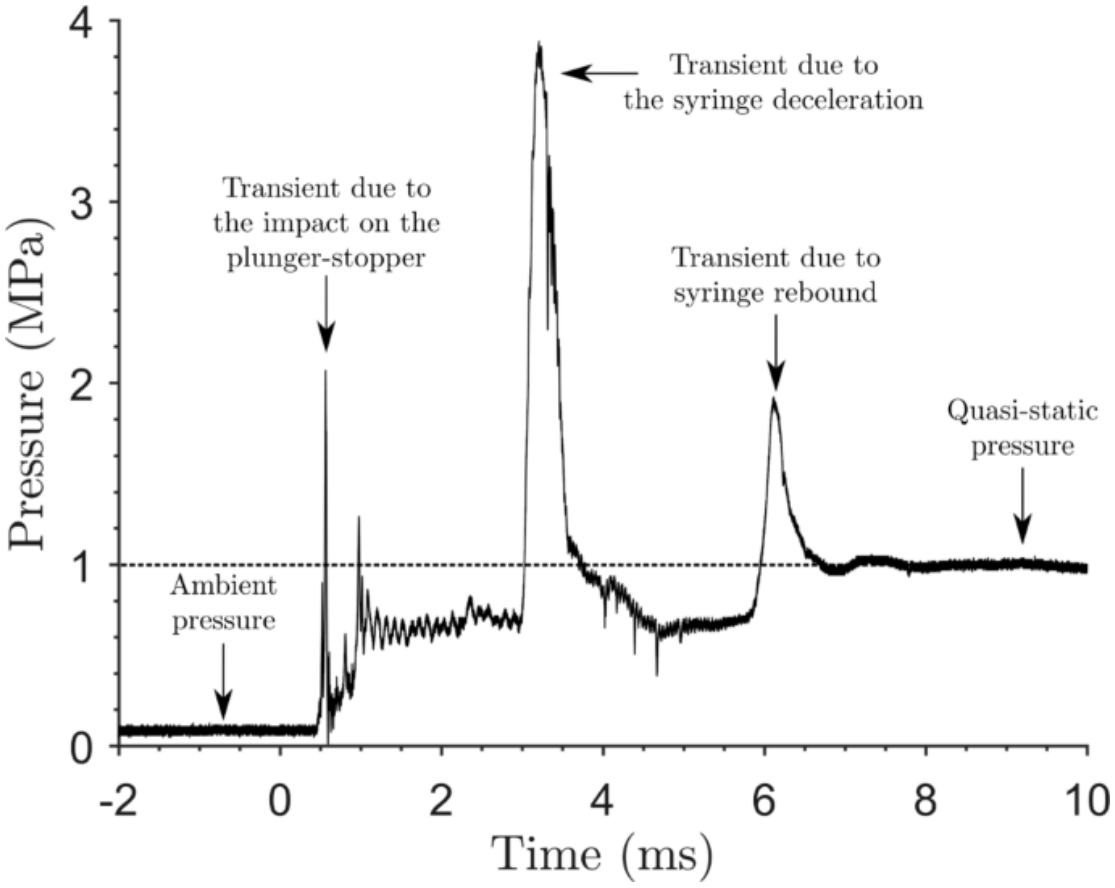

Figure 16: Pressure changes over time for an autoinjector (Veilleux et.al, 2018)

Although these studies show the mathematical relationship between shear rate profile, viscosity, injection force and pressure; the results are only relevant for surrogate fluids. There still exist a gap to understand the flow behavior of Newtonian and non-Newtonian drugs and concentrated solutions and their relations to injection forces, speed, and time.

Injecting large volumes of solutions possess complex delivery challenges. Historically, biologicals were administered intravenously. This was linked to prolonged treatment requiring patients to make appointments and be at the hospitals for hours at a time. Subcutaneous administration of biologicals has been introduced to promote self-administration of medication. Subcutaneous injections have been limited to 2ml as increased volumes lead to stability, manufacturing, and medication delivery challenges (Badkar, 2021). This volume limitation is due to the restriction of the extracellular matrix in the subcutaneous space (Badkar, 2021). Technologies need to enable subcutaneous and intramuscular injections of higher volumes or dosages without compromising the medication concentration.

Injection time is a critical parameter for the design of autoinjectors as accurate and effective drug delivery is time-dependent. Estimating injection time usually includes an injectability analysis. This can be done by measuring the formulation viscosity per shear rate to determine fluid behaviour or calculating the shear rate correlating to a specific needle gauge and flow rate. This can further be linked to other rheological tools such as injection force and injection speed to determine device performance. While there are models to predict injection time for an autoinjector by characterizing drug solutions, there is a need to link the kinematics and dynamics of an autoinjector to analyse fluid behaviour. Furthermore, sensitivity of device component dimensions should be explored in the autoinjector kinematics and dynamics study.

1.6 Research Question, Aim And Objectives

This research aims to design, develop, verify, and validate a dynamic model for an intramuscular autoinjector. This is done by answering the following research questions:

- How to mathematically represent the spring-loaded plunger motion during the injection process?
- How does medication characterisation defined by fluid viscosity affect the syringeability of an autoinjector?

The objectives to be satisfied are:

- Design and develop an optimised mathematical model to describe the plunger motion of a spring-driven autoinjector.
- Conduct a Computational Fluid Dynamics (CFD) study to demonstrate the fluid behavior of different medications during the injection process.
- Verify and validate the CFD model for its context of use (COU) following requirements from the American Society of Mechanical Engineers (ASME) Verification and Validation Standards (V&V 40, V&V 20).

1.7 Rationale

The autoinjector market accounted for USD 46 billion in 2020 and is estimated to reach USD 104.9 billion in 2025 with a CAGR of 17.9% from 2020 to 2025 (Markets and markets, 2020). This expansion is fueled by the:

- Rising incidence and prevalence of anaphylaxis reactions, autoimmune and chronic diseases.
- Increased development of injectable biological molecules.
- Favorability of self-administration treatment therapies.

The incidence of anaphylaxis is approximated to be 52 -112 episodes per 100 000 person - years with a prevalence of 0.3 - 5.1% worldwide (Tejedor et.al. 2015). In a systematic review to analyse the epidemiology of anaphylaxis, it was reported that the incidence rate for food-induced allergies from 34 studies indicate 0.7 per 100 person years and 0.2 per 100 person-years for 0-4 years and 0-19 years (Umasunthar et.al., 2015). Children are susceptible to allergic reactions and have a higher incidence rate of anaphylaxis. This is often linked to the difficulty of controlling and avoiding allergens in younger children. The global availability and accessibility of adrenaline autoinjectors is limited. Only 32% of 195 countries worldwide have access to adrenaline autoinjectors (Kase et.al, 2018). The demand for adrenaline autoinjectors worldwide has created a need for local, fast-paced design and manufacturing of autoinjectors to increase accessibility.

A systematic review and meta-analysis study to determine the prevalence of rheumatoid arthritis reported a prevalence of 0.46% based on 67 studies (Almutairi et.al, 2021). Oral disease-modifying antirheumatic (DMARDs) drugs have been linked to serious adverse events such as attacking blood cells and the liver. This has led to the development of injectable biologicals that inhibit chemicals in the body from attacking the immune system. A study concluded that 50% RA patients preferred subcutaneous and intravenous administration of DMARDs while 26% preferred subcutaneous administration only (Hsiao et.al, 2019). The questions in the study survey revolved around comfort, adverse events, resulting infections and affordability. Multiple sclerosis prevalence is higher in Europe and North America (greater than 100 people /100,000 of the population) compared to Sub-Saharan Africa and East Asia (greater than 2 people /100,000 of the population) (Leray, 2016).

Chronic conditions such as diabetes, cardiovascular diseases and cancer are the leading cause of death worldwide. Management of chronic conditions requires regular, accurate and easy therapies to improve patient adherence and compliance. There were 287 million diabetes patients in 2011 (ISO 11608-2, 2012 & Buysman et.al, 2011). Diabetes patients are estimated to increase to 438.4 million in 2030 (Chernikova et.al, 2011). Many people in the older population suffer from multimorbidity or the occurrence of numerous chronic illnesses at once. This leads to polypharmacy or taking multiple treatments at a time. Multimorbidity affects 95% of adults above 65 years old (Violan et.al, 2014). Polypharmacy is linked to high medical costs, frequent hospital admissions and decreased medication compliance and adherence. Accessibility to autoinjectors that can inject multiple drugs simultaneously can improve medication adherence in multimorbidity patients.

Opioid overdose is a healthcare crisis in many parts of the world as it is one of the leading causes of deaths and disabilities in drug users. Individuals can be exposed to opioids as part of a treatment regimen for a particular disease, mistakenly exposed or choose to use opioids for pleasure. A study with 66 South African drug users, it was found that 63% of the people in Pretoria and 14% of the people in Cape Town overdosed in 2021 (Wilson, 2022). High risk individuals include people with substance abuse history, painkiller users who are prescribed large doses and sedative users. The availability of naloxone autoinjectors will prevent the deaths associated with opioid overdose.

New emerging needs and challenges are driving an increase in the autoinjector market. Patients need more autoinjectors due to the ease of use and opportunity of self-administration. These devices are ideal in emergency settings to save life's. Chronic disease patients prefer autoinjectors due to their ease-of-use. They offer promising opportunities for development such as injecting multiple drugs simultaneously. They are commercially viable for pharmaceutical companies as they induce product differentiation that directly correlates to high drug sales. Biologicals accounted for more than 50% of the highest-selling drugs in year 2020 (Roe, 2021).

Other instances where autoinjectors can be used include immunization injection, injection of immunoglobulins and toxoids, hormone and antibiotics injections. The preferred injection site for most vaccines is the intramuscular layer at either the deltoid or anterolateral aspect of the thigh. This reduces side effects and promotes immunogenicity. Toxoids are proteins with chemically suppressed toxicity through heat treatment whilst maintaining immunogenicity. These antigens cause immune response to protect the body against bacteria-secreted toxins. Tetanus is a bacterial-induced infection resulting in severe muscle spasm and locked jaws. It causes bone fracture, pneumonia and laryngospasms. Tetanus was linked to 79% (44612 of 56748) deaths in South Asia and Sub-Saharan Africa 2015 (Kyu et.al., 2015). Majority of these cases are from low- and middle-income countries. Neonatal tetanus occurring between 28 days from birth is the most common type, followed by maternal tetanus. Although Non-neonatal tetanus cases exist, there are not often recorded and reported.

Pertussis is a contagious whooping cough cause by respiratory tract infection. It was linked to 24.1 million cases with 160 700 deaths in children younger than 5 years in 2014 (Yeung et.al. 2017). Africa has the highest occurrence and death related to pertussis, accounting for 7.8 million cases with 58% deaths in 2014 (Yeung et.al, 2017). Conditions such as tetanus, influenza and pertussis can be easily prevented by intramuscular administration of toxoids. Diphtheria toxoids, tetanus toxoids and pertussis vaccines (DTPw) are 0.5 ml intramuscular injections given in 5 courses (Shukla et.al., 2018). 3 doses are given in the first two years of life (infancy) and 2 booster vaccines are given at 18 and 60 months.

To meet the autoinjector market demand, there is a need to gain insight and appreciation of the fluid-delivery system of an autoinjector. This means understanding the medication flow during the injection process and how this affects the general performance of an autoinjector. An appreciation of the fluid-delivery system will promote the design of high-performing autoinjectors that lead to

medication adherence and compliance. This will lead to less pain and improved patient experience during auto injections. Furthermore, its means more technological advancements to solve challenges related to polypharmacy, injecting highly viscous and large doses of drugs.

1.8 Limitation And Structure

This research is novel because it characterises medication flow in the fluid delivery system of an autoinjector during the injection process. The spring is considered the main source of the plunger motion. Studied plunger kinematics relate to the displacement and velocity of the plunger during the injection. The computational fluid dynamics model is created assuming of steady-state conditions, laminar flow and incompressible fluids.

This dissertation is divided into 6 chapters. The current chapter introduces the research background and highlights the different types of autoinjectors in the market. The rheological characterisation of fluid is defined including tools such as the power law and rheometry. The relevant literature is reviewed in this chapter. Literature on Industrial performance parameters like injection time, injection speed and injection site is investigated. Pharmacokinetics, usability, pain perception and tolerance related to an autoinjector are explored in this chapter. Models designed to describe the relationship between viscosity behaviour of injectables and other parameters are summarized and compared. The research objectives, aim and research questions are describe in this chapter to lay the foundation for this research.

Chapter 2 introduces the methodology used to conduct this research. The design, validation and optimisation of a mathematical describing the plunger motion is highlighted in this chapter. The methodology to conduct the CFD study is featured in chapter 2. This includes the system design, governing equations and discretisation. The verification and validation of the CFD model as per the American Society of Mechanical Engineers Verification and Validation standard (V&V40) and Verification and Validation for CFD and Heat transfer (V&V20) is described in this chapter.

Chapter 3 presents the mathematical model, validation and optimisation results. These results are discussed in this chapter and compared to the literature. Chapter 4 presents the CFD results and comparison of these results to the literature. Chapter 5 depicts the verification and validation assessment and related discussion. Chapter 6 presents the conclusion and future recommendations.

CHAPTER 2: METHODOLOGY

2.1 Introduction

Mathematical modelling represents real-life problems and systems using mathematical equations. These models are adopted to deduce, simulate, and discern the behaviour of systems at a specific point in time or over a certain duration. They are divided based on linearity, state, time-dependency and variable-parameter relationship. The linear behaviour is defined by the straight-line relationship between model parameters. It represents direct proportionality between two parameters. Mathematical models can be developed under equilibrium conditions (static) or under time-dependent changes (dynamic). They are termed deterministic when distinct variables depend on model parameters. Stochastic models use probability distributions to represent distinct values.

Computational modelling is the art of using numerical analysis to simulate complex system and solve problems associated with these systems. In health sciences, computational models have been applied in areas such as medical device design and application, tracking infectious diseases, support clinical decisions, supplementing bench testing for regulatory submissions and predict adverse events related to different treatments (Morrison et.al, 2017). Computational models are useful throughout the entire medical device lifecycle to predict performance, safety, and effectiveness of a device (ASME, V&V40, 2019). Computational models are the only viable option in scenarios where conducting a physical experiment is impossible or unethical.

A study to assess the role of computational modelling and simulations in the total product cycle of vascular devices categories computer modelling as the most cost-effective and most effective in predicting performance under certain acceptable assumptions (Morrison et.al, 2017). Verification refers to the extent that the computational simulation coincides with the fundamental mathematical analysis and derived solutions. This is conducted to assess that the model meets the specification and assumptions for its intended use. Validation assesses the accuracy of the computational simulation to represent real-life systems. Models can be validated by conducting subjective reviews, statistical tests or physical experiments.

This chapter outlines the methodology followed in this research. The methodology is represented in Figure 17 below. The process followed to develop, validate and optimize the mathematical model created to define the plunger motion is described in this chapter. The design, verification and validation of the CFD model follows thereafter.

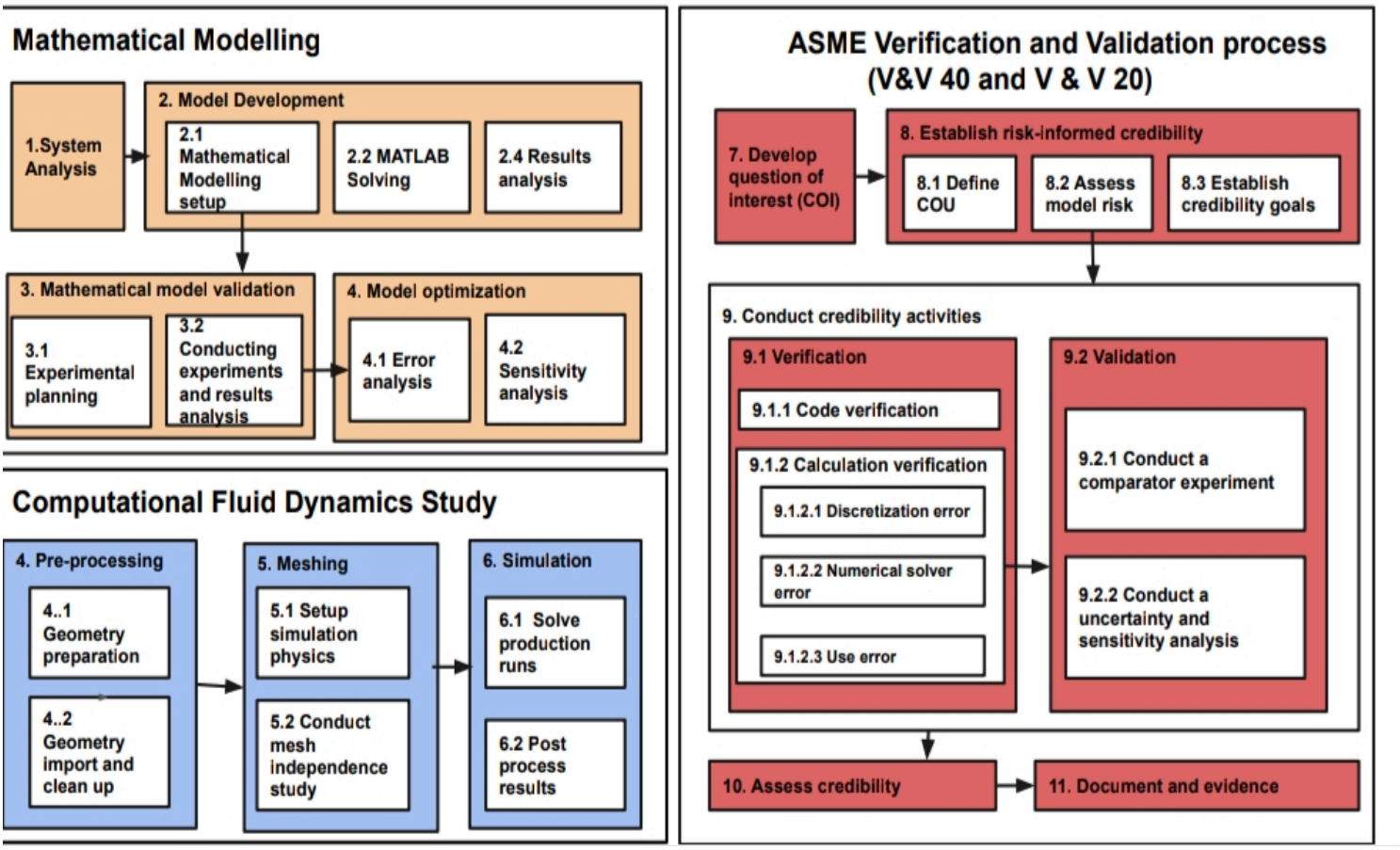

Figure 17: Methodology flow chart

2.2 Development And Optimization Of The Mathematical Model

A dynamic model that comprises of a mathematical and CFD model was chosen for this research. The mathematical model is used to explore the kinematic properties associated with a plunger. The model type is ideal to allow for an understanding of how different variables such as plunger force and fluid force interact and how this can be used to predict autoinjector performance. The CFD aims to develop relations between medication viscosity, volume, needle length, needle diameter and fluid flow. This is important in optimizing the performance of any autoinjector. A CFD model is chosen because it allows for the flow phenomena related to the autoinjector to be modelled and studied.

2.2.1 Development Of The Mathematical Model

In spring-driven autoinjector, the compression of the spring forces the plunger into motion. To move, the plunger must overcome the effects of friction and fluid resistance. Newton's second law of motion equates the sum of the forces to the product of the mass and acceleration. This law is applied on the plunger as follows:

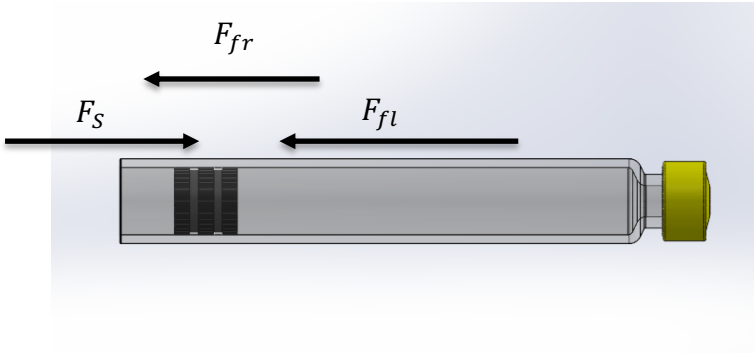

Figure 18:Free-body Diagram Showing Forces Acting on the Plunger

$$\Sigma F = m.a \qquad 2.1$$

$$F_s - F_{fr} - F_{fl} = m_p a_p \qquad 2.2$$

According to the Hooke's Law, the extension of the spring is proportional to the spring force such that:

$$F_s = -kx \qquad 2.3$$

During needle insertion, the spring is preloaded. This changes the spring force to:

$$F_s = -k(x_i - x) \qquad 2.4$$

Static friction can be measured when the plunger is stationary. This is defined as:

$$F_{sf} = \mu_s F_N = \mu_s mg \qquad 2.5$$

When the plunger moves, the friction becomes the sum of the viscous and dynamic friction. The viscous friction is defined as:

$$F_{vf} = \mu_{viscous} \frac{dx}{dt} sgn(x) \quad 2.6$$

Where: $sgn = -1\ when\ x < 0, 0\ when\ x = 0\ and\ 1\ when\ x > 0$

The dynamic friction is defined as:

$$F_{df} = \mu_{dynamic} F_N sgn(x) \quad 2.7$$

Hence, the total frictional force during the plunger motion is:

$$F_{fr} = \mu_{viscous} \frac{dx}{dt} sgn(x) + \mu_{dynamic} F_N sgn(x) \quad 2.8$$

The fluid resistance force is due to the fluid pressure and the pressure losses along the syringe and the needle. Assuming incompressible, Newtonian fluids and laminar flow through a syringe of constant circular cross-section, the fluid force is defined as per Hagen Poiseuille such that:

$$\Delta P = \frac{8\mu L}{4R^4} \frac{dx}{dt} \quad 2.9$$

Kinetic energy in the fluid causes dynamic pressure and the dynamic pressure loss can be describe using the Darcy - Weisbach equation as follows:

$$\Delta P = f_d \frac{L}{D} \frac{\rho v^2}{2} \quad 2.10$$

The inertial pressure terms include the static pressure as a result of gravity and pressure losses due the pressure difference between the inlet and the outlet. This is the difference between atmospheric pressure and the tissue resistance.

$$P_{static} = \rho g h \quad 2.11$$

$$P_{medium-losses} = P_{atm} - P_{tissue} \quad 2.12$$

Combining equation *2.9*, *2.10* and *2.12*. The total pressure is defined as:

$$\frac{dP_{total}}{dt} = \frac{8\mu L}{4R^4} \frac{dx}{dt} + f_d \frac{L}{D} \frac{\rho v^2}{2} + \rho g h + (P_{atm} - P_{tissue}) \quad 2.13$$

Equation *2.13* above is used to calculate the fluid force such that:

$$F_{fluid} = P_{total} A \quad 2.14$$

Using equation the above equations, a system of differential equation were obtained as follows:

$$\frac{dx}{dt} = v \quad 2.15$$

$$\frac{dv}{dt} = \frac{d^2x}{dt^2} = \frac{F_s - F_{fr} - F_{fl}}{m} \quad 2.16$$

$$\frac{dP_{total}}{dt} = \frac{8\mu L}{4R^4} \frac{dx}{dt} + f_d \frac{L}{D} \frac{\rho v^2}{2} + \rho g h + (P_{atm} - P_{tissue}) \quad 2.17$$

These equations were solved using MATLAB.

2.2.2 Model Validation

A validation experiment was conducted using the tensile tester, Testometric x350-5. The fluid delivery system of a reloadable autoinjector was used. This consists of a plunger, a vial, needle and fluid. The apparatus used for this model are:

- High speed camera (Figure 21 below)
- Light sources (Figure 21 below)
- Testometric force machine x350-5 (Figure 21 below)
- Testometric component clamps (Figure 20 below)
- Injector model consisting of a vial, plunger, needle and a holder (Figure 20 below)
- Actuation model consisting of a spring, spring compressor and holder (Figure 19 below)
- Fluid - Water

Figure 19: Actuation Model

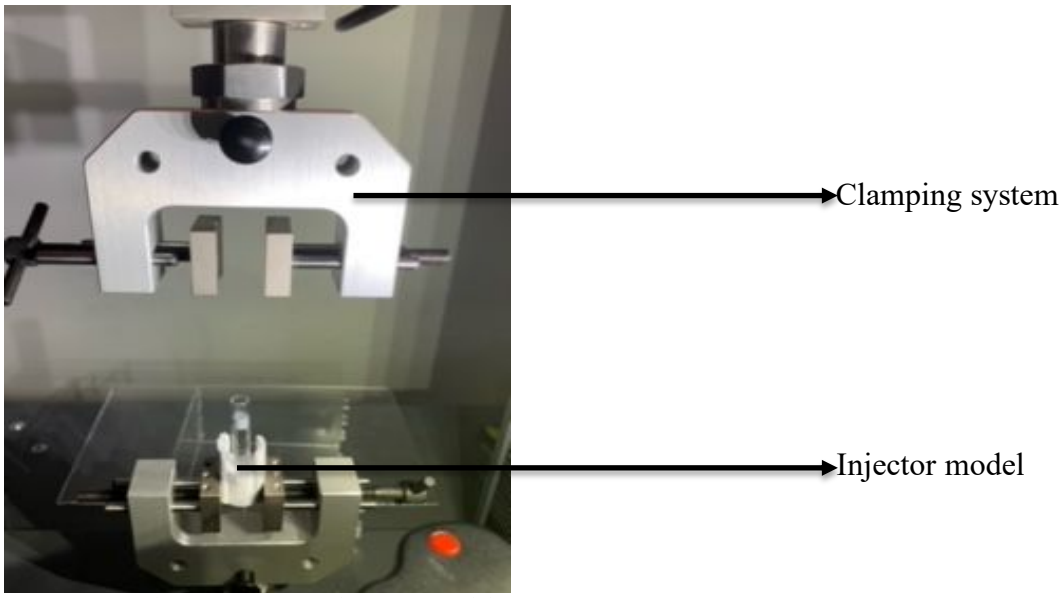

Figure 20: Clamping system and Injector Model

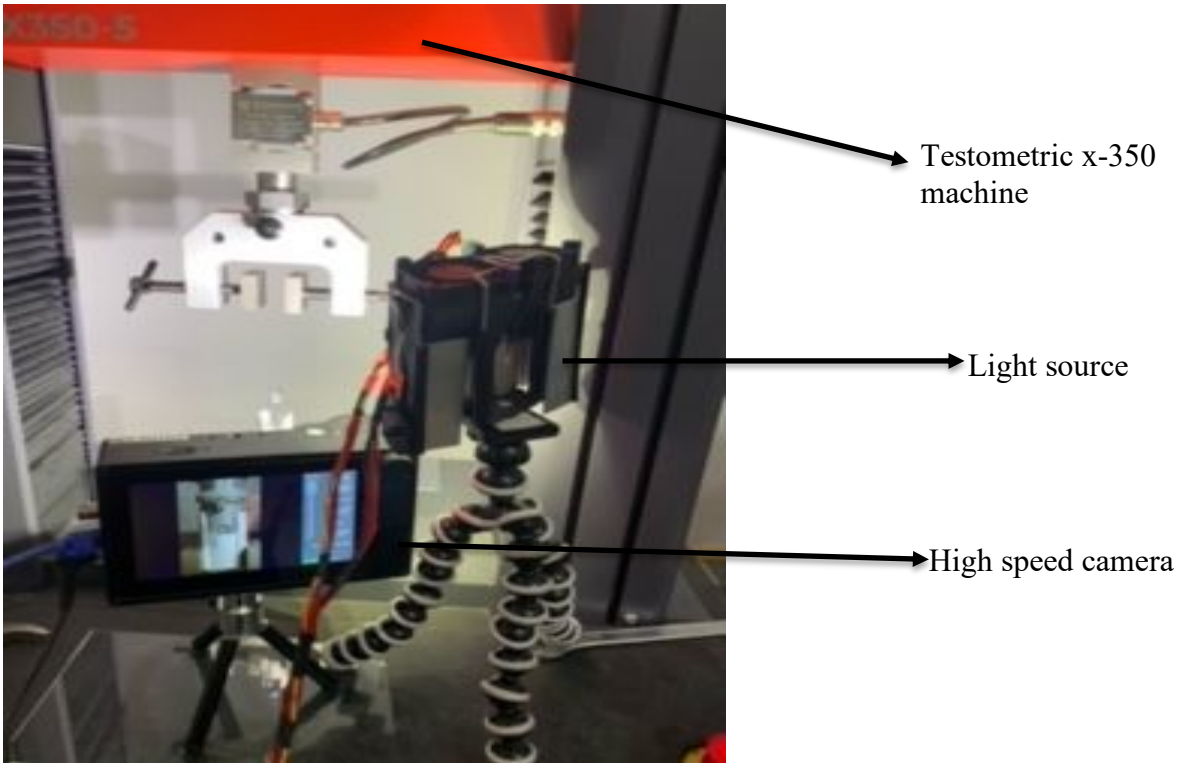

Figure 21: Validation Experiment Setup

The spring properties were verified by conducting a compression test on the Testometric machine to measure the spring force and deflection. The spring deflection and force overtime were plotted in the same set of axes. A sticker with clear graduations was used to correctly read the plunger displacement on the injector model during the experiment. The injector was clamped at the machine's base and positioned visible to the high-speed camera. The actuation components were clamped in the Testometric machine. Once the components were correctly set up, the holding

ring had to be moved to release the spring. The spring would impact the plunger to inject the water out. The camera captured the motion on the plunger. The experiment was repeated twice to ensure that similar measures were taken both times and a 10% margin of error was factored for human error purposes. The recorded plunger displacement results were analysed and used to calculate plunger velocity.

2.2.3 Model Optimization

Mathematical models are calibrated to establish a closer agreement between the model and real system results. Determining how well a model deals with time and randomness promotes good model optimization. The error associated with the mathematical model was determined by comparing model results with validation results. Parameter adjustment and analysis of model outputs formed the two part optimization technique used in this research. A sensitivity analysis was conducted to determine sensitive parameters and parameters that can be adjusted. Parameters were divided into three parts; those related to friction, parameters that include spring force and those that include pressure. Possible assumptions were listed for each group of parameters and system of differential equations were solved for each assumption. The following assumptions were explored:

Friction

Assumption 1: Friction has no effect on the motion of the plunger - $F_{fr} = 0$

Assumption 2: Kinetic friction is negligible - $F_{df} = 0$

Assumption 3: Viscous friction is negligible- $F_{vf} = 0$

Spring and fluid force

Assumption 4: Spring force does not affect the plunger displacement and velocity - $F_s = 0$

Assumption 5: Spring force is constant throughout the plunger motion - $F_s = 20\ N$

Assumption 6: Fluid force does not affect the plunger motion - $F_{fl} = 0$

Assumption 7: Fluid force is constant throughout the plunger motion - $F_{fl} = 60\ N$

Pressure

Assumption 8: There are no viscous pressure losses - $\Delta P = \frac{8\mu L}{4R^4}\frac{dx}{dt} = 0$

Assumption 9: There are no dynamic losses - $\Delta P = f_d \frac{L}{D}\frac{\rho v^2}{2} = 0$

Assumption 10: Static pressure terms can be neglected - $P_{static} = 0$

The results recorded for each assumption were matched with the validation results and the closest match was used to identify parameters to be adjusted. Error was determined between the calibrated and uncalibrated model. The model outputs (plunger displacement, velocity and volume of the fluid injected per unit time) were evaluated using statistical root-mean-square errors (RMSE).

The RMSE was calculated by the equation:

$$RMSE = \sqrt{\frac{\sum_{I=1}^{N}(x_i - \hat{x}_i)^2}{N}} \quad 2.18$$

Where N is the number of observed points, x_i is the actual observed data points, $\hat{x}_i$is the estimated data values and i is the variable.

The performance of the model was then rated as per *Moriasi et.al, 2007* model performance criteria defined in the table below.

Table 1: Model Performance Rating (Moriasi et.al, 2007)

Performance rating	R^2	RMSE
Very good	$0.65 < R^2 < 1$	$0 < RMSE < 0.6$
Good	$0.55 < R^2 < 0.65$	$0.6 < RMSE < 0.7$
Satisfactory	$0.40 < R^2 < 0.55$	$0.7 < RMSE < 0.8$
Unsatisfactory	$R^2 \leq 0.04$	$RMSE > 0.8$

2.3 Computational Fluid Dynamics Model

The CFD study is divided into 4 minor studies. Study A is conducted to analyse the effects of viscosity, Study B is conducted to analyse the effects of needle length, Study C is conducted to analyse the effects of needle diameter and Study D is conducted to analyse the effects of medication volume.

2.3.1 Governing Equations And Discretisation

The governing equations of CFD are the Navier stokes equations. The mass continuity equation in its strongest form is :

$$\frac{\partial \rho}{\partial t} + \nabla \rho u = 0 \quad 2.19$$

Where ρ is the density, t is the time and u is the flow velocity. For an incompressible fluid, the density, ρ = constant and the time derivative, $\frac{\partial \rho}{\partial t} = 0$. Therefore the mass continuity equation becomes:

$$\rho \nabla u = 0 \quad 2.20$$

This is only true if:

$$\nabla . u = \frac{\partial u_x}{\partial x} + \frac{\partial u_y}{\partial y} + \frac{\partial u_z}{\partial z} = 0 \quad 2.21$$

This is the strong form of the mass conservation equation for incompressible fluids. Consider the conservation of momentum equation in the x-direction:

$$\frac{\partial(\rho u_x)}{\partial t} + \nabla(\rho u_x u) + \frac{\partial \rho}{\partial x} - \frac{\partial}{\partial x}\left[2\mu \frac{\partial u_x}{\partial x} + \lambda \nabla u\right] - \frac{\partial}{\partial y}\left[\mu \frac{\partial u_x}{\partial y} + \frac{\partial u_y}{\partial x}\right] - \frac{\partial}{\partial z}\left[\mu \frac{\partial u_x}{\partial z} + \frac{\partial u_z}{\partial x}\right] = \rho g_x \quad 2.22$$

Where, $\frac{\partial(\rho u_x)}{\partial t}$ is the change in velocity with respect to time, $\nabla(\rho u_x u)$ is the convection momentum, $\frac{\partial \rho}{\partial x}$ is the surface force, $\frac{\partial}{\partial x}\left[2\mu \frac{\partial u_x}{\partial x} + \lambda \nabla u\right]$ is the diffusion term in the x-direction, $\frac{\partial}{\partial y}\left[\mu \frac{\partial u_x}{\partial y} + \frac{\partial u_y}{\partial x}\right] - \frac{\partial}{\partial z}$is the diffusion term in the y-direction, $\frac{\partial}{\partial z}\left[\mu \frac{\partial u_x}{\partial z} + \frac{\partial u_z}{\partial x}\right]$ is the diffusion term in the z-direction and ρg_x is the mass force. For incompressible fluids, only the viscous term is relevant as all the other terms depend on volumetric deformation.

The viscous term becomes:

$$\nabla.\tau_x = \mu\left[\frac{\partial^2 u_x}{\partial x^2} + \frac{\partial^2 u_x}{\partial y^2} + \frac{\partial^2 u_x}{\partial z^2}\right] + \mu\left[\frac{\partial^2 u_x}{\partial x^2} + \frac{\partial^2 u_y}{\partial x \partial y} + \frac{\partial^2 u_z}{\partial x \partial z}\right]$$
$$\nabla.\tau_y = \mu\left[\frac{\partial^2 u_y}{\partial x^2} + \frac{\partial^2 u_y}{\partial y^2} + \frac{\partial^2 u_y}{\partial z^2}\right] + \mu\left[\frac{\partial^2 u_x}{\partial x \partial y} + \frac{\partial^2 u_y}{\partial y^2} + \frac{\partial^2 u_z}{\partial y \partial z}\right]$$
$$\nabla.\tau_z = \mu\left[\frac{\partial^2 u_z}{\partial z^2} + \frac{\partial^2 u_z}{\partial y^2} + \frac{\partial^2 u_z}{\partial z^2}\right] + \mu\left[\frac{\partial^2 u_x}{\partial x \partial z} + \frac{\partial^2 u_y}{\partial x \partial y} + \frac{\partial^2 u_z}{\partial z^2}\right] \quad 2.23$$

Assuming that u has a continuous derivative of f, the above equation can be written as:

$$\nabla.\tau_x = \mu\left[\frac{\partial^2 u_x}{\partial x^2} + \frac{\partial^2 u_x}{\partial y^2} + \frac{\partial^2 u_x}{\partial z^2}\right] + \mu\frac{\partial}{\partial x}\left[\frac{\partial u_x}{\partial x} + \frac{\partial u_y}{\partial y} + \frac{\partial u_z}{\partial z}\right]$$
$$\nabla.\tau_y = \mu\left[\frac{\partial^2 u_y}{\partial x^2} + \frac{\partial^2 u_y}{\partial y^2} + \frac{\partial^2 u_y}{\partial z^2}\right] + \mu\frac{\partial}{\partial y}\left[\frac{\partial u_x}{\partial x} + \frac{\partial u_y}{\partial y} + \frac{\partial u_z}{\partial z}\right]$$
$$\nabla.\tau_y = \mu\left[\frac{\partial^2 u_y}{\partial x^2} + \frac{\partial^2 u_y}{\partial y^2} + \frac{\partial^2 u_y}{\partial z^2}\right] + \mu\frac{\partial}{\partial z}\left[\frac{\partial u_x}{\partial x} + \frac{\partial u_y}{\partial y} + \frac{\partial u_z}{\partial z}\right] \quad 2.24$$

The above equation is equal to the sum of the double Laplacian, the $\mu\frac{\partial}{\partial x}$ term and the divergence gradient. So this equation becomes:

$$\nabla.\tau_x = \mu[\nabla.\nabla u_x] + \mu\frac{\partial}{\partial x}[\nabla.u]$$
$$\nabla.\tau_y = \mu\left[\nabla.\nabla u_y\right] + \mu\frac{\partial}{\partial y}[\nabla.u]$$
$$\nabla.\tau_z = \mu[\nabla.\nabla u_z] + \mu\frac{\partial}{\partial z}[\nabla.u] \quad 2.25$$

Applying the constraint for incompressible flow, this becomes:

$$\nabla.\tau_x = \nabla(\mu\nabla u_x)$$
$$\nabla.\tau_y = \nabla\left(\mu\nabla u_y\right)$$
$$\nabla.\tau_z = \nabla(\mu\nabla u_z) \quad 2.26$$

All spatial derivatives should be expressed as divergence as per conservative adjective. The expanded convective term becomes:

$$\nabla.(\rho u_x u) = \rho u_x \nabla.u + \rho u(\nabla u_x) \quad 2.27$$

Since ρ = constant, $\nabla.u = 0$, replacing the viscosity with the viscous term, we get:

$$\frac{\partial(\rho u_x)}{\partial t} + \rho u(\nabla u_x) + \frac{\partial \rho}{\partial x} - \mu\nabla.(\nabla u_x) = \rho g_x$$
$$\frac{\partial(\rho u_y)}{\partial t} + \rho u(\nabla u_y) + \frac{\partial \rho}{\partial y} - \mu\nabla.(\nabla u_y) = \rho g_y$$
$$\frac{\partial(\rho u_z)}{\partial t} + \rho u(\nabla u_z) + \frac{\partial \rho}{\partial z} - \mu\nabla.(\nabla u_z) = \rho g_z \quad 2.28$$

These are the Navier stokes equations for incompressible fluids. It is impossible to solve these equations analytically because a continuous distributions of variables cannot be produced in a solution domain. To solve this challenge, we define discrete solution values for individual points in time and space that cover the entire solution domain. This process is called discretisation.
The finite volume method discretises the solution domain into a finite range of controlled cells. These cells or volumes form a mesh.

Applying the pressure projection method, the Navier stokes equations can be written as:

$$\frac{\partial w}{\partial t} + \nabla(w \times u) + \nabla p - \mu\nabla^2 u = 0 \quad 2.29$$

Where $w = \begin{bmatrix}\rho u_x & \rho u_y & \rho u_z\end{bmatrix}^T = \begin{bmatrix}\rho u_x \\ \rho u_y \\ \rho u_z\end{bmatrix}$

So $w \times u = w.u^T = \begin{bmatrix}\rho u_x \\ \rho u_y \\ \rho u_z\end{bmatrix}\begin{bmatrix}u_x & u_y & u_z\end{bmatrix} = \begin{bmatrix}\rho u_x u_x & \rho u_x u_y & \rho u_x u_z \\ \rho u_y u_x & \rho u_y u_y & \rho u_y u_z \\ \rho u_z u_z & \rho u_z u_y & \rho u_z u_z\end{bmatrix}$

Using the pressure projection, we get:

$$\frac{\partial w}{\partial t} \approx \frac{w^{n+1} - w'}{\Delta t} + \frac{w' - w'}{\Delta t} = -\nabla(w \times u) - \nabla\rho + \mu\nabla^2 u \quad 2.30$$

Where Δt is the time step size, n is the term evaluated at the present time step, $n+1$ is the term evaluated at the subsequent time step.

$$\frac{w' - w^n}{\Delta t} = \frac{\Delta w^*}{\Delta t} = -\nabla(w \times u) + \mu\nabla^2 u \quad 2.31$$

Where $\Delta w^* = w' - w^n$ and setting $-\nabla\rho = \frac{w^{n+1} - w'}{\Delta t}$

Rearranging the equation and replacing $w = pu$,

$$u^{n+1} = u^n - \frac{\Delta t}{p}\nabla\nabla p + \frac{1}{\rho}\nabla(\Delta w^*) \quad 2.32$$

Considering incompressibility, $\nabla u^{n+1} = 0$, we get

$$0 = \nabla u^n - \frac{\Delta t}{\rho}\nabla^2 p + \frac{1}{\rho}\nabla(\Delta w^*) \quad 2.33$$

The discretized differential equations become algebraic equations that can be solved to produce a solution.

2.3.2 System Configuration

The geometry for the fluid delivery system is modelled using Solidworks and implemented in three dimensions. The flow domain is made up of three autoinjector components namely, a:

- Needle
- Vial
- Plunger

This components are shown in Figure 22 below.

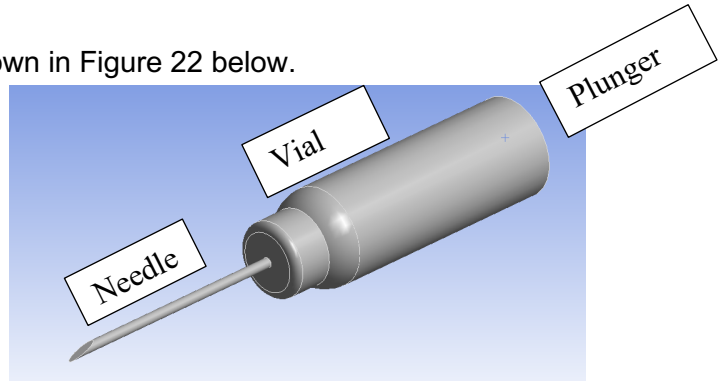

Figure 22: Flow domain for the simulations

The dimension for the flow domain for the four studies are shown below:

Table 2: CFD Study Components Dimension

	Study A	Study B	Study C	Study D
Vial	0.3 ml vial, Diameter = 11.6 mm, Length = 32 mm	0.3 ml vial, Diameter = 11.6 mm, Length = 32 mm	0.3 ml vial, Diameter = 11.6 mm, Length = 32 mm	5 x vials, volume = 0.1 ,0.3, 5, 8 and 10 ml
Needles	25 gauge O.D = 0.514 mm I.D = 0.260 mm Length = 32 mm	6 x 25 gauge needles, O.D = 0.514 mm I.D = 0.260 mm, Length = 16, 18, 20, 25, 30 and 32 mm	5 needles, Size = 14, 16, 20, 25 and 27 gauge, Length = 30 mm	25 gauge, O.D = 0.514 mm I.D = 0.260 mm, needle length = 30 mm
Plunger	Diameter = 11.6 mm, Length = 5 mm	Diameter = 11.6 mm, Length = 5 mm	Diameter = 11.6 mm, Length = 5 mm	Diameter = 12, 11.6, 22 and 24 mm, Length = 5 mm

The dimensions of the vials and needles used were chosen based on commercially available components used for reloadable autoinjectors. To generate the solution, each geometry was uploaded into ANSYS Fluent. Meshing was done using ANSYS meshes. The system properties were then defined.

2.3.3 System Properties

Medications with viscosity 1-20 cP were modelled as incompressible, Newtonian fluid. The density was kept constant at 997 $\frac{kg}{m^3}$. The power law was used to model non-Newtonian fluids with viscosity range 21 – 100 cP. All simulations were conducted under steady state conditions.

2.3.4 System Conditions

The inlet, wall and outlet boundary of the geometry is shown in Figure 23 below. A moving wall is defined as the first boundary. Wall speed corresponds to the plunger speed and is 200 mm/min or 3.33m/s. No slip shear conditions are defined for the wall. The second boundary condition defined at the outlet which corresponds to the needle tip. A pressure of 1333.22 Pa is defined as the outlet pressure. This pressure corresponds to the pressure of the active skeletal muscle, which is 10 mmHg according to *Wheatlet et.al, 2018.*

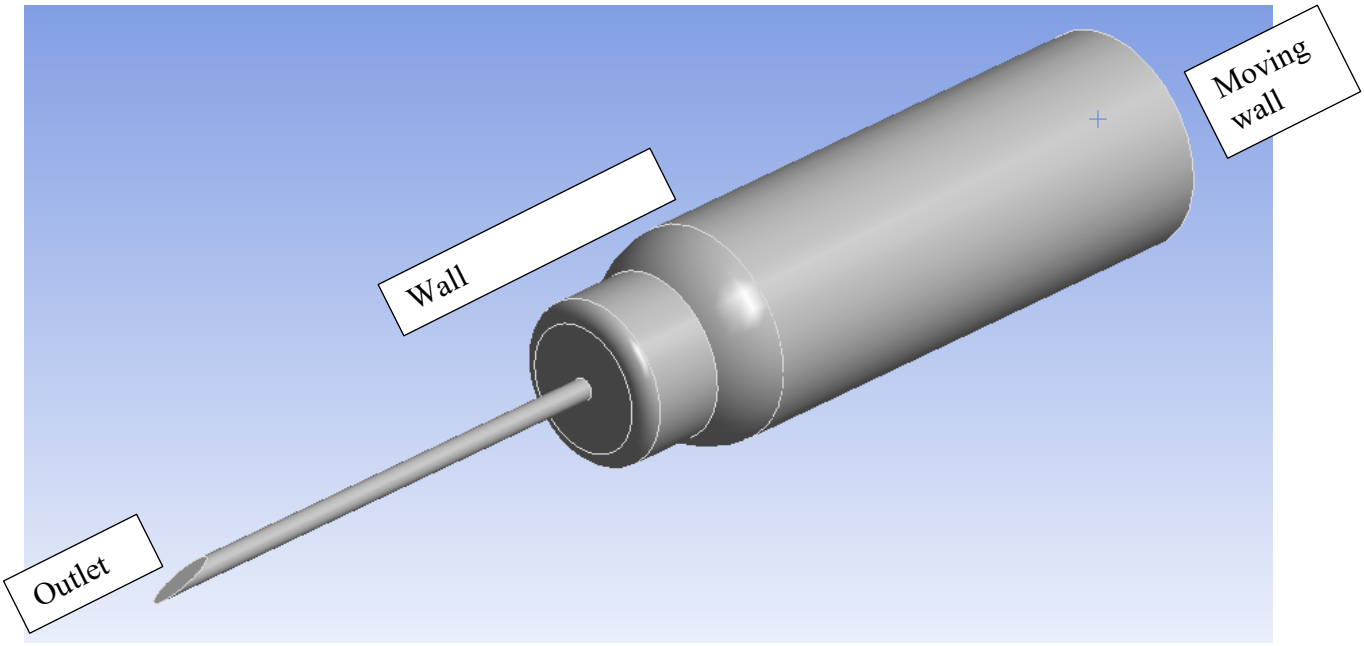

Figure 23: Named selection for the Boundaries of the Geometry

A grid independence study is conducted to define the grid size for each of the geometry configurations and to ensure that the solution is independent of the mesh. The following conditions are assessed to confirm convergence, otherwise the number of iterations are increased:

- The imbalance of the domain must be less than 1%.
- The residual RMS error must reduce to 10^{-6}.
- The pressure and velocity values have reached steady state.

Once the grid size has been defined, the actual simulations are conducted. The computational framework used is ANSYS Workbench 19.2 (ANSYS, Lebanon, NH, USA). Simulations are conducted in Fluent. On ANSYS, the momentum equations are evaluated sequentially. Thereafter, the pressure equation is solved via mass flux and velocity. Convergence criteria is examined and the solution is generated when convergence criteria is met, otherwise steps are

iterated until convergence is reached. Post-processing follows the ANSYS solutions are generated. Post-processing includes reviewing results, confirming convergence of the solution, displaying results in graph and contour plots and assessing viability of results. Post -processing is conducted on CFD – Post.

2.4 Risk-informed Credibility Assessment

The American Society of Mechanical Engineers (ASME),US Food and Drug Administration (FDA) and some medical device companies and software providers collaborated and developed a risk-informed credibility assessment framework called the ASME V&V40. This framework aims to assess credibility of a computational model for a specific context of use (COU) (ASME V&V40, 2018). The risk-informed credibility assessment is conducted in this research to assess the credibility of the developed computational model. The framework is divided into a series of steps, namely:

Step 1: Establish question of interest (QOI)
Step 2: Define the COU
Step 3: Assess model risk
Step 4: Establish credibility activities
Step 5: Assess credibility
Step 6: Documenting results

This frameworks follows an iterative approach that allows for redefining the COU if insufficient credibility is achieved as shown in Figure 24 below. Only once sufficient credibility is achieved, the computational model can be used to make a decisions for the specific COU.

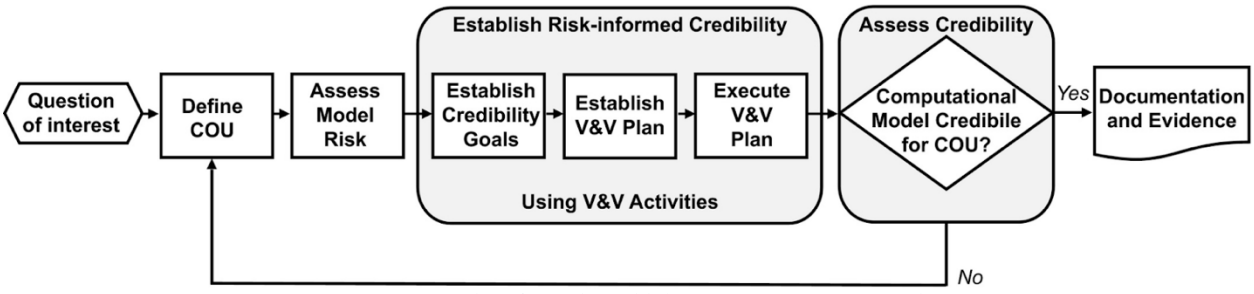

Figure 24: Risk- informed Credibility Assessment Framework

2. 4.1 Define Question Of Interest

The QOI is the specific question or decision to be addressed by the computational model (ASME V&V40, 2018).

2.4.2 Specify Context Of Use

The COU defines the specific scope and role of the computational model used to address a QOI (ASME V&V40, 2018). It is a detailed statement of what will be modelled and how it will be used to inform the QOI. The COU is different from the intended use which describes the use of a

medical device in a clinical setting. COU can be used for technical performance investigation or supporting patient inclusion criteria in a clinical trial (ASME, V&V40). The model risk should be assessed for each COU if multiple COU are defined for a single computational model.

2.4.3 Evaluate Model Risk

The use of a computational model is associated with some risk or undesirable impact. This risk must be meticulously evaluated and communicated to the user beforehand. Model risk is a combination of model influence and decision consequence. Model influence and decision consequence are evaluated individually using a specific degradation scale defined by the relevant organisation. The product of the model influence and decision consequence indicates the model risk as shown in Figure 25 below.

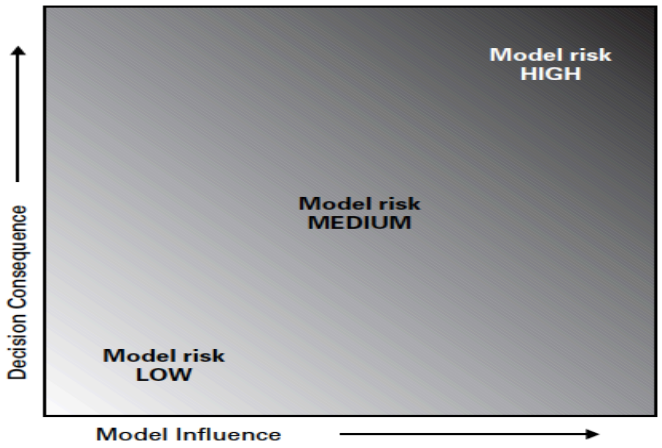

Figure 25: Model Risk Defined As Per ASME Standards

Model influence is the contribution of the computational model relative to other contributing evidence in making a decision (ASME V&V40, 2018). It is defined by a degradation scale representing low to high risk for a specific COU.
The proposed degradation scale for the model influence is:

Table 3: Model Influence Degradation Scale

Model influence	Description
Low	There is none/insufficient evidence provided by the computational model to inform a decision.
Medium	There is moderate evidence provided by the computational model to inform a decision.
High	There is a lot of evidence that the computational model provides to inform a decision.

Decision consequence is the significance of an adverse outcome resulting from an incorrect decision (ASME V&V40, 2018). Decision consequences may be patient-related e.g. harm to the patient or non-patient related e.g. financial loss or delayed of patient access to medical device. The degradation scale used for decision consequence in this research is:

Table 4: Decision Consequence Degradation Scale

Decision consequence	Description
Low	An incorrect decision will adversely result in no or minor malfunctioning of the autoinjector that may be corrected with less effort during device testing.
Medium	An incorrect decision will adversely result in malfunctioning of the autoinjector that may be corrected with moderate effort during device testing.
High	An incorrect decision will adversely result in a malfunctioning of the autoinjector such that it does not serve it intended use. The malfunction cannot be corrected and a complete design change.

2.4.4 Evaluate Credibility

Every computational model is associated with a mathematical model. Verification includes assessing that the relevant mathematical model is executed and applied correctly (ASME V&V40, 2018). Verification encompasses code and calculation verification. Code verification is not evaluated in this research due to the use of commercial software. As part of calculation verification; discretisation, numerical and use error associated with the computational model are determined. Discretization error is conducted to quantify numerical error as a results of spatial or temporal discretisation. It includes analysis of spatial and temporal convergence behaviour of the solution and the refinement of discretisation parameters and solver convergence. Numerical error is characterised by the solver parameters selected. It is related to the numerical solutions and the solver properties. Use error is accredited to the simulations errors due to human error.

2.4.4.1 Verification Activities

The following verification activities are conducted for the computational model:

- Conduct a grid independence or a time step analysis.
- Observe and meet grid independence criteria for all solution.
- Estimate the discretization error.
- Verify inputs and output of the simulation model.

2.4.4.2 Validation Activities

Validation assesses the agreement between the computational model and a real-life system. This includes confirming model accuracy, sensitivity and uncertainty. Model form and model inputs make up the credibility factors of a computational model. They include system conditions,. configuration, properties and governing equations. Model form is the formulation of the

computational model. Model inputs refers to the estimation of the parameters used in the system condition, properties, configuration and governing equations.

The validation activities conducted include:

- Exploring model form assumptions and characterizing their influence.
- Conducting a sensitivity analysis on key performance of model inputs.
- Quantification of uncertainty related to the model input parameters.
- Conducting a comparator experiment.

2.4.4.2.1 Comparator Experiment

The comparator experiment is made of two kinds of tests: Fluid characterisation testing and force testing. Fluid characterisation testing is conducting to categorise medications as either Newtonian or non-Newtonian by measuring the viscosity per shear rate using a rheometer. Force testing is done to measure the force per displacement during the injection process using the ZwickRoell universal tester. Both sets of tests are set up as per the ASME V&V40 and V&V20 standards for assessing credibility of computational fluid model. Medications used for both sets of tests are:

Adrenaline (shown in Figure 26A)

- Pharma-Q adrenaline
- 1 ml vial with adrenaline base as tartrate.
- Injected in the intramuscular layer to manage an anaphylactic shock. It is useful due to its sympathomimetic ability allowing relief of acute allergy, anaphylactic shock, bronchial spasm and cardiovascular resuscitation.

Basalgar (shown in Figure 26B)

- A solution of insulin glargine (modified insulin with similar properties with human insulin).
- The solution contain 100 units/ml of insulin and is injected in the subcutaneous layer.
- It is prescribed to adults patients with type 1 or 2 diabetes or children older than 12 years with type 1 diabetes.

Amikacin (shown in Figure 26C)

- A vial of amikacin contains a 2 ml solution with 12.88 mg of sodium.
- It is an aminoglycoside antibiotic used against multiple gram-negative organisms e.g. Escherichia coli, klebsiella and salmonella etc.
- It is given intramuscularly or intravenously to patients with infections caused by gram-negative organisms e.g. bacterial septicaemia, respiratory trach infections or intra-abdominal infections etc.

Vaxigrip (shown in Figure 26D)

- Tetra-prefilled syringe containing a 3 ml vaccine.
- The vaccine protects kids (6 months and older) against influenza virus haemagglutinin.
- It is injected in the intramuscular layer, usually in the thigh.

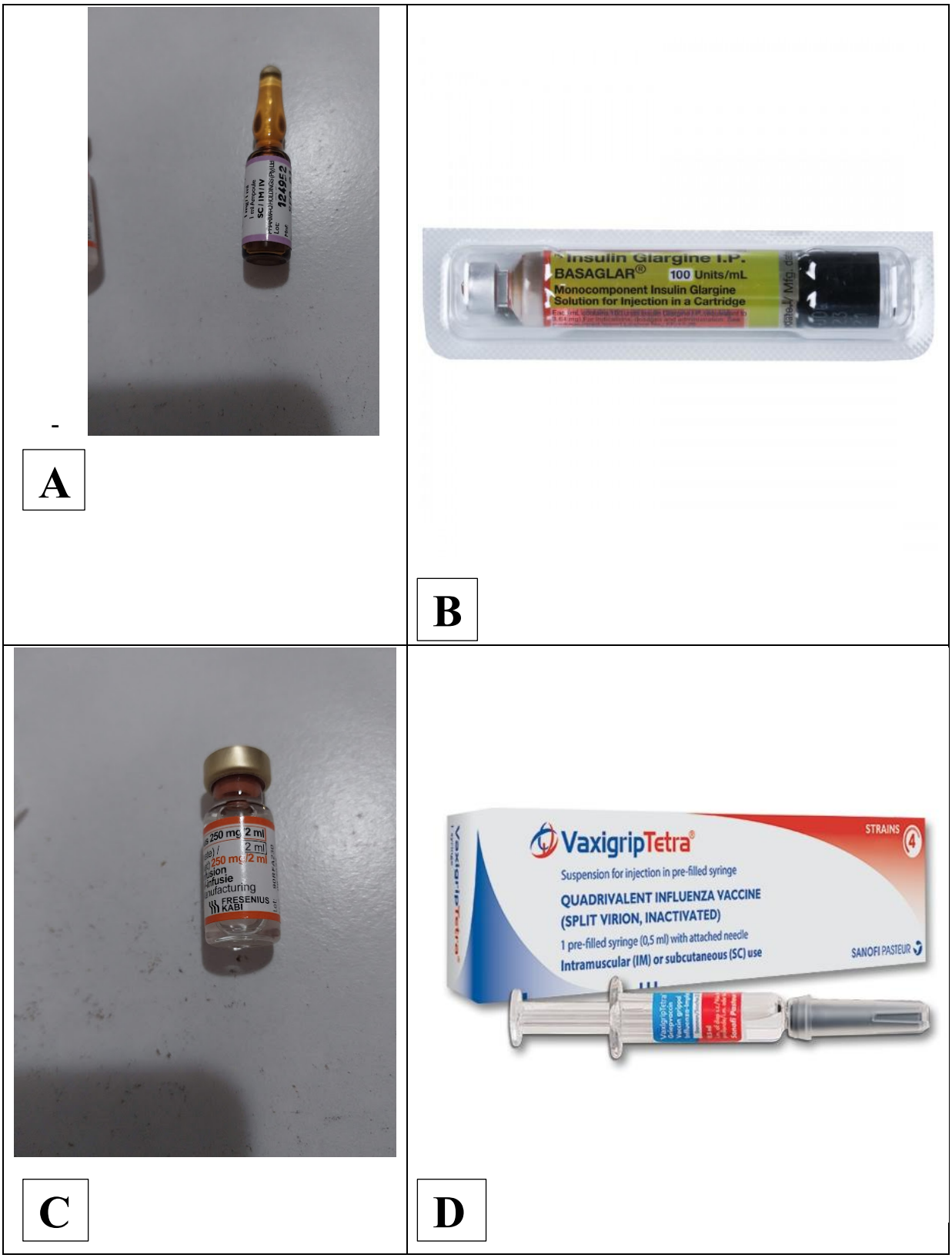

Figure 26: Medications used for Validation Testing. A: Pharma Q-Adrenaline, B: Basalgar, C: Amikacin and D: Vaxigrip Tetra.

A) Fluid Characterisation Testing

Aim: To characterise medication as Newtonian or non-Newtonian.

Apparatus

- Hybrid Rheometer HR-2 (Maximum torque: 200 mN.m, Maximum angular velocity: 300 rad/s) shown in Figure 27 below.
- Samples (Insulin, Adrenaline, Amikacin, Vaxigrip)

Figure 27: Fluid Characterisation Set-up with the hybrid rheometer hr-2

Methodology

The rheometer is connected to the computer with the data capturing software. Drops of medication are poured into the Peltier plate. The gap between the Peltier plate and the geometry is set to 0.15 mm. The geometry is rotated at a set speed to determine the shear rate. The shear rate is calculated as follows: $\dot{\gamma} = \frac{n}{x_{gap}}$, where $\dot{\gamma}$ is the Shear rate, n is the speed and x_{gap} represents the gap distance. Thereafter the viscosity is determined using the shear stress and rate such that: $\mu = \frac{\tau}{\dot{\gamma}}$, where μ is the Viscosity, τ is the shear stress and $\dot{\gamma}$ represents the shear rate. The lab temperature is controlled and kept at room temperature at all times. Viscosity measures are repeated 3 times for each medication to ensure consistency in measurements.

Results are generated and used to plot viscosity vs shear rate curves. A 5% margin of error was factored to account for human error.

b) Force Testing

Aim: This experiment aims to validate the computational model by comparing the dynamic pressure of the results calculated as per experiment and those captured by the computational model. This experiment is further used to analyse sensitivity of medication fluid behaviour to variations in component dimensions, and how this affects general autoinjector performance.

Apparatus

- Zwick universal tester (Speed range:0.00001 to 2000mm/min, Force capacity: 5 kN) shown in Figure 28 below.
- Syringe support rig
- Medications (Insulin, Adrenaline, Amikacin, Vaxigrip)
- Syringes x 4 sizes (1ml, 2 ml, 5ml, 10 ml)
- Needle gauges x 6 sizes (18, 21,22,23 and 26 gauge)

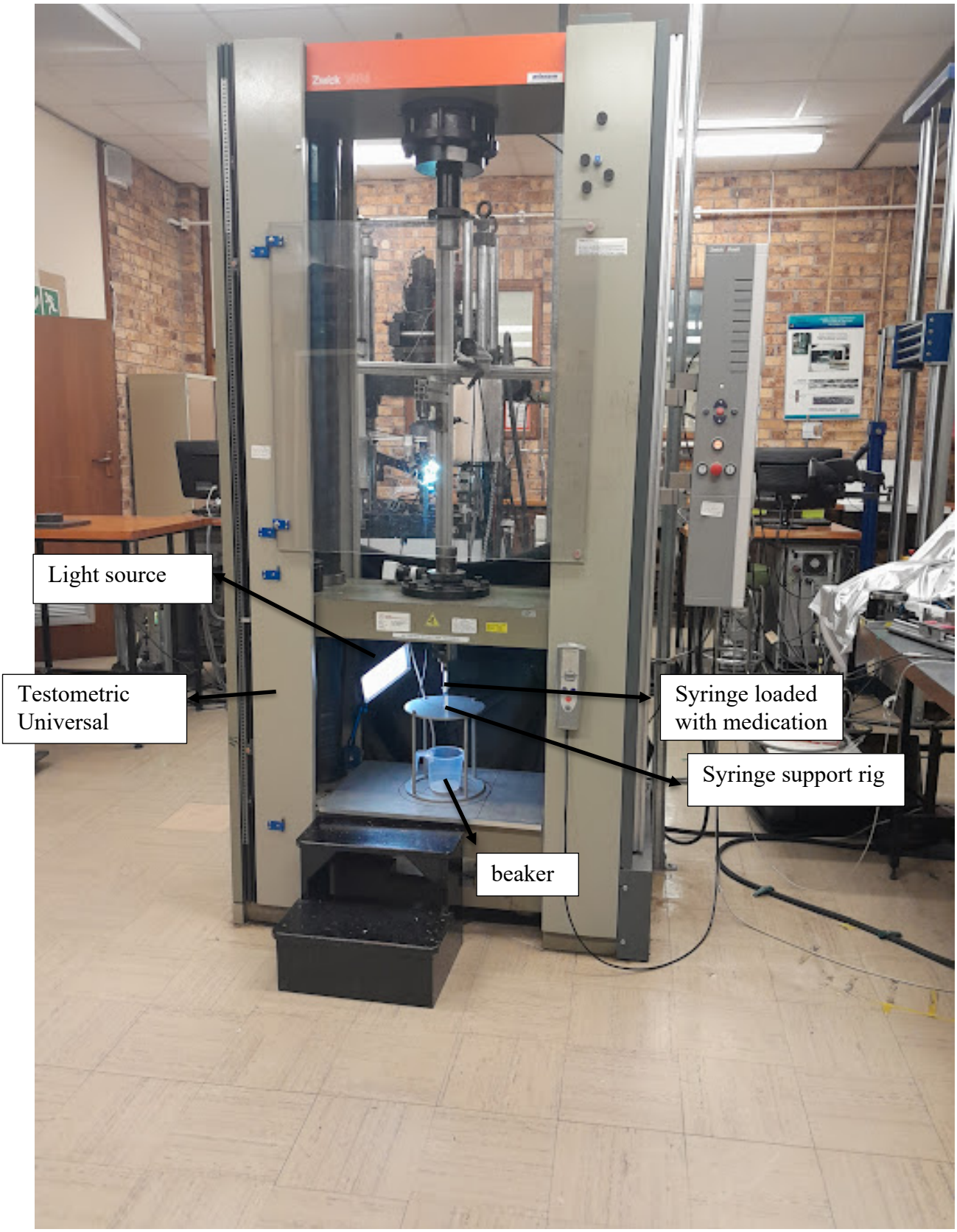

Figure 28: Force testing setup with the ZwickRoell Universal Tester

Methodology

The syringe support rig was designed on Solidworks and machined from aluminium foil. The rig setup is shown in Figure 29 below. Four plates were used for the different syringes diameters.

Figure 29: Force testing setup Showing Syringe, beaker and Syringe Support Rig

To set up for testing, the ZwickRoell universal tester was connected to the data capturing software. The rig was place at the base of the ZwickRoell. A beaker was then placed at the rig;s based and used to collect all injected medications. Different needles and syringe combinations were connected and different medication were drawn into the syringes. Syringe containing medication is placed concentric into the support rig plate directly below the ZwickRoell plunger. The ZwickRoell was set to compress a distance of 40 mm at a speed of 200 mm/min. The outlet pressure in the needle tip is atmospheric pressure and is equal to 101,325 Pa. The experiment was repeated to ensure consistency in measurements and a 5% margin of error was factored to account for human error. The force per distance travelled is measured by the machine. This force represent the actuation force and is used to calculate the dynamic pressure as follows:

$$P_{dynamic} = \frac{F_{actuation}}{A} \qquad 2.34$$

The calculated dynamic pressure are compared to the dynamic pressure results captured from the computational model to validate the model.

CHAPTER 3: MATHEMATICAL MODEL

3.1 Introduction

This chapter details the results obtained from the developed mathematical model to describe the motion of the plunger. This motion results from the spring force and initiates the injection process. This mathematical accounts for the effect of the spring force on the plunger and the fluid resistance due to the fluid being injected by an autoinjector. Thereafter, the validation experiment results are presented to compare the model results with a real-life medication delivery system. The optimized model is presented in this chapter and is compared to the pre-optimization model, real-life delivery system and literature.

3.2 Results

3.2.1 Un-optimized Model

A polyisoprenes plunger of mass 0.005g, 20 mm diameter and 10 mm thickness is used in this research. The plunger displacement is shown in Figure 30 below. The results were limited to the first 3 s of the plunger motion as this portion of the rapid injection mainly encompasses plunger motion and minimal fluid motion. An average constant fluid velocity is assumed for this model and this assumption results in minimal error as the model is valid for the first 3 s after actuation. Initially the displacement increase slowly and then rapidly increases after a second until maximum displacement is reached. At 2.5 s, a maximum displacement calculated to be 8 mm is reached. This displacement marks the end of the plunger motion. To determine the injection time, the plunger displacement time must be added to the needle insertion time.

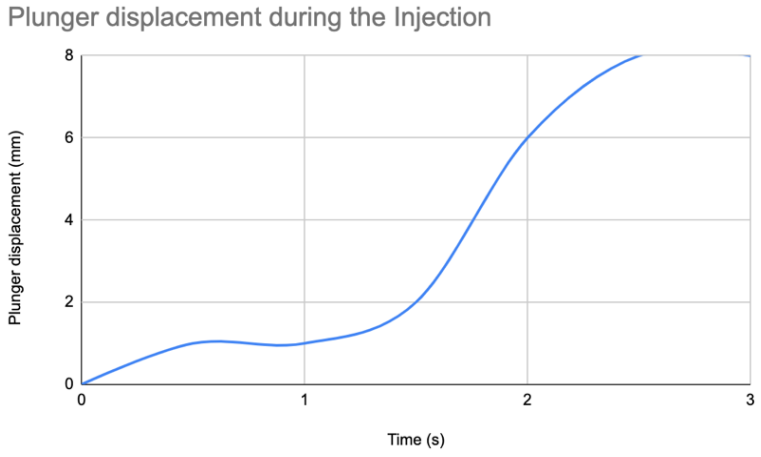

Figure 30: Plunger displacement vs time

The plunger velocity during the injection process is recorded in Figure 31 below. The plunger velocity increases linearly for the first 0.56s of the plunger motion. Thereafter, a constant velocity is produced. This velocity is 0.0078 m/s in the direction of the plunger displacement. A velocity decay was recorded between 0.56 – 1s. The deceleration recorded between 0.56-1s correspond to a displacement decay just before an exponential increase in plunger displacement. The

constant velocity is maintained for the entire motion of the plunger and duration of the injection process. The maximum velocity of the plunger is 0.008 m/s and is recorded at 0.56s.

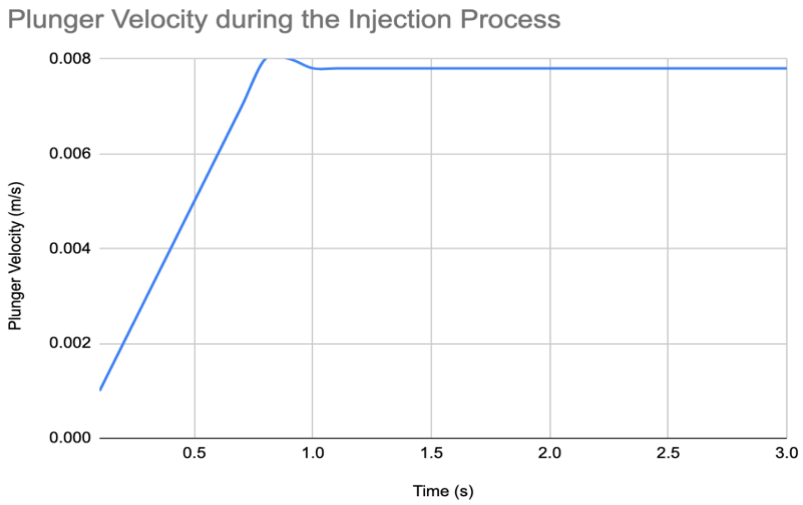

Figure 31: Plunger velocity during the injection process

3.2.3 Validation Experiment Results

The properties of the spring used for the validation results were confirmed via a spring compression test to determine the relationship between the spring deflection and displacement. The spring versus force deflection curves for the three tests conducted are shown in Figure 32 below. The spring force and deflection are directly proportional. This is in line with the Hooke's law. The maximum spring force recorded is 105 N and this corresponds to a maximum displacement of 49.7mm. The spring constant was therefore calculated to be 20 kN/m.

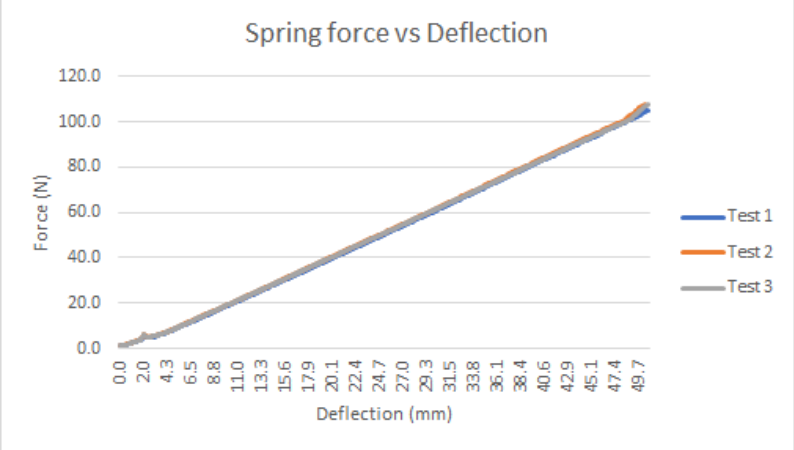

Figure 32: Spring Force vs deflection

The plunger displacement curves for the mathematical model and validation experiment are shown in Figure 33 below. According to the validation results, the plunger displacement increases linearly until maximum displacement is reached. This displacement is 8 mm. It is the same maximum displacement captured in the mathematical model, however was reached sooner in the validation experiment. The plunger displacement and injection process ended at 2s in the

validation experiment. This displacement was reached 0.5s later in the mathematical model. The percentage error between the model and validation results is 34. 2% at a 95% confidence interval.

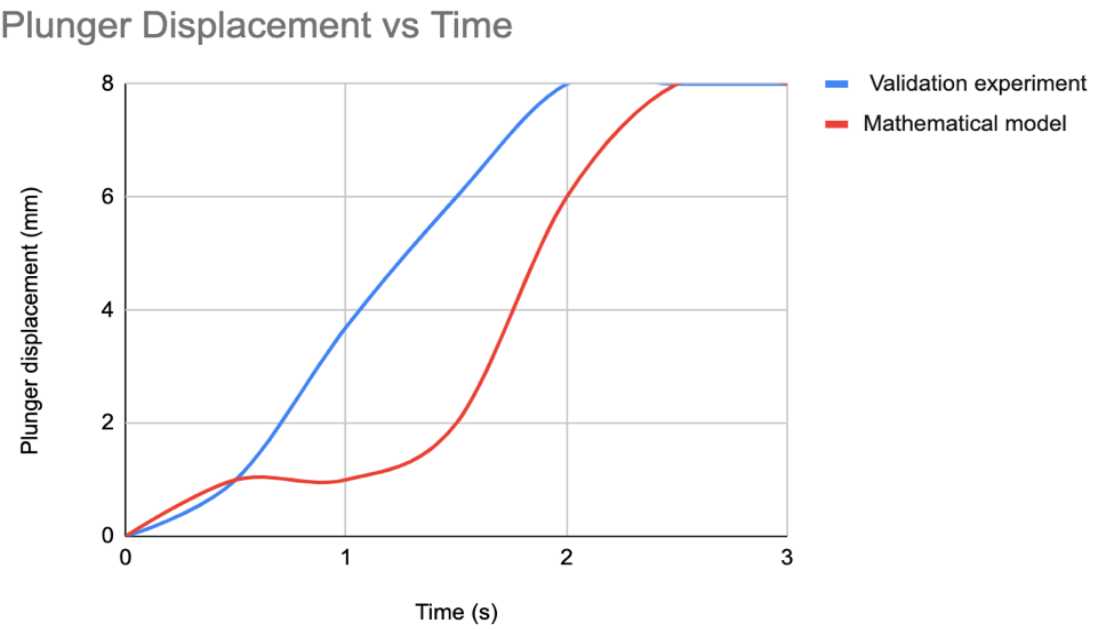

Figure 33: Plunger displacement vs time graph from the mathematical model and validation experiment

The plunger velocity as captured by the mathematical model and validation experiment are shown in Figure 34 below. According to the validation results, the plunger velocity increases linearly for the first 0.6s of the injection process. A maximum velocity of 0.006 m/s is recorded at 0.06s. The velocity dropped by 0.002 m/s and then remained constant for the entire injection process. This constant velocity is 0.005 m/s. The plunger velocity is higher in the mathematical model than it is in the validation experiment from 0.6s until the end of the injection process. Similar trends are observed in the plunger velocity change during the injection process for both the model and experimental results. The statistically significant difference between the two results is the time taken to reach maximum and equilibrium plunger velocity.

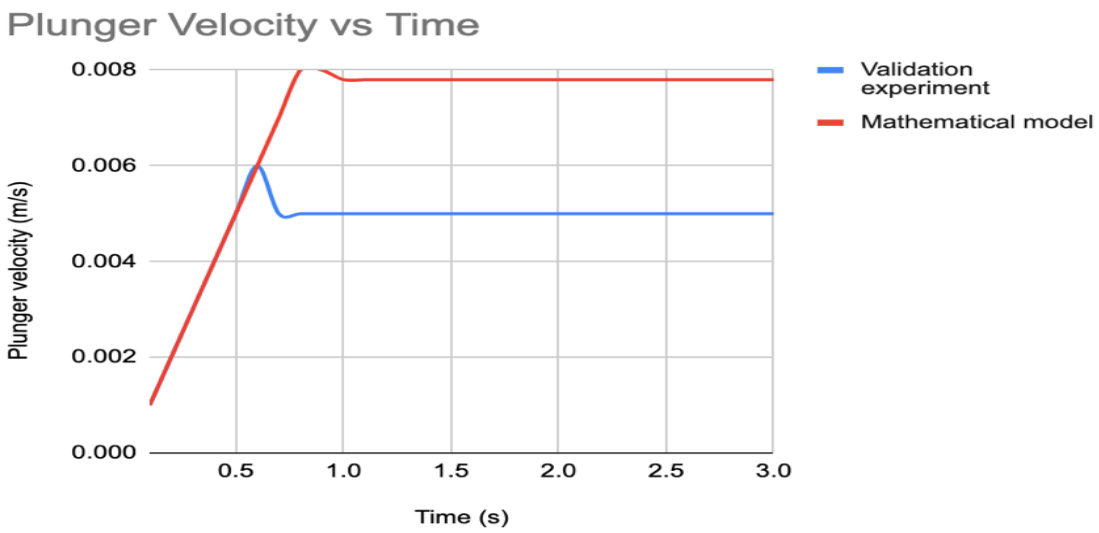

Figure 34: Plunger velocity during the injection process as per mathematical model and per validation experiment.

3.2.4 Sensitivity Analysis

The plunger displacement and friction relationship is analysed and displayed in Figure 35 below. Assuming that there is no friction during the injection process exhibits the largest variation and sensitivity in the model results when compared to the validation results. This assumption depicts an abrupt decrease in the plunger displacement followed by an exponential increase until the plunger comes to a complete stop. The assumption with the closest agreement to the validation results is the absence of kinetic friction. The assumption that leads to results most similar to the mathematical model is the absence of viscous friction. This curves resembles the experiment results, but is displaced in time and hence leading to high error. The correlation between the plunger displacement validation results and the results under the assumption of no friction, no viscous friction and no kinetic friction is 25%, 50% and 62,5% namely.

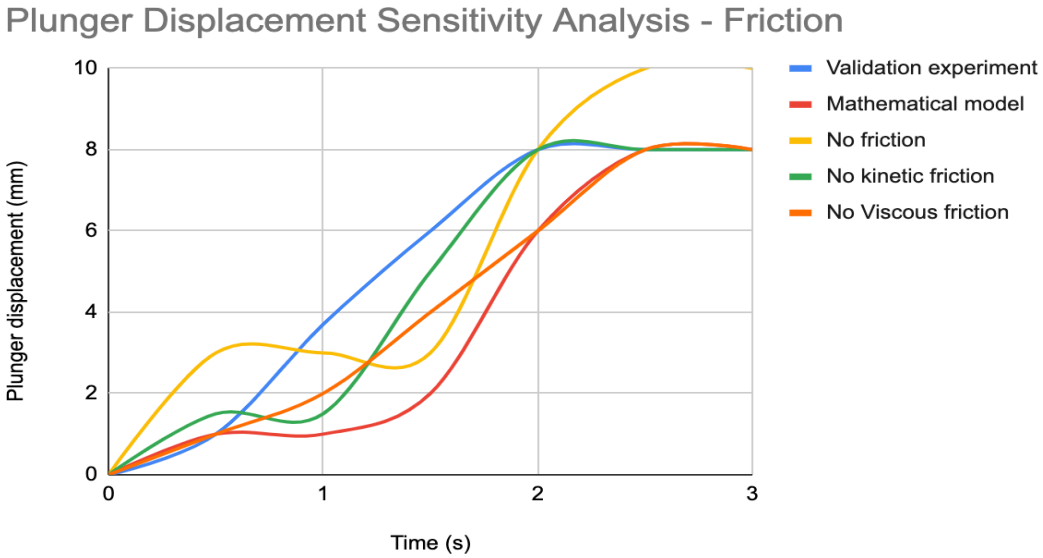

Figure 35: Plunger Displacement vs Time Under Assumptions Involving Friction

The correlation in the plunger displacement results under assumptions related to spring and fluid forces is shown in Figure 36 below. Assuming the absence of spring force results in minimal plunger displacement and assuming a constant fluid force results in a non-linear increase in the plunger displacement followed by a displacement decrease. At 2 s a peak plunger displacement of 8 mm is reached. The decrease in displacement is observed immediately after the peak displacement. The highest increase in the plunger displacement is captured under the assumptions of negligible fluid force. None of the used assumptions results in a strong correlation between the model and validation experiment results.

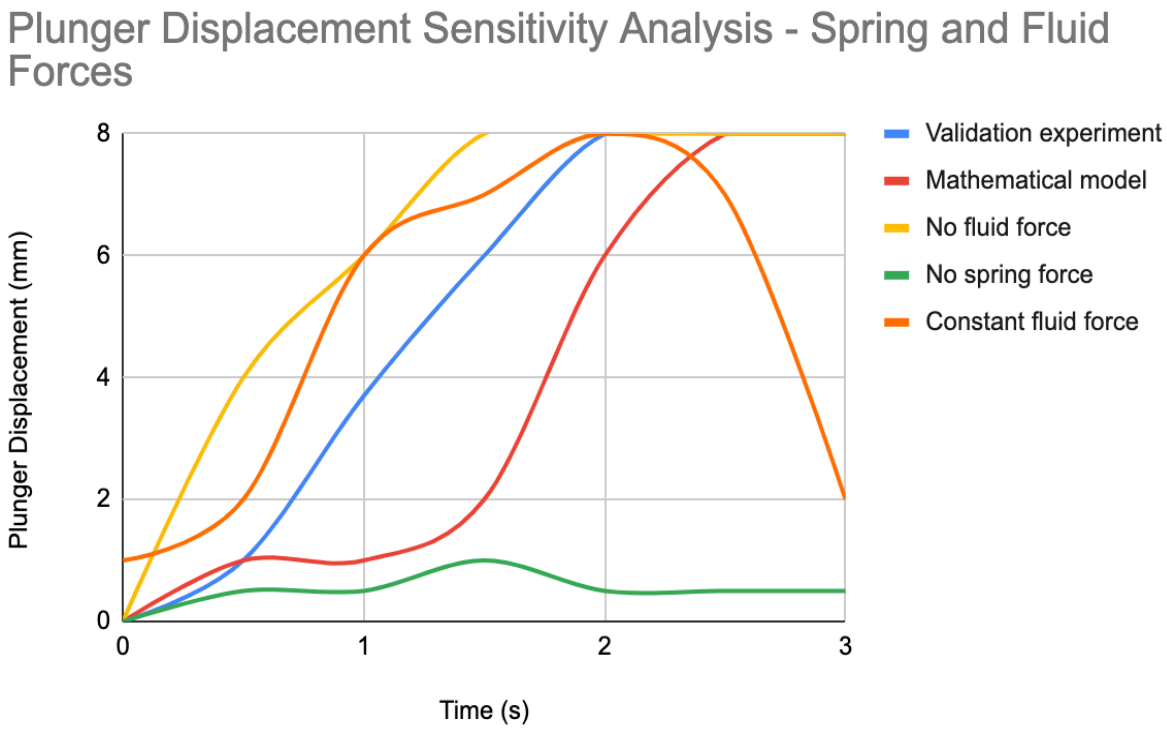

Figure 36: Plunger Displacement For the Mathematical Model under Assumptions Related To Spring and Fluid Forces

The plunger displacement model curves under fluid pressure assumptions are shown in Figure 37 below. All the observed results depicts a slow plunger motion when compared to the validation model. Assuming negligible static pressure results in zero plunger velocity followed by an increased plunger velocity after 1.5s. The maximum plunger velocity recorded in this curve is 0.002 m/s. Neglecting dynamic and viscous fluid pressure results in curves that exhibit similar trends to those observed in the validation experiment. An increase in plunger displacement characterises these trends until a peak displacement is reached. Thereafter, the plunger comes to a constant stop. The peak plunger displacements are 8, 8 and 6 mm for the validation experiment, model results under the assumptions of no dynamic pressure and model results under the assumptions of no viscous friction. The peak displacement is reached earlier in the validation experiment. The peak displacement is reached at 2.4 s in the mathematical model

under the assumption of no dynamic friction and at 2.6s under the assumptions of negligible viscous pressure.

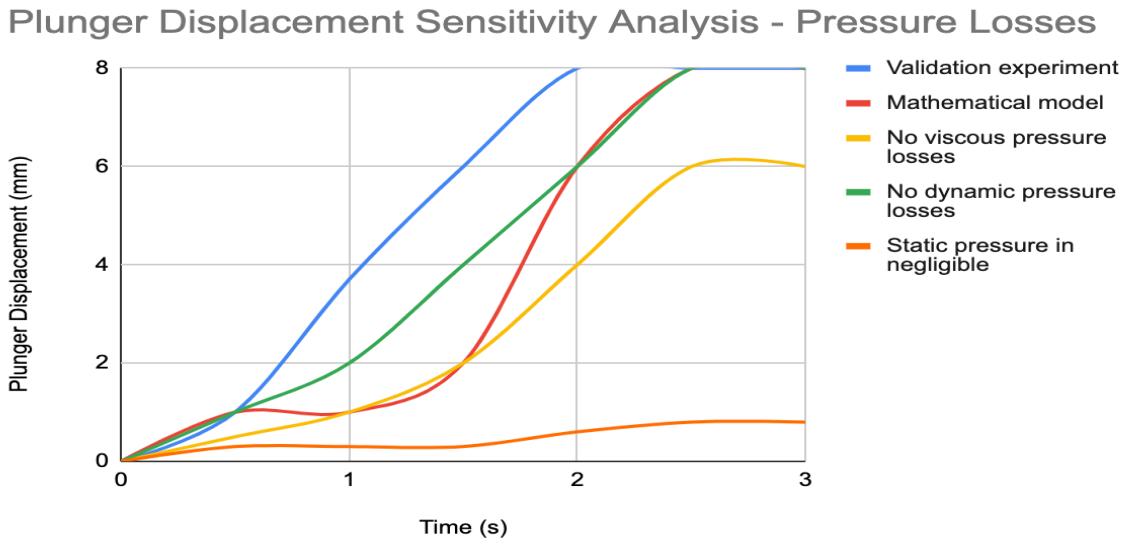

Figure 37: Plunger Displacement Results under Assumptions Involving Pressure

The plunger velocity results under the assumptions related to friction is shown in Figure 38 below. All the results observed in the mathematical under the different assumptions related to friction exhibit plunger velocity lower than that recorded in the validation experiment. The strongest correlation in the plunger velocity results is observed between the validation experiment and the model results under the assumption of negligible kinetic friction. Another strong correlation is observed between the mathematical model under assumptions of negligible friction and the un-optimised mathematical model. The most substantial variation and sensitivity is observed in the mathematical model under the assumptions of no viscous friction.

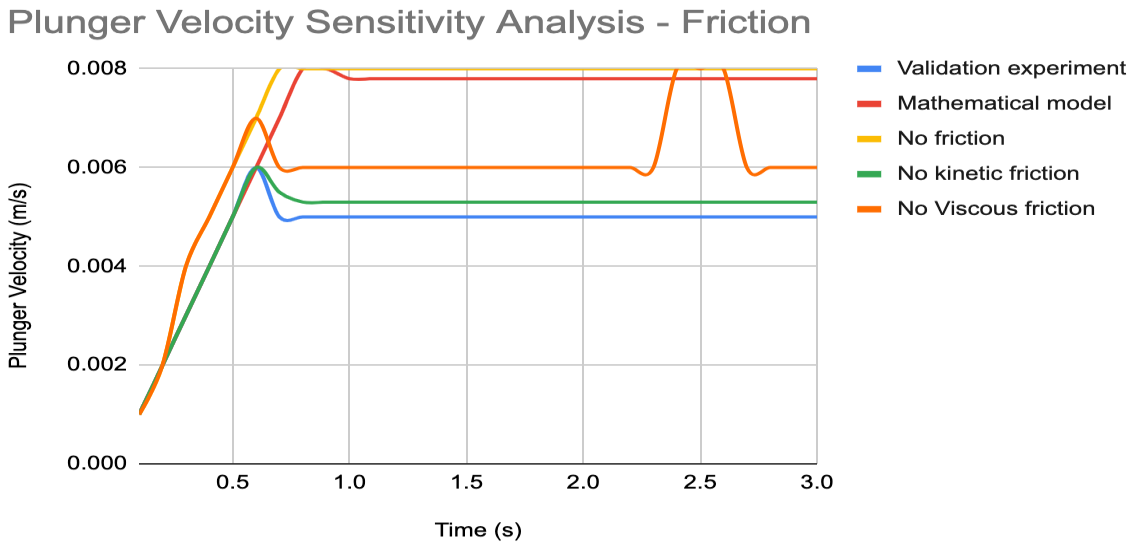

Figure 38:Plunger Velocity Results under Assumptions Involving Friction

The plunger velocity results under assumptions related to fluid and spring forces are shown in Figure 39 below. Assuming negligible spring force results in the lowest plunger velocity. This curve shows constant velocity throughout the injection process with a small deviation between 1.50 - 1.54 s. Assuming negligible fluid force results in an increase in plunger velocity until a peak velocity of 0.003 m/s is reached. A constant velocity is maintained thereafter until 1.51 s. The period between 1.51 - 1.54 s is characterised by an abrupt velocity decrease. Thereafter, a constant velocity of 0.002 m/s is maintained for the duration of the plunger motion. All the other curves under this category exhibit similar trends to the validation results.

Assuming constant fluid force results in a steeper velocity increase. The peak velocity calculated for this assumption is 0.003 m/s and is recorded at 0.35 s. A constant velocity is maintained thereafter for the duration of the plunger motion. Neglecting viscous pressure losses results in 66% difference between the validation and model results.

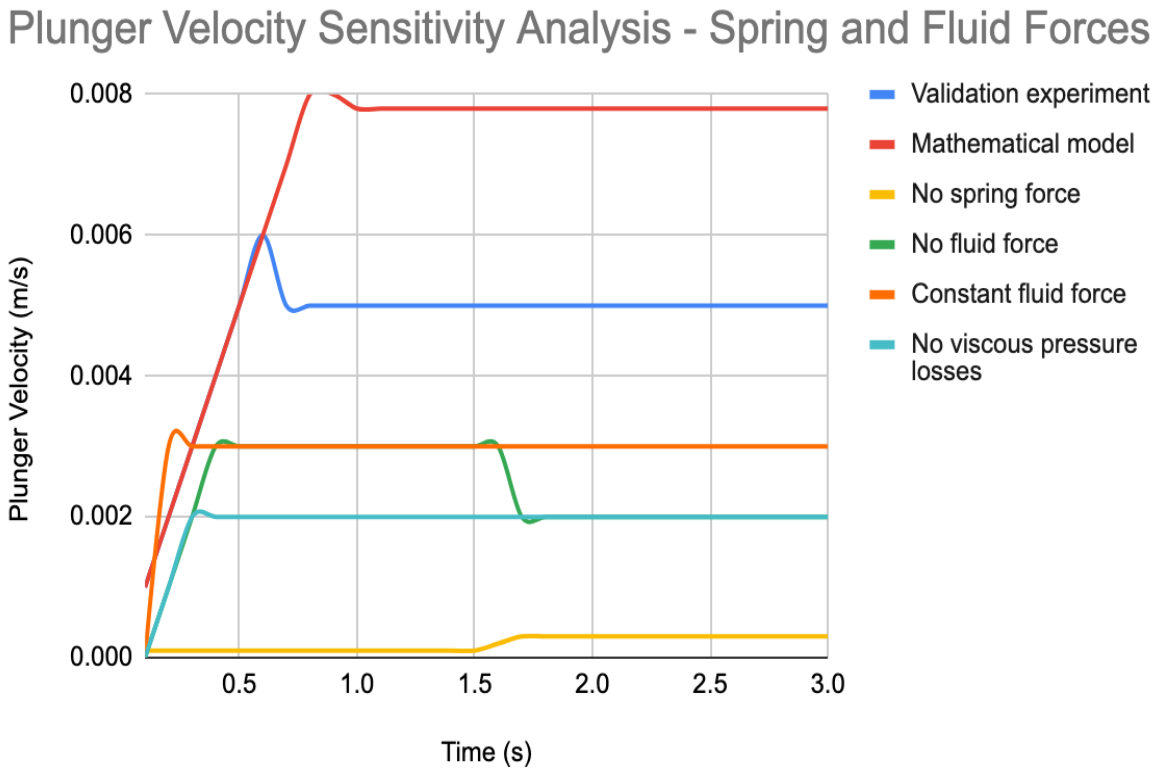

Figure 39: Plunger Velocity Results under Assumptions Involving Spring and Fluid Forces

The plunger velocity under the assumption related to pressure is shown in Figure 40 below. The most variable and sensitive plunger velocity results are recorded under the assumption of negligible static pressure. This curve exhibit a linear increase in plunger velocity until maximum velocity of 0.006 m/s is reached. The plunger velocity is unstable between 0.55 s to 1.1 s. Thereafter, a constant velocity of the 0.002 m/s is maintained for the duration of the plunger

motion recorded. The same constant velocity is reached under the assumption of negligible dynamic pressure, however this is reached 0.5 s earlier then negligible static pressure. Assuming no dynamic pressure losses results in lower plunger velocity peaking at 0.003 m/s.

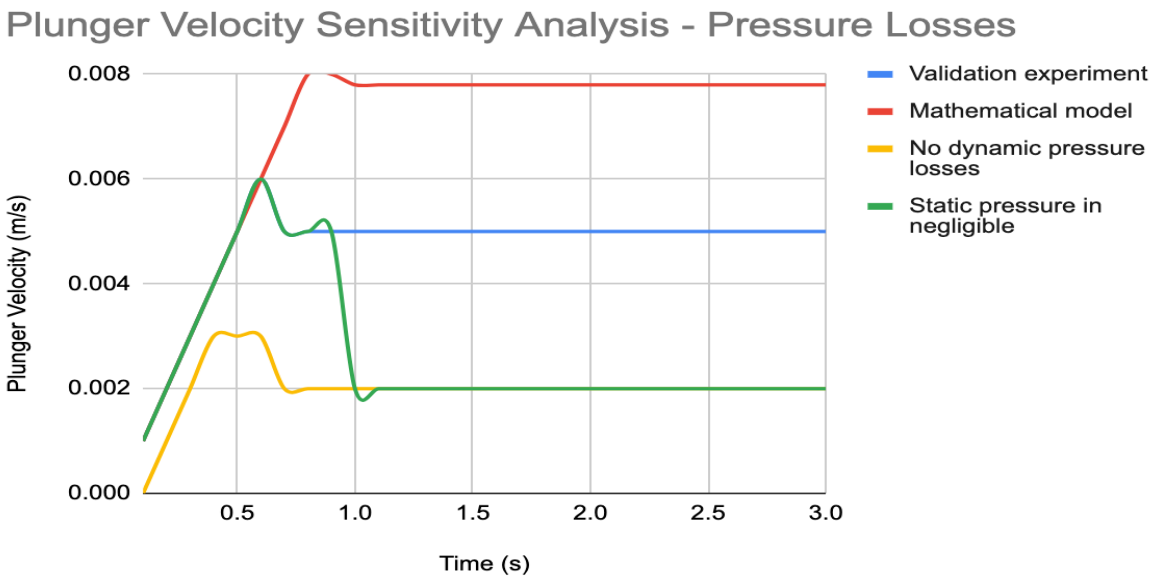

Figure 40: Plunger Velocity vs Time Under the Assumptions Related to Fluid Pressure

3.2.5 Optimized Model

To optimize the mathematical model, the pressure in the syringe is redefined using Bernoulli's equation. Under the assumptions of steady state conditions, incompressible flow and negligible viscous friction in the syringe, Bernoulli's equation becomes:

$$P_1 + \frac{1}{2}\rho {v_1}^2 + \rho g h_1 += P_2 + \frac{1}{2}\rho {v_2}^2 + \rho g h_2 + f_d \frac{L_s}{D_s}\frac{\rho {v_2}^2}{2} \qquad 4.1$$

Where P_1, is the pressure at the inlet of the syringe (market point A in Figure 41 below), ρ is the fluid density, $v_1$is the mean fluid velocity at the inlet of the syringe, g is the gravitational acceleration, h_1 is the initial height, P_2, is the pressure at the end of the syringe (marked point B in Figure 41 below), f_d is the frictional coefficient, D_s is the diameter of the syringe and L_s is the length of the syringe.

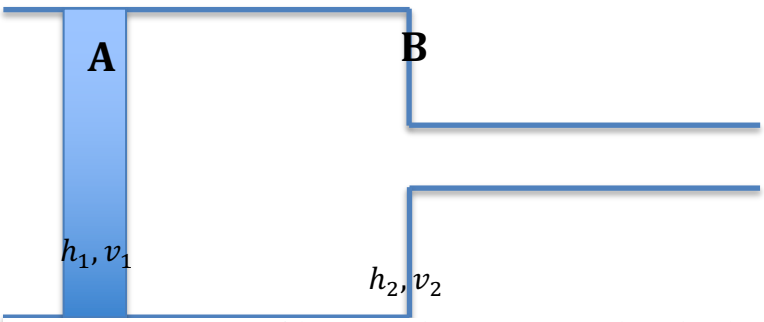

Figure 41: Representation of the Syringe, showing position A where the inlet pressure is measured and B where the outlet pressure is measured.

The pressure in the needle is still defined using the Hagen-Poiseuille equation. The mathematical model terms that were adjusted based on the sensitivity results include the inertial terms of the pressure losses in the plunger and needles, the viscous friction in the plunger and the dynamic pressure loss. The inertial terms and viscous friction are assumed to be negligible. The dynamic pressure losses are now defined for the syringe and needle separately. The dynamic pressure loss in the syringe is coupled in the Bernoulli's equation. The dynamic losses in the needle are defined by the equation *4.2* below, such that:

$$\Delta P = f_d \frac{L_n}{D_n} \frac{\rho {v_2}^2}{2} \qquad 4.3$$

Where $L_n$is the needle length and , D_n is the needle diameter, v_2 is the fluid flow in the needle. After parameter adjustments, the optimized mathematical model is defined as:

$$\frac{dx}{dt} = v$$

$$\frac{dv}{dt} = \frac{d^2x}{dt^2} = \frac{F_s - F_{fr} - F_{fl}}{m}$$

$$\frac{dP_{total}}{dt} = \frac{8\mu L}{4R^4}\frac{dx}{dt} + f_d \frac{L_s}{D_s}\frac{\rho {v_1}^2}{2} + f_d \frac{L_n}{D_n}\frac{\rho {v_2}^2}{2} + \frac{1}{2}\rho {v_1}^2 - \frac{1}{2}\rho {v_2}^2 \qquad 4.4$$

The optimized equations were solved using MATLAB to generate a plunger displacement and velocity graph shown in Figure 42 and 43 below. The post optimization plunger displacement curve exponentially increase until a peak displacement of 8 mm is reached. The displacement remains constant for the duration of the motion recorded. A 8% error at 95% confidence interval was calculated between the optimised model and the validation result.

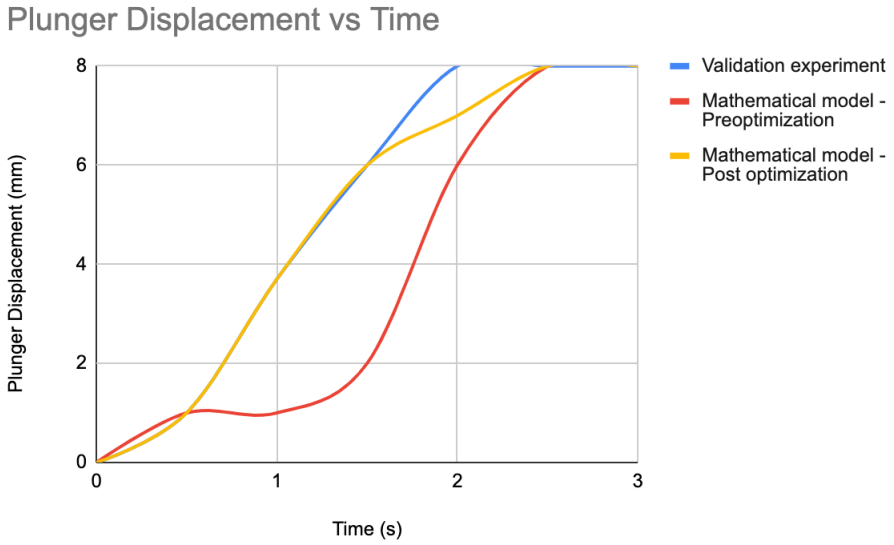

Figure 42: Plunger Displacement vs time Showing Optimized Mathematical Model Results

The plunger velocity is directly proportional to the injection time for the first 0.57s of the plunger motion. Thereafter, a peak velocity of 0.007 m/s is reached. A decrease in plunger velocity is recorded until a velocity of 0.005 m/s is reached and maintained for the duration of the motion recorded. The major difference between the post-calibration results and validation experiment is the peak plunger velocity and the time this velocity is reached. The peak plunger velocity is higher in the post optimisation model and is reached later compared to the validation model.

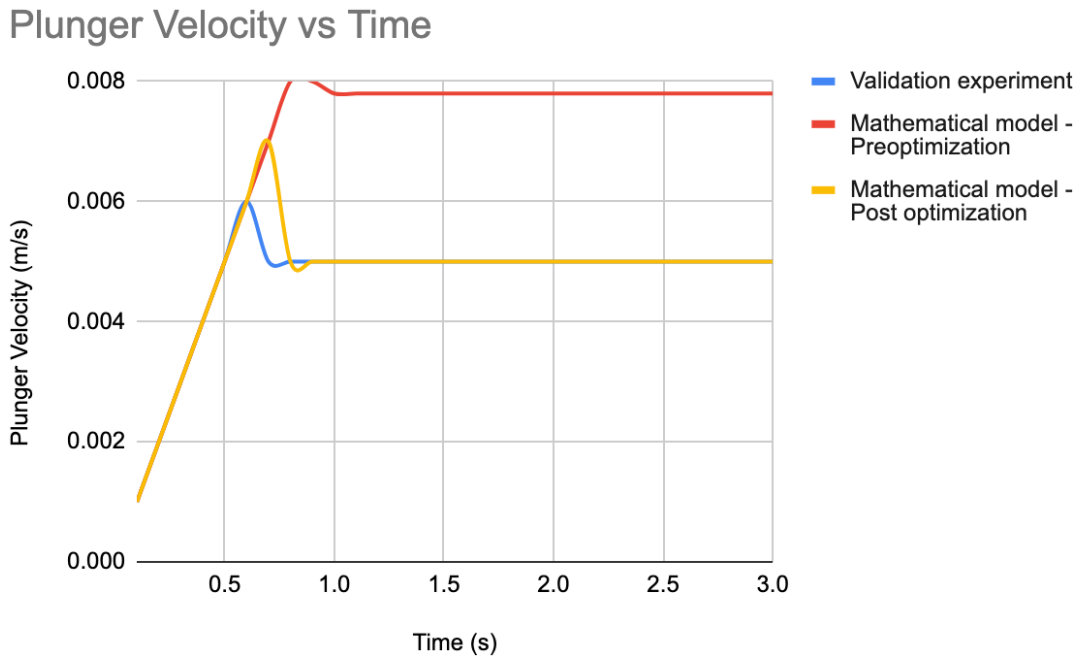

Figure 43: Plunger Velocity vs Time from The Optimized Mathematical Model

3.3 Discussion

The main function of the plunger inside an autoinjector is to move and seal medication. Medication is sealed to prevent premature injections and contamination. Estimating the plunger motion is challenging due to the multiple factors affecting the motion and the complexity of the interaction between these factors. These factors include ambient pressure variations, temperature, syringe volume and tribological factors. The tribological factors are due to the relative motion and friction between the syringe and the plunger during the injection process.

According to the optimised mathematical model and validation results, the plunger displacement increases linearly when the plunger motion is initiated until a maximum displacement is reached. This trend is acceptable because the plunger force is proportional to the spring force and hence if the spring force increases, the plunger force will increase. According to Hooke's law, the spring deflection is directly proportional to the spring force. When an autoinjector is actuated, the spring compression increases. This increases the spring force and hence the plunger force causing the plunger to be displaced. At this stage, there is minimum effects of friction between the syringe and the plunger and the fluid resistance as the fluid is just starting to move. These results align

with recent studies of Wilkins et.al (2012) and Thueer et.al (2018). Wilkins et.al (2012) as quoted in chapter 1.3.2, Figure 2 demonstrates an increase in plunger force as the plunger displacement increases. Thueer et.al (2018) illustrate similar results and is quoted in chapter 1.3.2, Figure 3. When the plunger is released, the plunger force increases to overcome the friction between the syringe barrel and the plunger.

The plunger accelerates until maximum velocity is reached. This is due to the increase in plunger force and dynamic pressure as a result of the moving fluid. The maximum plunger velocity is reached when the force due to the fluid dynamic pressure is equal to the plunger force. After that the fluid resistance force results in a slight plunger velocity decrease followed by a constant velocity maintained for the entire duration of the plunger motion.

The most sensitive results recorded as per the sensitivity analysis were due to the assumption of negligible friction. Without friction, the plunger displacement decreases abruptly and then exponentially increases. The plunger velocity increases rapidly under this assumption. These findings agree with the principles of tribology since in a frictionless surface, the plunger would slide on the syringe barrel. This would create a large variation in the plunger displacement and velocity. Possible resulting scenarios would include breakage of the seal between the plunger and the syringe, regurgitation of the medication or retrograde of the fluid between the plunger and the syringe barrel. Hence, the plunger will have no resistance resulting in large plunger displacement at high velocity. This would be dangerous for patients and clinicians.

In the sensitivity analysis, neglecting viscous friction produced a larger discrepancy between the model and validation results compared to neglecting the kinetic friction. These results demonstrate that the highest friction during the injection process is due of the viscous effects and fluid velocity. This means that viscous friction is higher than the dynamic friction during the plunger motion.

Assuming the absence of spring force results in no plunger displacement. This is as expected since the function of a spring in a spring-actuated autoinjector is to move the plunger and hence the medication. Assuming constant fluid force or zero fluid force are invalid assumptions as the motion of the plunger is bound to impact and move the medication in the syringe. If the medication in the syringe is in motion, the fluid force is present and changing. The fluid force varies due to the variation in the fluid pressure.

Assuming negligible dynamic pressure exhibits the closest results to the validation results because at the beginning of the plunger motion, the fluid starts to move and there is minimum effect of dynamic pressure. The highest pressure at this point is static and viscous pressure. As the fluid start to gain traction, the dynamic pressure increases. The pressure in the syringe increases with the increase in the plunger velocity. The optimised mathematical model is termed a good representation of the plunger motion in an autoinjector since an $RMSE$ of 0,55 was calculated and this represents good model performance as per Moriasi et.al, 2007. This model considers dynamic pressure in both the syringe and needle since pressure is inversely

proportional to the diameter as per the Hagen Poiseuille equation. The dynamic pressure in the needle is higher than the dynamic pressure in the syringe.

The mathematical model promotes the understanding of the force transfer between the spring, plunger and medication to bring about high autoinjector performance. The spring force is required to overcome friction and move the plunger to force the medication into motion. Understanding the motion of the plunger promotes an understanding of the glide and break-loose forces associated with the autoinjector. A slow plunger motion is associated with an increase in glide and break-loose force. This often leads an unacceptable increase in injection time, plunger stalling or lack of accurate medication delivery. Understanding the plunger motion encourages siliconization and choosing the correct plunger for medication delivery. Siliconization increases the glide force required to move the plunger. The correct plunger is important for drug integrity, limiting drug waste and simplifying the administration process.

CHAPTER 4: COMPUTATIONAL FLUID DYNAMICS MODEL

4.1 Results

This chapter details the results captured from the computational fluid dynamics model aimed at interpreting the fluid behaviour of different medications during the injection process. A comprehensive grid independence study was conducted to define the mesh size and ensure that the solutions are independent of the mesh. A total of 75 simulations were conducted post grid independence study. These simulations were divided into four types. Type A evaluating the effect of medication viscosity, Type B evaluates the effects of needle diameter, type C evaluating the effects of needle length and type D evaluates the effects of medication volume. 15 simulations were conducted under type A. In these simulations the viscosity of the medication was varied and defined as either constant or varying according to the Power law. 20 Simulations were conducted for each type, namely type B, C and D. Two main boundary conditions were used ; a moving wall velocity corresponding to the plunger velocity and an outlet pressure corresponding to the pressure in the injection site. The dynamic pressure, total pressure and wall shear stress results were therefore captured using CFD post.

4. 1.1 Grid Independence Study

A grid independence study is conducted to define the correct mesh size for the fluid domain. This study was conducted through running simulations at different mesh sizes and capturing the element size and resulting dynamic pressure. 15 geometry combinations were used in conducting the study. The mesh size range used was $5 \times 10^{-8} - 5 \times 10^{-2}\ mm$. Figure 44 below shows the grid independence results for the different geometries. The average relative errors, based on the pressure results for the geometry configurations was calculated to be 0.0474%. The configuration with the largest vial (10 ml) took longer to reach convergence and yielded the highest pressure at a larger element size. For this configuration the smaller relative error was generated at a mesh size of 0.0005 mm with 49879 elements. Convergence was reached quicker at a smaller element size for a 0.3ml vial with a 27 gauge needle. For this configuration, the smallest relative error was produced at a mesh size of 0.05 mm with 230 elements. The convergence criteria were carefully monitored with rms residuals kept at 1×10^{-5} rms. The mesh size with the smallest relative error for most of the geometry configurations (8/15) was 0.005 mm. A tetrahedral mesh generated at this mesh size is shown in Figure 45 below. The remaining configurations were generated at a mesh size of 0.05 mm.

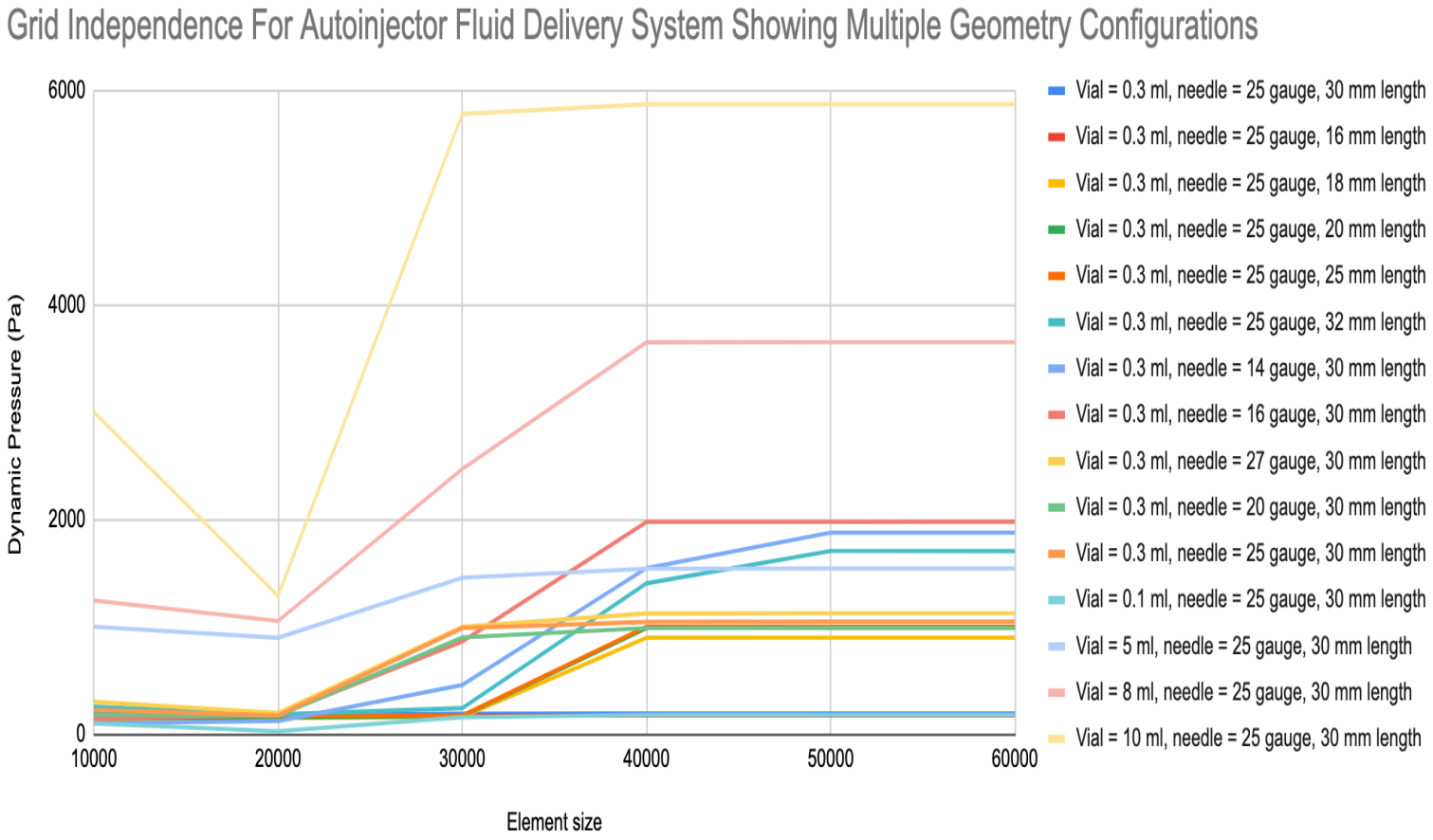

Figure 44: Grid Independence Study Dynamic Pressure vs Elements Size for Different Geometry Configurations

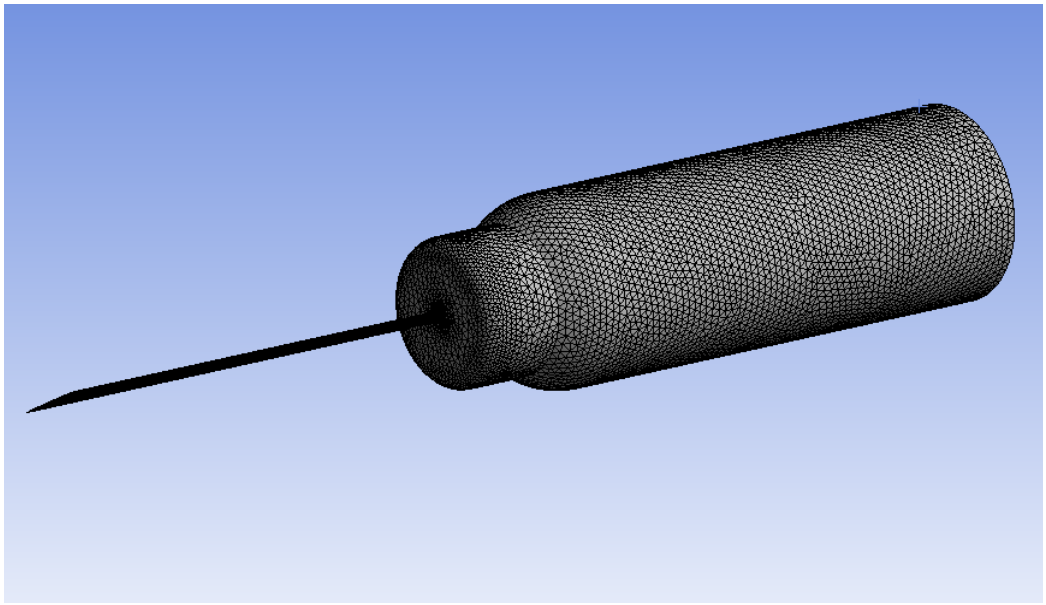

Figure 45: Mesh Generated at 0.005 Mesh Size for a 0.3 ml vial with a 20 Gauge Needle

4.1.2 Simulation Type A: Viscosity

10 Simulations were conducted by varying the viscosity of the injected medication and studying the resulting pressure and wall shear stress. Figure 46 below shows the dynamic pressure vs viscosity curve produced. Fluid dynamic pressure increases rapidly as viscosity increases. This increase is higher for fluids with viscosity less than 10 cP. The dynamic pressure captured for a fluid with viscosity 1 cP and 10 cP is 815 Pa and 2840 Pa respectively. At viscosities between 20 – 60 cP, steady increase in Dynamic pressure is observed. This region is marked by a dynamic pressure of 3500 Pa at 20 cP and 4445 Pa at 60 cP. For viscosities above 60 cP, dynamic pressure begins to stabilise.

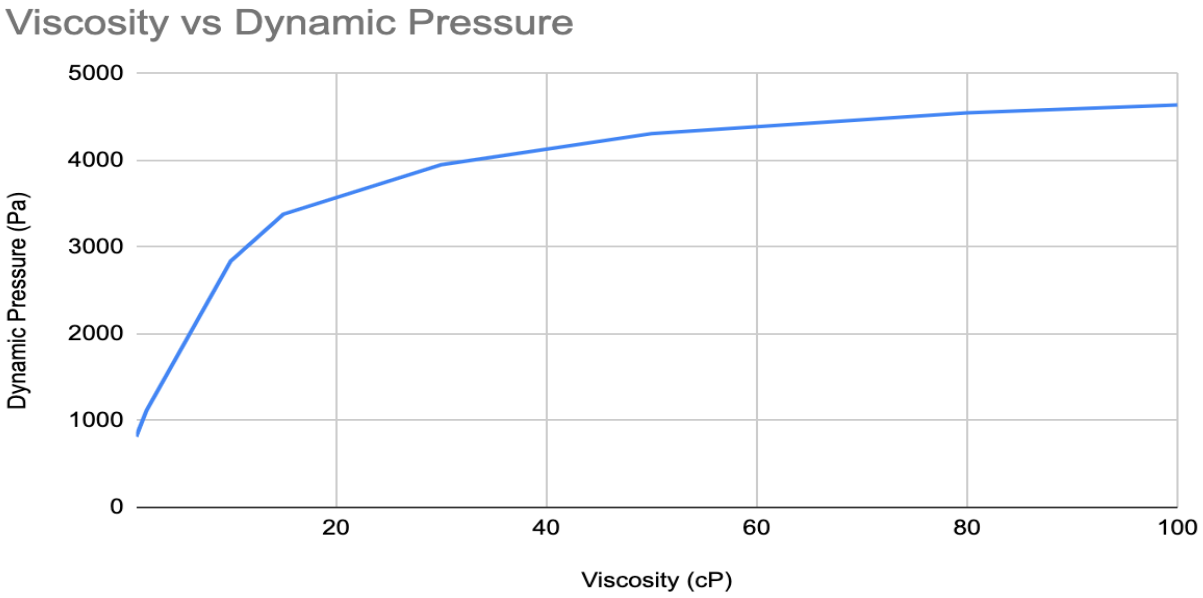

Figure 46: Viscosity vs Dynamic Pressure Results Observed in the Autoinjector Fluid Delivery System During Injection

Figure 47 presents the relationship between wall shear stress and viscosity during the injection process. Wall Shear Stress is directly proportional to the medication viscosity. The shear stress captured for fluids with viscosity 1, 20 and 100 cP is 57, 488 and 1810 Pa respectively.

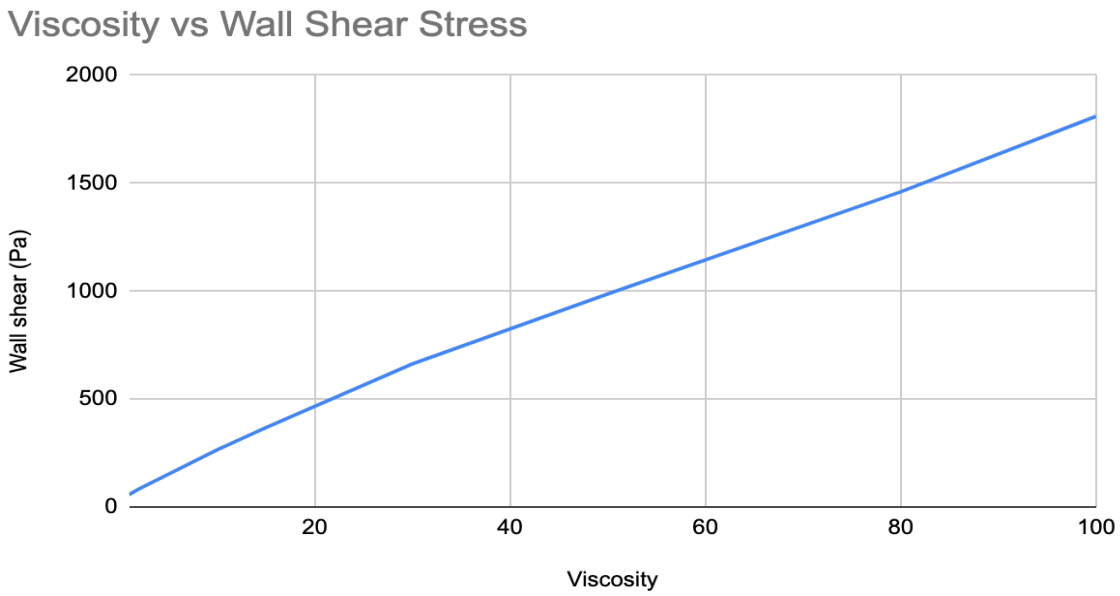

Figure 47:Viscosity vs Shear Stress Observed in the Autoinjector Fluid Delivery System During Injection

4.1.3 Simulation Type B: Needle diameter

Simulation Type B results are produced by injecting different medications via a needle to the injection site whilst varying needle gauge per simulation. The plunger motion initiates fluid flow and this is represented by the moving wall in the simulations. Figure 48 shows the maximum dynamic pressure captured per needle gauge. Dynamic pressure is constant for needle gauges below 20 irrespective of the fluid viscosity. High viscosity medications results in high pressures. For a 14 gauge needle, dynamic pressure was captured to be 827, 3510 and 4620 Pa for a fluid of viscosity 1, 20 and 100 cP respectively. The highest dynamic pressure is captured at 100 cP for a 16 gauge needle. The lowest dynamic pressure is captured at 1 cP for a 14 gauge needle.

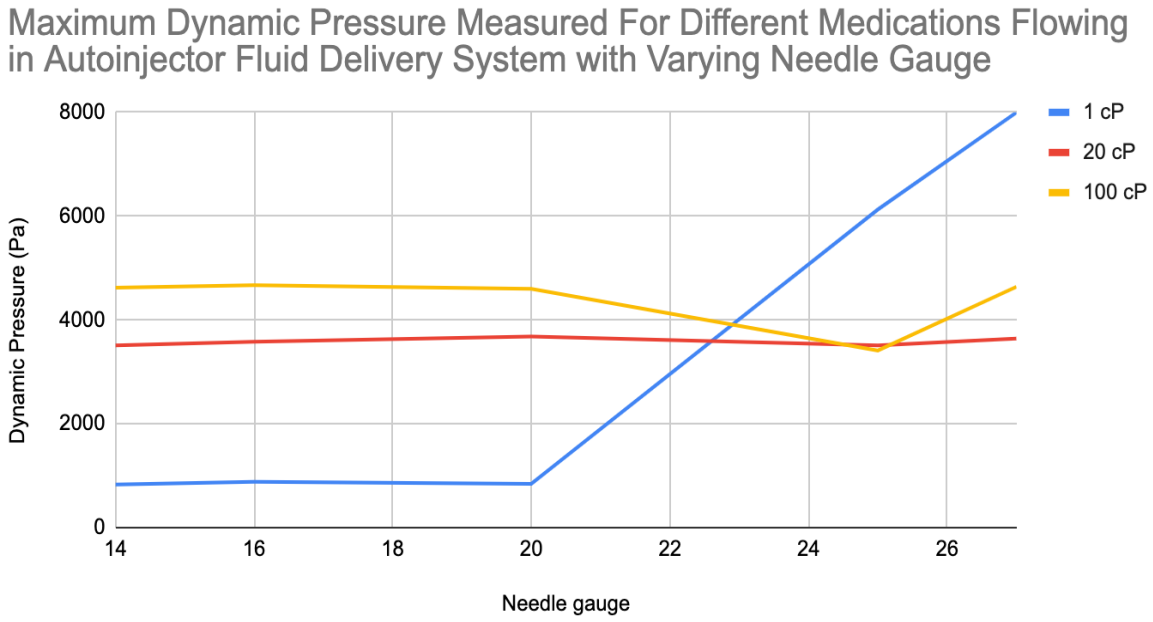

Figure 48:Maximum Dynamic Pressure Captured From CFD Model When Varying Needle Gauge

Figure 49 below shows the maximum shear stress captured at different needle gauges. Negligible change are captured at 1 and 20 cP. At 100 cP, no significant shear stress change is encapsulated at needle gauges below 20. Wall shear stress decreases for needle gauge between 20 to 24 . Thereafter increases when using needle gauges above 24.

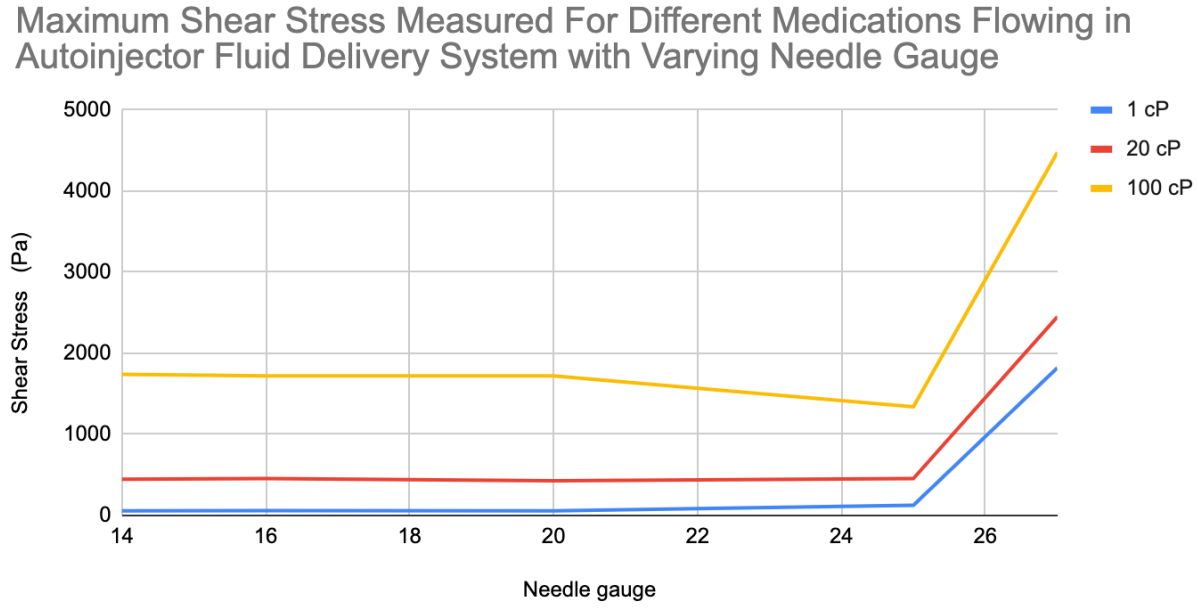

Figure 49: Maximum Shear Stress Recorded for Different Medications Flowing in the Autoinjector Fluid Delivery System Varying Needle Gauge

4.1.4 Simulation Type C: Needle Length

Simulations Type C were conducted by injecting different medications from the vial via the needle into the injection site varying needle length from simulation to simulation. Figure 50 below shows the dynamic pressure captured using the different needle lengths. Dynamic pressure increases with increasing length, irrespective of the fluid viscosity. The shortest needle length used for the study is 16 mm and dynamic pressure of 434, 1957 and 2475 Pa was recorded at 1, 20 and 100 cP. For a 32 mm needle, dynamic pressure is 869, 3914 and 4949 for a fluid with a viscosity of 1, 20 and 100 cP.

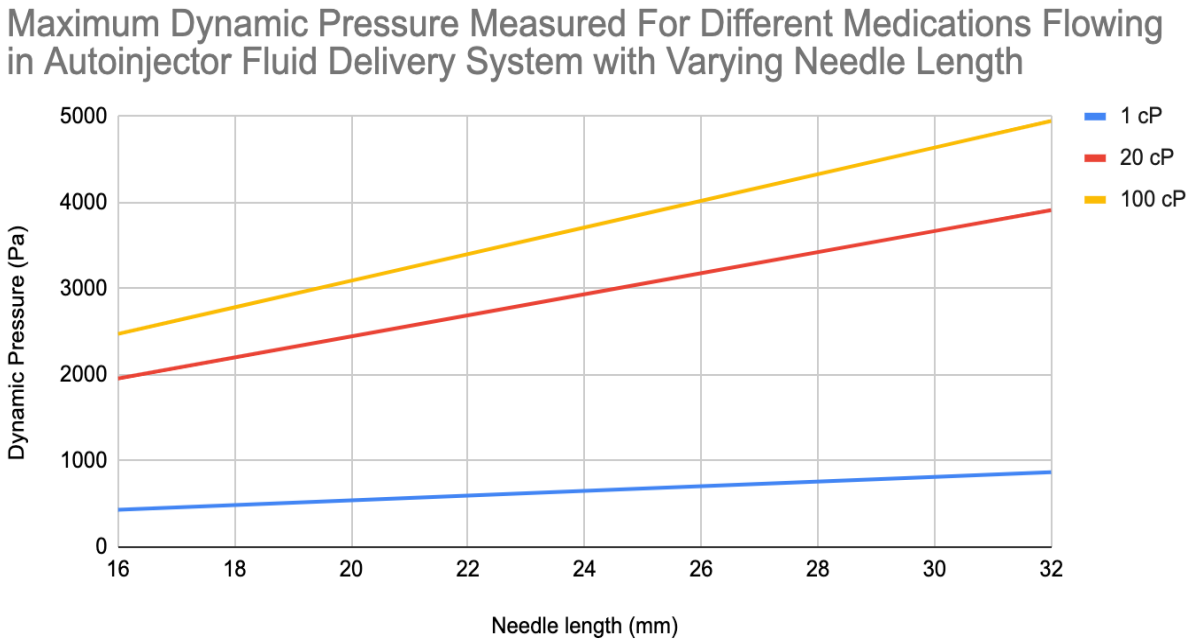

Figure 50: Maximum Dynamic Pressure Recorded for Different Medications Flowing in the Autoinjector Fluid Delivery System Varying Needle length

Figure 51 below shows the maximum shear stress recorded when varying needle length. Wall Shear stress is directly proportion to needle length. Larger viscosity medications result in higher wall stresses. For a 16 mm needle, the shear stress is 30, 261, 965 Pa recorded for a fluid with viscosity 1, 20 and 100 cP respectively. A needle length of 32 mm results in maximum wall shear stress of 61, 522 and 1931 Pa when a liquid of viscosity 1,20 and 100 cP is used.

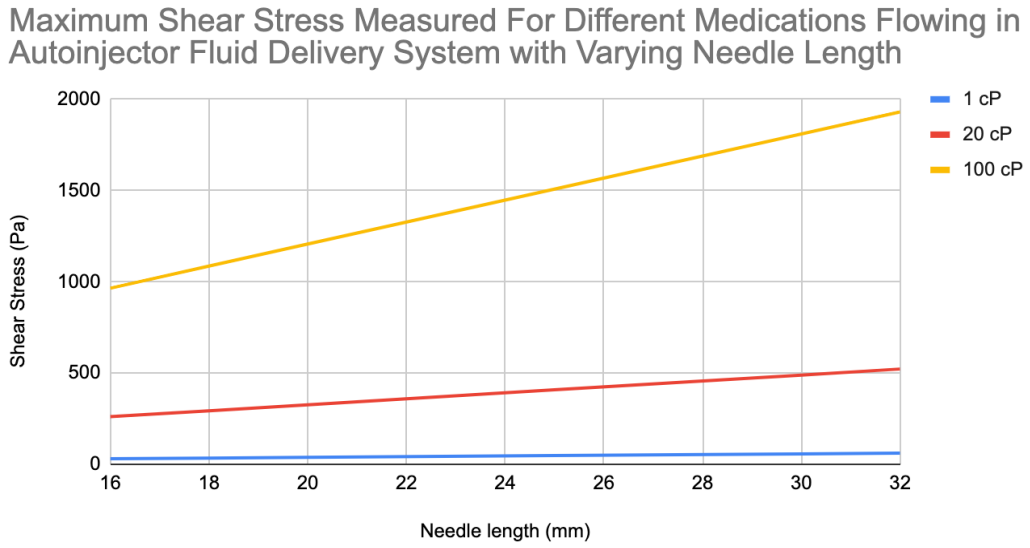

Figure 51: Maximum Shear Stress Recorded for Different Medications Flowing in the Autoinjector Fluid Delivery System Varying Needle length

4.1.5 Simulation Type D: Medication Volume

Simulations type D are conducted by varying the medication volume flowing in the fluid domain. Figure 52 displays the relationship between the maximum dynamic pressure and medication volume when fluids of different viscosities are forced into motion. A 1ml vial produces a dynamic pressure of 2717,12233 and 15466 Pa for a fluid with viscosity 1,20 and 100 cP respectively. Medications with the viscosity of 1,20 and 100 cP with a volume of 10ml generate a dynamic pressure of 27167, 122333 and 154666 Pa.

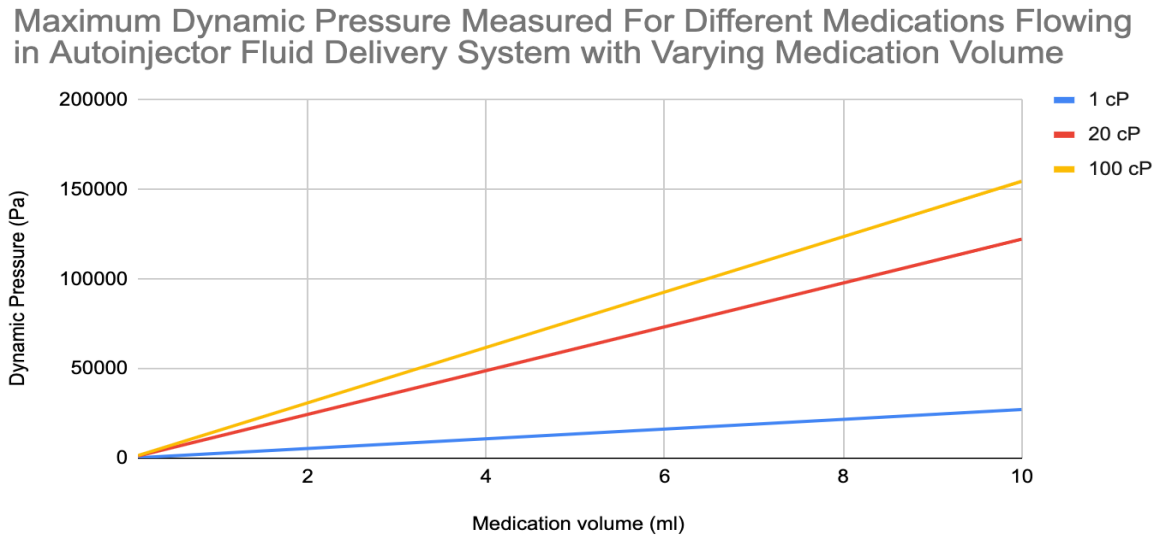

Figure 52: Maximum Dynamic Pressure Measured For Different Medications Flowing in Autoinjector Fluid Delivery System with Varying Medication Volume

Shear stress increases with increasing medication volume (Figure 53). The shear stress recorded for a 1 ml vial at 1,20 and 100 cP is 190, 1630 and 6033 Pa. The shear stress recorded for a 10 ml vial at 1,20 and 100 cP is 1900, 16300 and 60333 Pa.

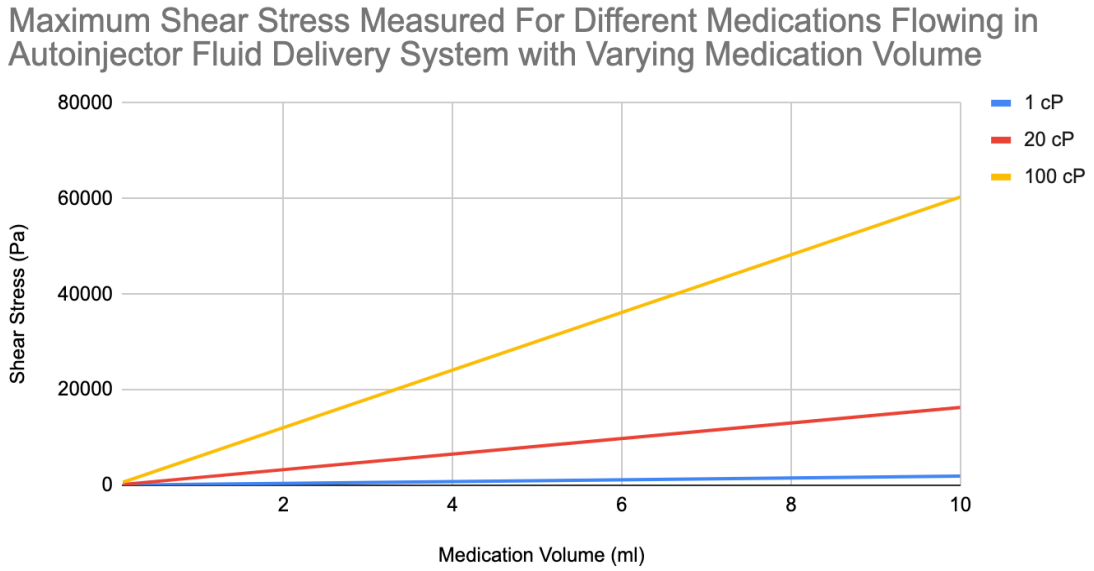

Figure 53: Maximum Shear Stress Measured For Different Medications Flowing in Autoinjector Fluid Delivery System with Varying Medication Volume

4.1.6 Flow Patterns

Figure 54 below shows the contour plots of the dynamic pressure for a 1 cP fluid. The dynamic pressure is the highest at the moving wall centre compared to anywhere else in the fluid system. Dynamic pressure decreases towards the needle. At low viscosities, the fluid travels faster and easier hence As viscosity increases, the dynamic pressure increases along the walls of the moving wall. The pressure profile is less visible at high viscosities.

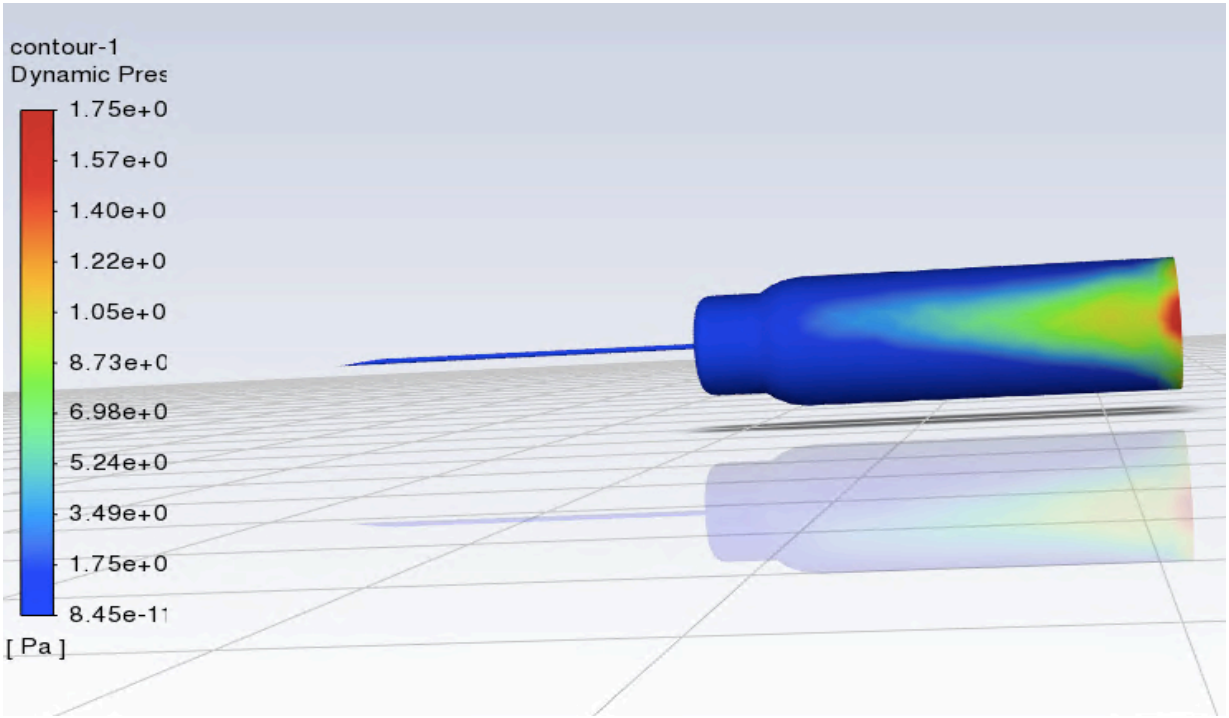

Figure 54: Dynamic Pressure Profile at Viscosity 1 cP

Figure 55 below shows the total pressure profile for medication at 1 cP. The pressure profile is clearly visible and comprises of high pressure at the edge of the moving wall. The pressure decreases as you move along the vial. High pressures are observed at the needle tip and pressure decreases as you move away from the needle tip towards the vial.

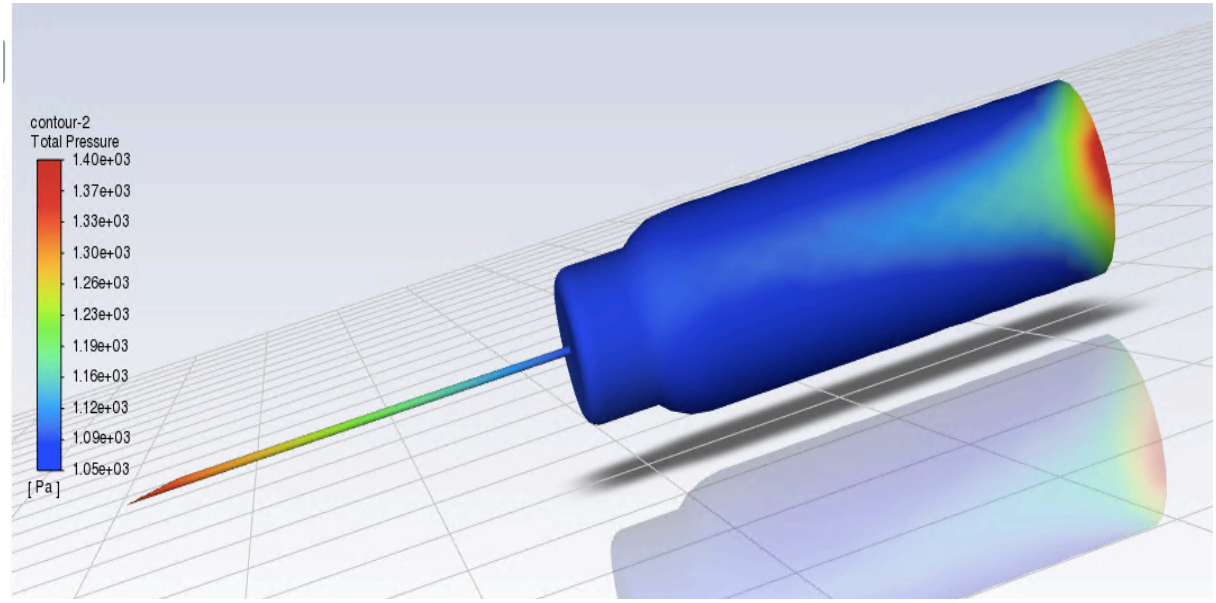

Figure 55: Total Pressure Contours at Viscosity 1 cP

Figure 56 below shows the wall shear stress contours captured for a 1 cP fluid. Shear stress is higher at the centre of the moving wall and decrease as you move towards the needle.

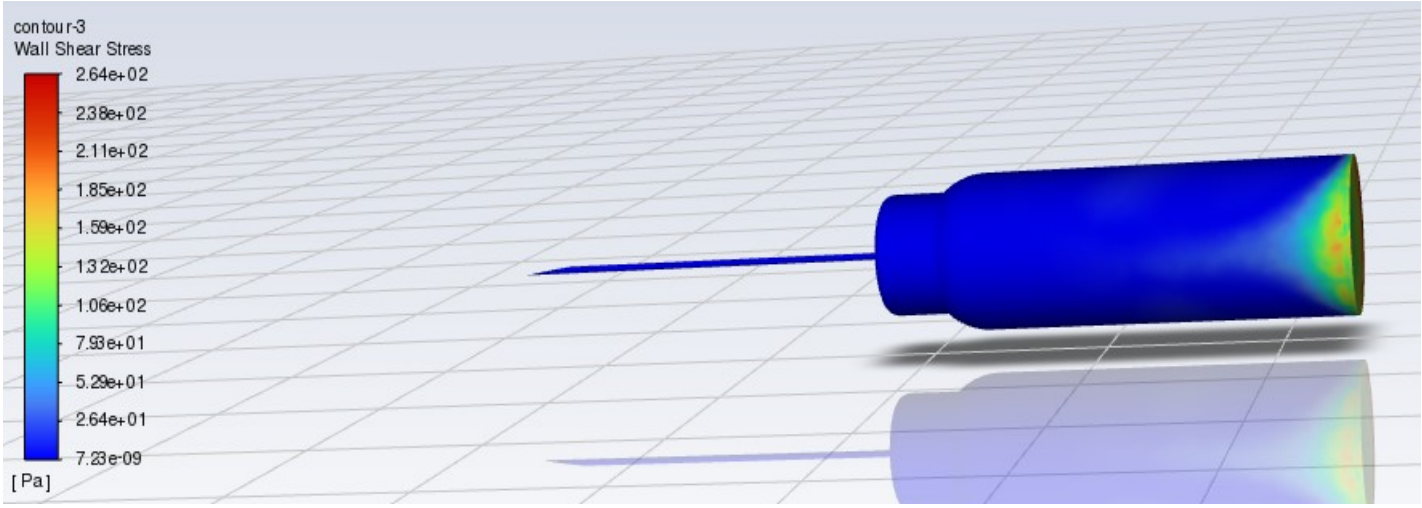

Figure 56: Wall shear stress at Viscosity 1 cP

4.3 Discussion

The aim of the CFD model is analyse the fluid behaviour of different medications during the injection process with a focus on syringeability and injectability. Syringeability refers to the force required to inject medication. Injectability explores the ease of injection taking into account drug formulation, administration, adverse events and general ergonomics. Both these properties depend on the fluid viscosity, needle and syringe geometry. Most autoinjectors are equipped with a 25 or 27 gauge needle and a 1 ml vial. These needle gauges work well for intramuscular injections. The most effective needle length for intramuscular injections is 13-19 mm. To the best of our knowledge, this research is the first of its kind to use CFD to analyse the effects of viscosity on the injection process, taking into account changes in dimensions of the medication delivery system.

4.3.1 Effects Of Viscosity On Auto-Injections

Type A Simulations were conducted to explore the effects of viscosity on the injection process. The viscosity of the medication was varied from 1 – 100 cP. Simulations with medications of viscosity above 20 cP only met the convergence criteria once the conditions were changed from constant viscosity to varying viscosity defined by the power law. Shear-thinning behaviour was therefore assumed for these fluids. The fluid domain was made of a 0.3 ml vial, 25 gauge needle with a length of 30 mm. A logistic growth was captured for the dynamic pressure when the viscosity was increased. This means that when viscosity increases, the dynamic pressure will increase. The rate at which this pressure increases will decrease until a constant pressure is reached and maintained. These results are consistent with the principles of fluid mechanics. The fluid velocity or motion of the molecules cause dynamic pressure. According to Bernoulli's equation, an increase in velocity results in a decrease in pressure to ensure that the algebraic sum of the pressure, kinetic and potential energy is constant. Following this principle, an increase in viscosity, increases the pressure but decreases the fluid velocity logistically.

Dynamic pressure is the highest at the centre of the moving wall and decreases as you move along the flow domain. The vial represent the region of developing flow, where the medications stick to walls of the vial as a results of the viscous effects. This is only true because of the no slip conditions. Separation flow is captured in the syringe and needle when the viscosity of the fluid is between 15 - 80 cP. Separation flow is characterised by deceleration of flow with increasing pressure. This confirms easier injections for Newtonian fluids than Non-Newtonian and hence higher syringeability and injectability. This implies that highly viscous medications will have a longer dwelling time in the needle. This will increase the chances of needle deformation and pain due to the damage in the muscle tissue.

The obtained results are consistent with the results from Kanair et.al, 2008, Badkar et.al, 2021 and Fry, 2014. Badkar et.al, 2021 state that high viscosity cause drug aggregation and dispersion, increasing injection force and pain. According to Fry, 2014, shear-thinning medications cause viscous resistance and increased pain perception. The results of these simulations exhibit direct proportionality between viscosity and shear stress. These results are consistent with Mahetab et.al, 2017. According to Mahetab et.al, 2017, shear stress remains zero at the centre of a syringe and needle and increases linearly to its highest value at the walls for all Newtonian fluids. This trend is observed for shear-thinning fluids when the flow is in steady state. The results thereby shown that it easier to inject lower viscosity medication and hence these would have higher injectability and lower syringeability.

4.3.2 Effects Of Needle Gauge

The correct needle sizes for an injection is determined by factoring the type of medication to be injected, the dose, body size and injection site. The higher the needle gauge, the smaller the diameter of the needle. Needle gauges below 20 result in constant dynamic pressure and negligible shear stress. This results in extremely slow medication flow in needle gauges below 20 and hence these gauges are not recommended for intramuscular injections. Using needle gauges from 20 - 25 exhibit an increase in wall shear stress (observed more clearly at high viscosities), increase in dynamic pressure at 1 cP and a decrease in dynamic pressure at 20 and 100 cP. This can be interpreted as decreasing needle diameter, increases dynamic pressure when injecting Newtonian fluids but decreasing dynamic pressure when injecting Shear-thinning Non-Newtonian fluids.

These results are consistent with the principles of fluid mechanics considering that flow in a needle is describe by the Hagen-Poiseuille equation. In this equation, the pressure along the needle is directly proportional to the needle length but inversely proportional to the needle diameter. Therefore, a decrease in needle diameter (increase needle gauge) will decrease the pressure. Large needle diameters are also associate with haemorrhage in the injection site, discomfort and increased pain. These factors all contribute to lack of medication compliance and adherence. Needles gauges above 25 gauge exhibit an increase dynamic pressure, total pressure and wall shear stress with increasing needle gauge. These results support the rationale of recommending either a 25 or 27 needle gauge for intramuscular injections of Newtonian medications. This means that even higher needle gauges are required for more viscous medications.

4.3.3 Effects Of Needle Length

The choice of needle length for an injection is often linked to the desired injection site and the patients skin-to-muscle depth. These factors must be correctly determined to ensure that the medication is delivered to the correct layer at the required injection time. According to the simulation results, an increase in needle length results in an linear increase in dynamic pressure and wall shear stress. These results are consistent with the Hagen-Poiseuille equation showing direct proportionality between pressure and needle length. Increasing the needle length means that the medication will remain in the autoinjector for longer. For rapid injections, higher injection forces are required to ensure timely medication delivery. These forces are even higher for high viscosity fluids than there are for lower viscosity medications. The length of the needle also affects the bioavailability of the drug being injected.

4.3. 4 Effects Of Medication Volume

Vial dimensions depend on the volume of medication being injected. Increasing medication volume increases dynamic pressure and wall shear stress but decreases total pressure. This also implies that static pressure decreases with increasing medication volume. These results are consistent with the Hagen-Poiseuille equation, which displays direct proportionality between the pressure and fluid volume. Intramuscular and subcutaneous injections have been kept below 2 ml. Volumes above 2 ml result in wall shear stresses above 1000 Pa. These stresses are too large and may result in syringe or needle breakage. Increasing the medication volume also means a higher syringe dwelling time. This slows down the flow of the medication and hence longer injection time. High volumes of medications require lower gauges. This is to ensure that medication will be deliver faster. This will however result in more pain and discomfort.

4.3. 5 Influence Of The Results On The Autoinjector Operations

4.3.5.1 Cavitation

Injectable fluids like any other liquids have vapour pressure. This is the pressure reached during evaporation, when there is an imbalance between particles that exist in the vapour phase and those that are escaping from the liquid. If the static pressure of a fluid drops below this vapour pressure, cavitation occurs. The phenomenon is a major problem in autoinjectors as it results in syringe damage and drug molecule separation. There is no indication of cavitation captured in the simulation result. This is due to the assumption of no slip conditions and that only the plunger is moving during the injection process.

Activation of spring autoinjectors results in mechanical impact between the components. This impact causes components to accelerate and induce high peak stresses and pressure in the fluid (Veilleux et.al., 2018). These stresses produce tension waves in the liquid and hence cavitation. To explore this phenomenon simulations were run under the assuming that all the components (syringe, plunger and needle) are moving at a speed of 3.33 m/s during the injection process. Figure 57 below shows a planar view of the fluid domain under this assumption. The results show that when autoinjector components e.g. the syringe, needle and plunger are in motion during the injection, tension waves are created and cavitation occurs. These results align with Eshraghi et.al,

2021, proving that cavitation occurs due to the relative motion between the syringe and the medication arising from needle insertion.

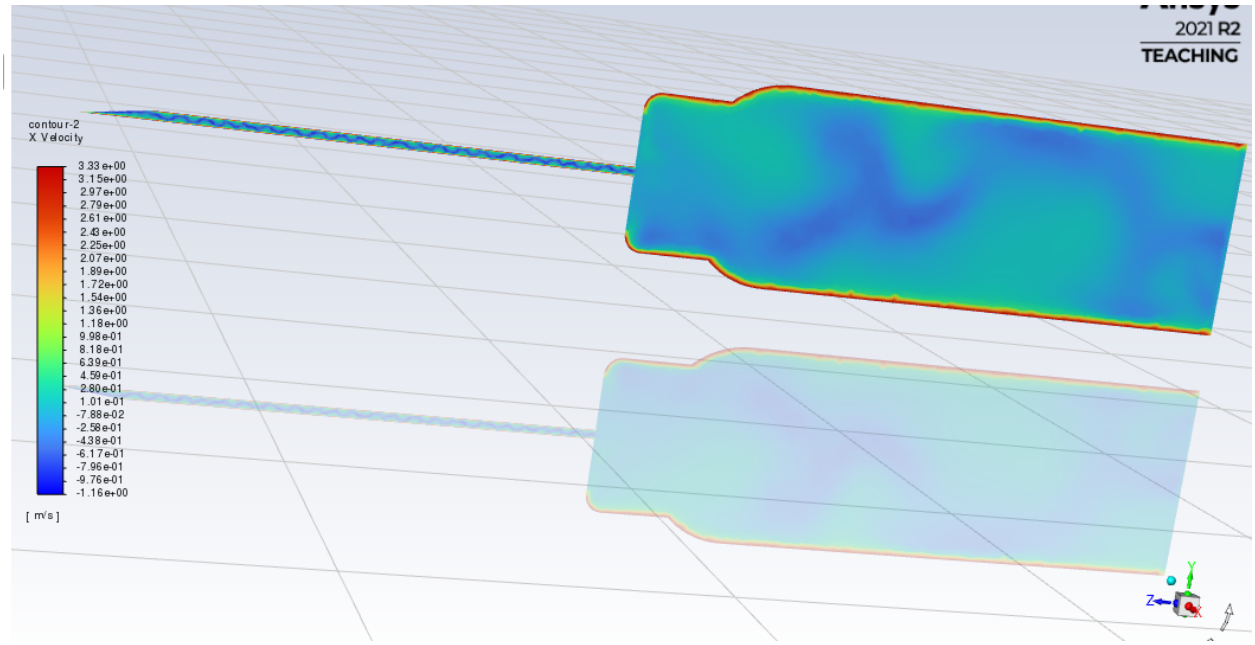

Figure 57: Planar View of the Velocity Profile of an Autoinjector Fluid Delivery System With Accelerating Components

4.3.5.2 Bioavailability Of A Drug And PK

Drug bioavailability refers to the active drug in the systematic circulation. It depends of food intake, physiological aspects, physiochemical properties and dosage form. The presence of separation flow in high viscous medication indicates medication aggregation and dispersion during injections and this may affect the PK properties of the drug and the bioavailability. According to Hill et.al, 2016, IM injections influence dispersion and uptake of injected material. Hence, they affect medication effectiveness and PK.

4.3.5.3 Patient Experience

Injecting medication with high viscosity induces separation flow. A decrease in flow rate characterises this as pressure increases. This causes challenges in injecting these medications and hence affects the usability of the overall autoinjector device. These results align with Badkar et.al, 2021 and Fry, 2014 linking shear-thinning injectables with high viscosity fluids. Both these studies show that high viscosity drugs induce drug aggregation and dispersions, injection pain and viscous resistance. Injecting large medication volumes increases dynamic pressure and wall shear stress. Large wall shear stresses are linked with device malfunction such as needle or syringe breakage. This is also linked to higher chances of infections and injection pain as more volume is forced under the skin (Hirsch et.al, 2012). Using lower needle-gauges does not induce any flow in the fluid domain. This means that injection force must be increased to force the medication into motion. There is no direct relationship between needle gauge and viscosity that has been found in this study, however increasing the needle length does mean an increase in needle dwelling time. This influences injection time and drug pharmacokinetics.

CHAPTER 5: RISK - INFORMED CREDIBILY ASSESSMENT

5.1 Introduction

This chapter outlines the results and discussion of the risk-informed credibility assessment conducted as part of this research. This assessment is conducted to assess the credibility of the computational model as per the ASME V&V 40 and V&V20 guidelines. The scope of the computational model is described by defining the QOI, COU and model risk. Thereafter verification and validation activities are conducted to establish credibility of the computational model.

5.2 Results

5.2.1 Scope

QOI: Does the viscosity of the intramuscular injectables influence autoinjector fluid system configuration?

COU: A CFD model was used to simulate the flow of different medications during the injection process. Each medication was defined by viscosity and density. The autoinjector fluid system configuration formed by the plunger, syringe and needle represents the flow domain. Medication viscosity, syringe and needle dimensions were varied to evaluate the pressure and stress changes during the injection process. This model was then used to evaluate sensitivity of medication fluid behaviour to variations in component dimensions, and how this affects general autoinjector performance.

Table 5: Table Showing Model Risk

	Model influence	Decision consequence	Model risk
COU	The model influence is high because the results from the CFD model show clear trends and relations between viscosity and syringe or needle dimensions.	If autoinjector designers finalise autoinjector design decisions based on the CFD results without any further considerations, then a malfunctioning auto injector fluid-delivery system will be incorporated into the design. The specific autoinjector will malfunction and fail to deliver the correct medication dosage into the intramuscular layer at the required time. A redesign will be required and consequently loss of time and money for the company. The decision consequence is high.	The model risk is high.

5.2.2 Verification Results

The verification process aims to confirm that the computational model matches the underlying mathematical model. For this study, calculation verification as per the ASME V&V 40 is conducted. This includes estimating discretization, numerical solver error and setting measures to mitigate use error. An extensive grid independence study was conducted as part of CFD pre-processing to identify the correct mesh size for each geometry via computing the relative error per mesh size. This mesh independence study is a vital verification component that demonstrates that the numerical error converges to the exact solution. The average discretisation error calculated via the grid independence study is 0.0474 %.

The numerical solver error stems from the selection of the solver parameters of the numerical solution. This error was estimated by verifying and monitoring the convergence tolerance. The convergence criteria for the solver equation residuals was varied to ensure that the difference between the results is minimum. More simulations were conducted using a 0.3ml vial, 25 gauge needle of length 30 mm and a 1 cP fluid. The resulting dynamic pressure corresponding to the different rms residuals was captured. The numerical solver error was then calculated for these results.

Table 6: Numerical Solver Error Determined for the CFD Model

RMS Residuals	Dynamic Pressure (Pa)	Numerical Solver Error (%)
1 x 10^{-1}	805.254	9.746
1 x 10^{-2}	812.412	2.588
1 x 10^{-3}	814.257	0.743
1 x 10^{-4}	814.881	0.119
1 x 10^{-5}	815.010	0.01
1 x 10^{-6}	815.010	0.01

The numerical solver error is shown in table 6 above. The minimum solver error was generated at 1 x 10^{-5} and 1 x 10^{-6} residuals and this error was calculated to be 0.01%. All simulations were then monitored to ensure that an rms residual of 1 x 10^{-6} is met. Use errors refers to the error due to the user oversight. For this research, the main sources of user error were analysed to be:

- Fault in inserting boundary conditions e.g. incorrect moving wall speed or outlet pressure.
- Using the incorrect mesh size.
- Using the incorrect solver model.
- Adding the incorrect geometry
- Failure to monitor or reach convergence.
- Incorrect definition of the material e.g. incorrect medication viscosity or density.

A checklist was used to ensure that the listed sources of error are avoided. If there was any perceived error, the simulations were recalculated to confirm the results.

5.2.5 Validation Results

Validation activities are conducted to ensure that the computational model represent real-life fluid delivery system of an autoinjector. The validation activities include assessing model form assumption, characterisation of medications and force testing. The formulation of the computational model was evaluated. This assessment mainly focused on assessing assumptions used for the system configuration and conditions of the computational model. The main model form assumptions were evaluated and these a listed in table 7 below.

Table 7: Model Form Assumptions

Model form	Model Form Assumptions
Complexity of the geometry	Eliminating small features of the geometry edges e.g. fillets, does not influence the results.
Fluid characterisation as per model	According to literature, viscosity above 20 cP represents non-Newtonian medications. Even after checking and refining the mesh, simulations with fluids of viscosity above 20 cP did not converge using constant velocity model. Convergence was only reached once the Power law was applied for these simulations.
Plunger-syringe friction	There is friction between the moving wall and the syringe. This friction was not captured in the computational model but is accounted for in the force testing.
No slip condition on the moving wall	There is no relative velocity between the wall and fluid.

5.2.6.2 Fluid Characterisation Testing

The viscosity and shear rate of four medications was determined using a rheometer. These medications are adrenaline Pharma Q, Amikacin 2 ml, Insulin basaglar and Vaxigrip tetra-filled 3ml. A total of 12 tests were conducted on the rheometer to determine the fluid characteristics of each of the four medications hence three tests for each medication. Figure 58below shows the relationship between the viscosity and shear rate of the four medications measured 25°C using a rheometer. Adrenaline viscosity increases slightly with increasing shear rate. A viscosity of 0.83 cP is measured for a shear rate of 63.1 s^{-1}. The highest adrenaline viscosity measured is 0.93 cP measured at a shear rate of 500 s^{-1}. The viscosity measured for Amikacin is almost constant at different shear rates. The average viscosity of amikacin is 0.88 cP. The results show that Vaxigrip viscosity decreases slightly with increasing shear rate. The highest viscosity measured for Vaxigrip is 1.28 cP for a shear rate of 63 s^{-1}. A linear increase in insulin viscosity as shear rate increases is captured. The lowest and highest insulin viscosity values measured are 2.04 and 3.32 cP at a shear rate of 50 and 500 s^{-1}.

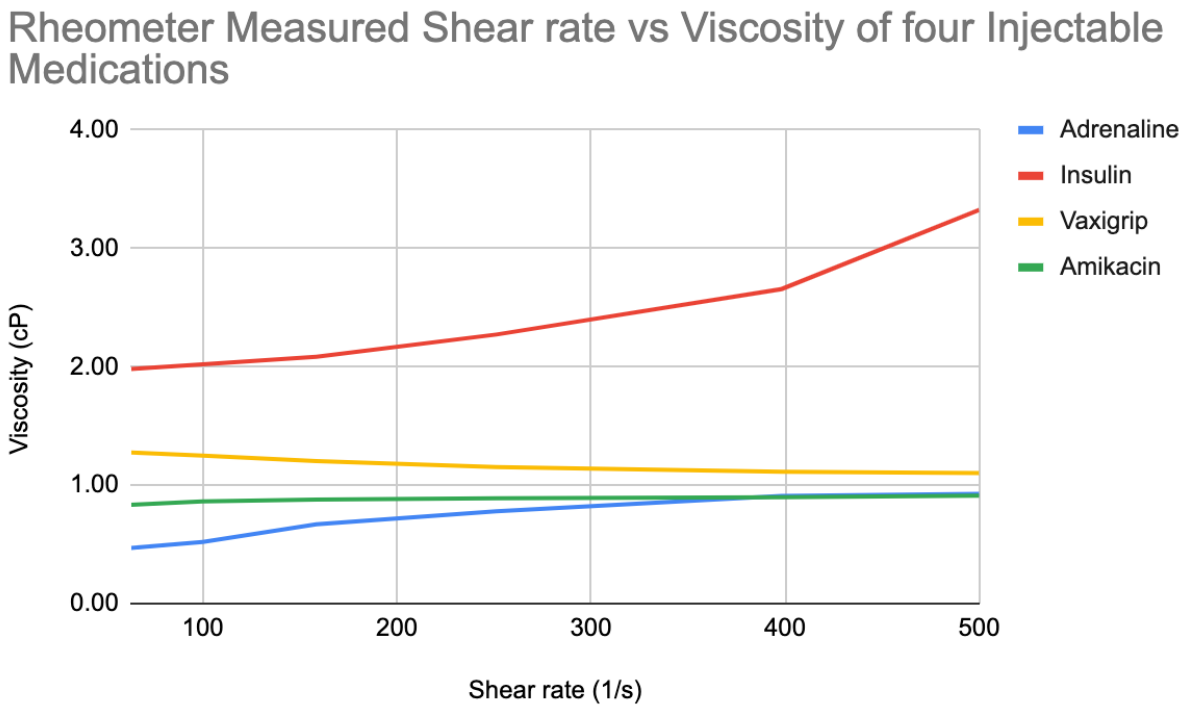

Figure 58: Viscosity vs Shear Rate of Four Medications

5.2.6.3 Force Testing

The syringe force per displacement was measured for the different medications using the ZwickRoell Universal tester. 80 tests were conducted as part of the model validation. The medications used for testing were adrenaline pharma Q, Amikacin, Vaxigrip and Insulin basaglar. The influence of needle gauge on the injection was evaluated by injecting each of the four medications using a 1ml syringe and varying the needle gauge. 5 different needle gauges were used, an 18, 21, 22, 23 and 26 gauge. The influence of medication volume on the injection process was assessed by injecting each of the four medications using a 26 gauge needle using different syringe volumes. Four different syringes were used and these had a volume of 1, 2, 5 and 10 ml. The plunger force per displacement was then captured for each of the injections.

Figure 59 presents the relationship between the syringe force and displacement of adrenaline injected using different needle gauges. At the beginning of the plunger displacement, the syringe force increases. Noise is detected at peak syringe forces. The syringe force decreases by half after the plunger has been displaced 3 mm. Thereafter a constant force is maintained throughout the injection process. The syringe force is higher for high gauge needles. The highest peak syringe force captured for adrenaline is 4.5 N for a 26 gauge needle and the lowest is 0.9 N for a 22 gauge needle.

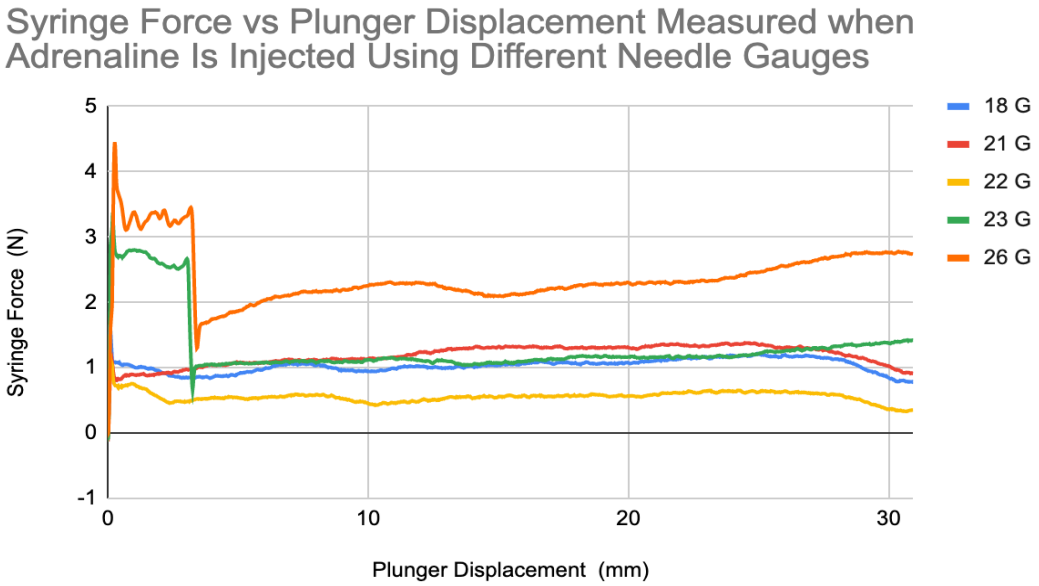

Figure 59:Relationship Between Plunger Displacement and Force When Adrenaline is Injected Using Different Syringe Gauges

Figure 60 below shows the syringe force per plunger displacement measured when Amikacin is injected using different needle gauges. When the plunger motion commerce, syringe force increases to its peak value. Noise is detected at peak syringe forces. This is followed by a decrease in syringe force resulting in a constant force that is maintained for the entire duration of the plunger motion. The highest syringe force is captured for a 23 gauge needle and the lowest is captured for 26 gauge needle. 4 N is the peak syringe force measured for 23 gauge needle. Negative syringe forces are captured for a 21 gauge needle.

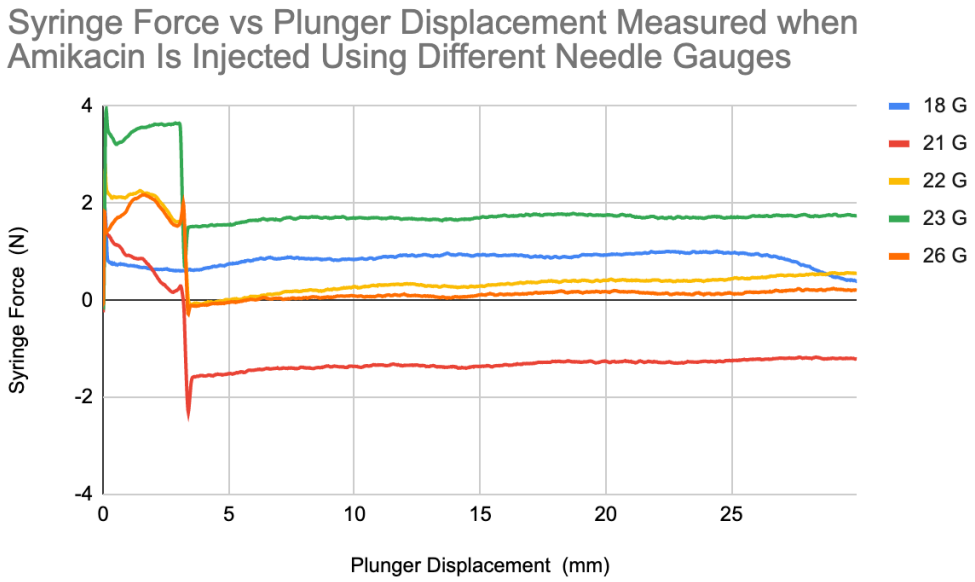

Figure 60: Plunger Force vs Displacement Captured When Amikacin is Injected Using Different Needle Gauges

Figure 61 displays the relationship between the syringe force and displacement measured when Vaxigrip is injected using different needle gauges. Immediately after actuation, the syringe force

increases to its highest value. A noisy decrease in syringe force is captured in the first 3 mm of the plunger displacement. Thereafter a constant syringe force is maintained for the duration of the plunger motion. The highest peak force is measured for a 26 gauge needle, followed by 23 gauge needle. These peak syringe forces are 4 N and 3.3N respectively. The lowest syringe force is 1.1 N captured for a 22 gauge needle.

Figure 62 below shows the syringe force vs displacement captured when Insulin basaglar is injected using different needle gauges. The syringe force increase immediately as the plunger begins to move. Peak syringe force is reached and a decrease follows this until a certain force is reached and maintained for the duration of the motion. Peak syringe forces are captured for 26 gauge needle, followed by 23 gauge. A longer transition period from peak force to constant force is recorded for both these gauges.

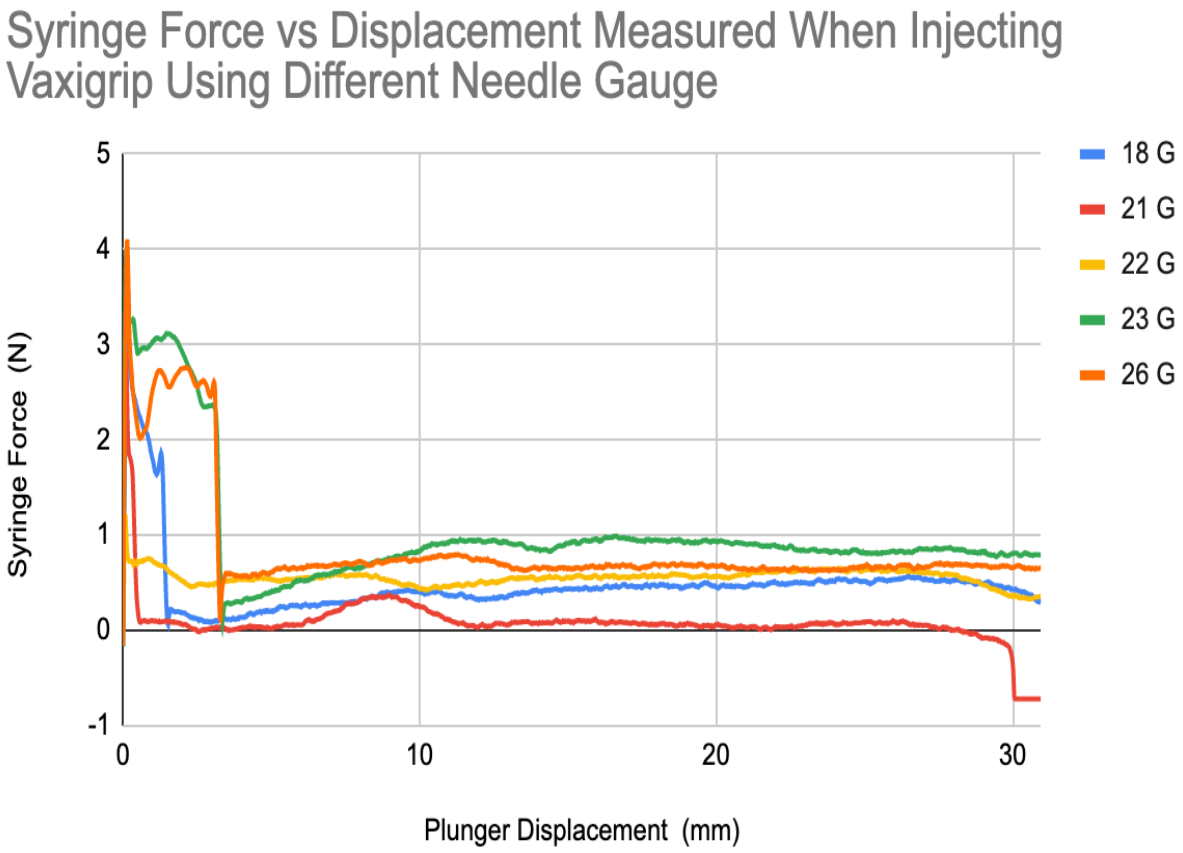

Figure 61:Plunger Force vs Displacement Captured When Vaxigrip is Injected Using Different Needle Gauges

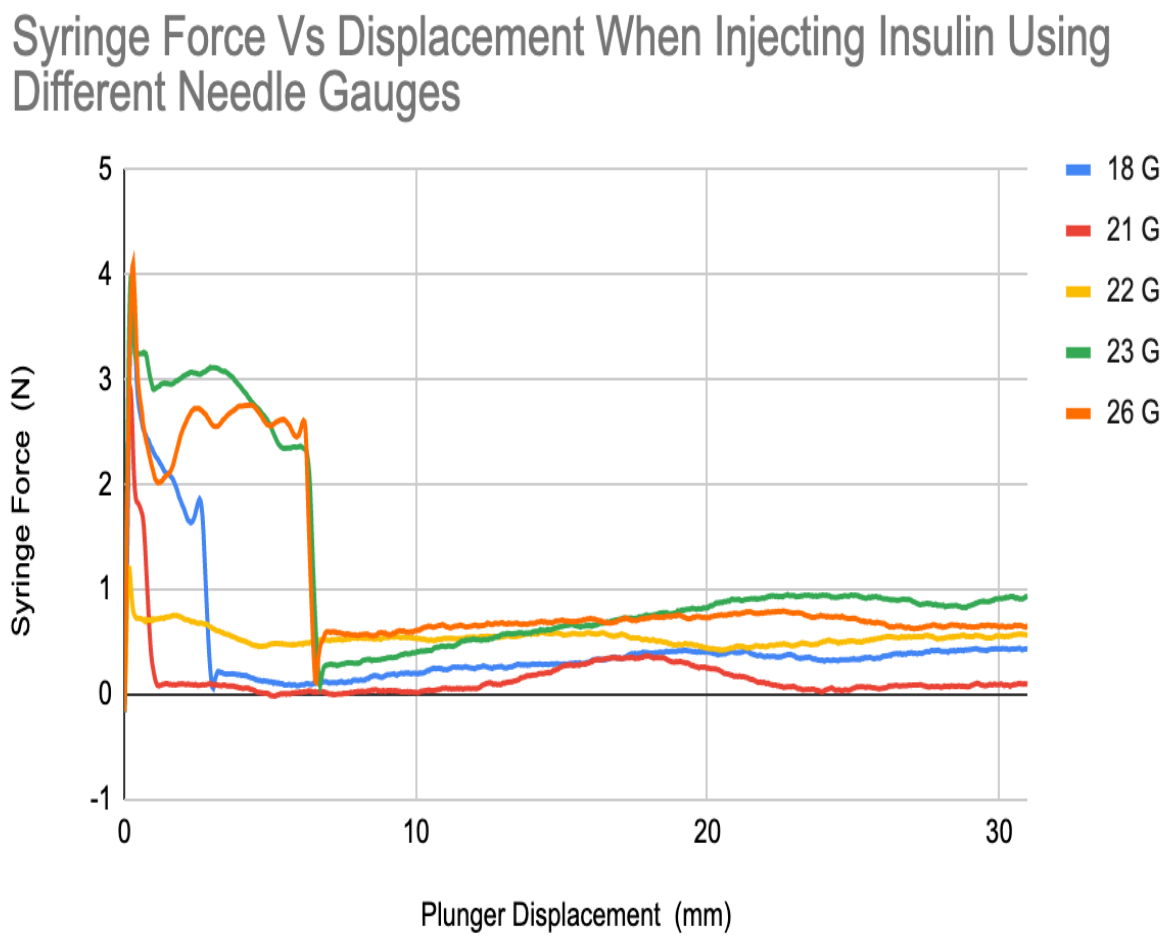

Figure 62:Plunger Force vs Plunger Displacement When Insulin Basalgar Is Injected Using Different Needle Gauges

The syringe forces captured for the different needle gauges and volumes are divided by the area of the medication in the syringe to calculate the dynamic pressure in the syringe. The dynamic pressure is plotted against the needle gauge and medication volume to match the results recorded for the CFD model. Figure 63 below shows the dynamic pressure changes per needle gauge as captured from the CFD model and the amikacin validation tests. Amikacin is chosen because it was characterised to have a viscosity of 0.91 cP and this is closest to 1 cP in the simulation results. A significant difference is observed in the results for gauges below 22. For these gauges, the dynamic pressure is higher in validation tests than the model results. For needle gauges above 22, the measured dynamic pressure is lower than the model results. The percentage error calculated between the model and validation results is 14.3%.

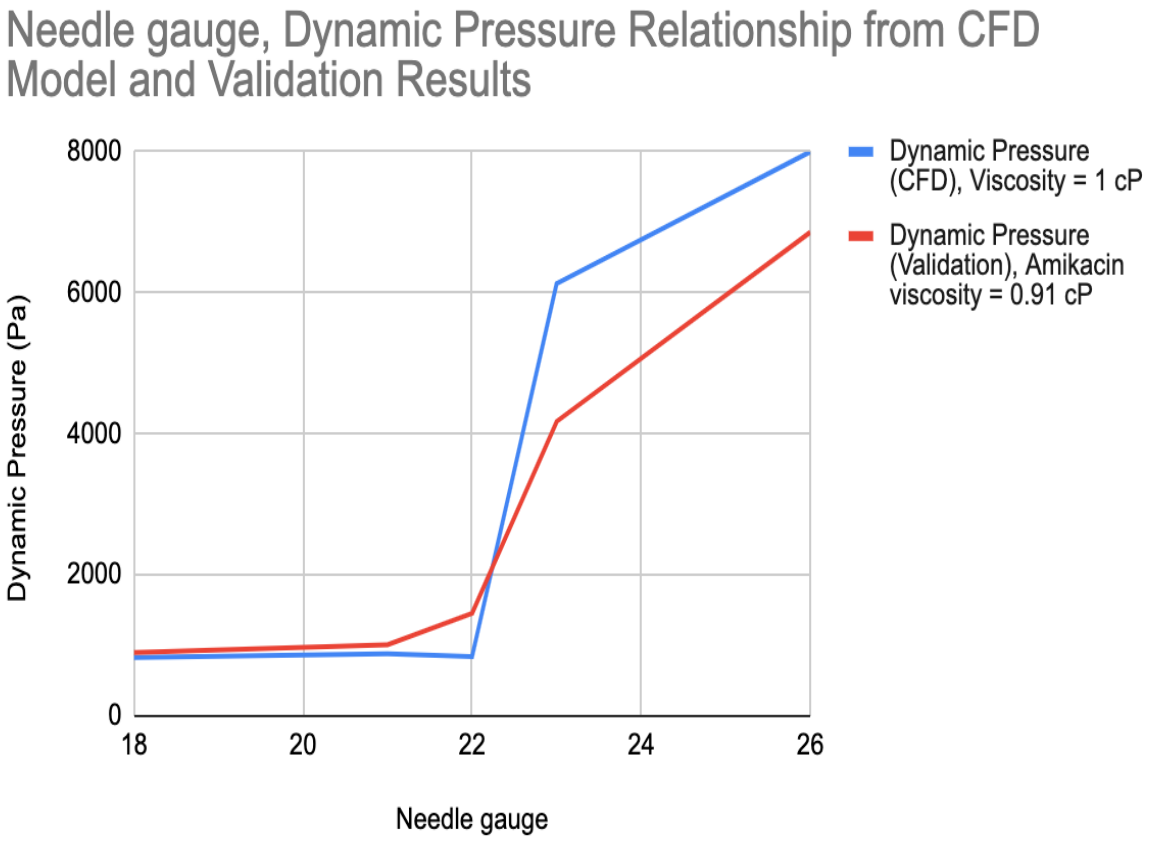

Figure 63:Dynamic Pressure Recorded At Different Needle Gauges As Per CFD Model Results and Validation Tests

Figure 64 below shows the dynamic pressure captured when different medication volumes are injected as per CFD model and validation tests. There is a significant difference in the model results when compared to the validation test results. For both sets of results, the dynamic pressure increases with increasing volume. These sets of results are similar for medication volumes less than 2 ml. Higher dynamic pressures are captured in the CFD model for volumes greater than 2 ml. The highest dynamic pressure is captured for a 10 ml volume and this is equal to 27167 cP as per the CFD model and 8588 cP according to the validation results. The percentage error between the sets of results is 28%.

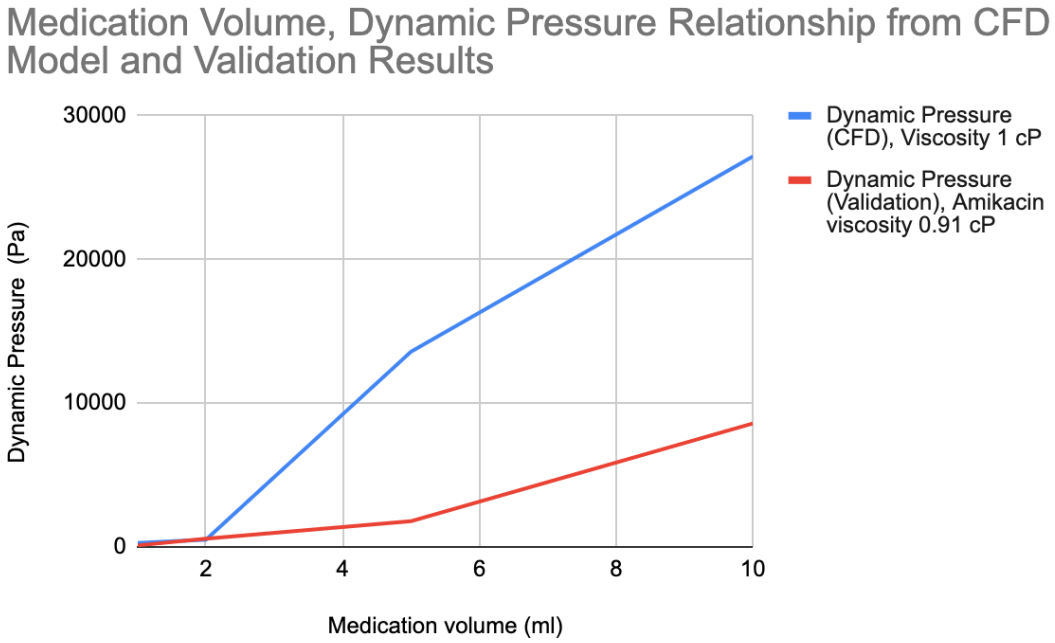

Figure 64:Relationship Between the Medication Volume And Dynamic Pressure from CFD Model and Validation Results

5.3 Discussion

Computational models are established as part of different medical device to either analyse device performance, assess operational conditions or explore new aspects of device. These models influence the risk and harm associated with the medical device and hence it is crucial to ensure that they are credible and match the real-world operations of the device in question. The ASME V&V 40 presents a framework to assess credibility of a computational model through conducting V&V activities. The V&V activities are quantified using a gradation system to rank the model from lowest to highest credibility.

The QOI and COU for the CFD model were assessed such that the COU gives information on how the model aims to answer the QOI. The computational model developed as part of this research aims to assess the effect of the viscosity of injectable medication on the configuration of the fluid delivery system. This was assessed through running simulations on ANSYS, varying the fluid viscosity and studying the fluid behaviour as these injectable medications through different fluid delivery geometry configurations. Medication volume, syringe and needle dimensions were varied to assess the pressure and stress changes during the injection process.

The associated risk for this computational model is defined to be high. This is defined after ranking the model influence and decision consequence. The biggest risk stems from assuming that the model results are to directly impact the autoinjector design without any further testing to inform the design process. Under this assumption, an incorrect model would result in poor performing autoinjectors that fail to deliver the desired dose of medication into the intramuscular layer at the required injection time. Injections may be too fast that they results in immature injections linked

with high pain perception and severe adverse events. Resulting injections could also be too slow leading to drug segregation, poor PK performance and incorrect medication delivery. All these factors affect patient experience and hence medication adherence and compliance.

As part of the CFD pre-processing, a grid independence study was conducted to determine the correct mesh size to be used for the simulations and to ensure that solutions are independent of mesh size. The average discretisation error calculated as part of this study was 0.0474%. The numerical solver error was calculated under the verification activities. This error is linked to divergence tolerance in the dynamic pressure results and was calculated to be 0.01%. The use error was not calculated as part of this study; however measures such as using a checklist to limit the amount human error done were set in place. Assessing all of the three types of errors associated with computational modelling and ensuring that they are all under 1% result in a verified computational model.

According the rheometer results, the viscosity increases slightly with increasing shear rates for adrenaline, amikacin and Vaxigrip. This increase is neglected such that it can be concluded that the viscosity does not change with shear rates for these medications and hence they are Newtonian medications. The viscosity of these medications is independent of shear rate and flow stresses. It has a linear correlation to the changes in shear deformation with respect to time. The viscosity of adrenaline, amikacin and Vaxigrip is therefore measured to be 0.71, 0.91 and 1.18 cP respectively. These results align with the CFD model since all medications with viscosity below 20 cP are Newtonian fluids. The viscosity measured for insulin increases with increasing shear rate. This means that insulin basaglar is a shear-thickening fluid. The minimum shear rate measured for insulin is 39.8178 s^{-1} and this was measured at a viscosity 1.93 cP. The maximum shear rate captured for insulin is 500.07 s^{-1} at a viscosity of 3.33 cP.

There are two types of pressures necessary for plunger motion. The pressure required to force the plunger into motion by overcoming the static friction that exist between the plunger and the syringe. This pressure is associated with the break-loose force. The second type of the pressure is required to overcome the kinetic friction that exist between the plunger and the syringe when the plunger is already in motion. This pressure is associated with the gliding force. The plunger force increased to its peak value and decreases thereafter to maintain a constant force for the entire duration of the plunger motion. This is a common trend observed for all the four medications tested. Peak force indicates the break-loose force required to overcome the static friction between the plunger and the syringe.

The constant force therefore represent the gliding force required to overcome the kinetic friction and keep the plunger moving until final displacement is reached. Once the peak pressure is reached, noise is detected during the tests. The possible explanation for this is the effect of fluid resistance force in the syringe and the atmospheric pressure as a result of injecting into the air. These results align with Genesheimer et,al, 2015 showing that there are two force profiles to discharge content in a syringe. A parabolic curve showing the force required to overcome the resistance of the plunger motion and a constant force required to glide the plunger in order to discharge the content in the syringe.

Insulin takes longer to transition from break-loose force to gliding force. This means that more time is required to overcome static friction for this drug. This is expected because Insulin is a long acting drug. According to Davis et.al, 2018 Insulin basaglar is created for prolonged absorption into the circulatory system and hence slow and steady delivery is required to achieve the correct PK of the drug. This also means that this drug needs to be injected into the subcutaneous layer rather than the intramuscular layer. According to Hirsch et.al, 2019 the PK and pharmacodynamics of insulin are more consistent in the subcutaneous layer compared to the intramuscular layer and hence this makes this layer desired for insulin delivery.

There is a significant difference in the dynamic pressure measured from the validation results and the pressure captured from the CFD model at different needle gauges and volumes. The dynamic pressure from the CFD model is higher than the tests results. A possible explanation for this is the difference in the needle tip pressure. A 1333 Pa pressure was defined as an outlet boundary condition in the CFD model. In the V&V, medications were injected into air and hence the needle tip pressure was the atmospheric pressure.

The credibility of the computational model is therefore determined in table 8 below:

Table 8: Credibility of The Computational Model

ASME V&V 40 guidelines	Low Credibility	Medium Credibility	High Credibility	Score	Reason
Code verification	Little or no software assurance method was detailed and followed	Software assurance method was specified and documented.	Software assurance method was specified and documented; Anomality list and software environment was well established and understood	High credibility	Although no code verification was conducted in this research, ANSYS code has been verified and hence high credibility can be assumed.
Discretization error	No grid independence study was performed to approximate discretization error	Grid independence study was conducted; discretisation error was not approximated. convergence	Grid independence study was conducted; discretisation error was approximated. convergence	High credibility	A comprehensive grid independence study was conducted as part of pre-processing and the discretisation error was estimated as part of the verification activities.

		criteria was noted	criteria was noted		
Numerical error	Sensitivity of Numerical Solver was not evaluated.	Sensitivity of Numerical Solver was not evaluated. Solver parameters were determined from previously validated computational models	A sensitivity study of the numerical parameters was conducted or convergence tolerance was used to estimate numerical error	High credibility	A convergence tolerance was used to estimate the numerical error associated with the dynamic pressure results.
Use error	Model inputs and outputs were not substantiated	The main inputs and outputs were substantiated by the researcher	The main inputs and outputs were substantiated through an internal peer review or external peer review.	Medium credibility	A checklist was used by the researcher when running simulations to avoid use errors.
Model form	Influence of model form assumptions were not evaluated	Influence of the main model form assumptions was evaluated	A throughout influence of model assumptions was evaluated	Medium credibility	Influence of the main model form assumptions was explored, such as the influence of the preparation of geometry on the results.
Quantification of sensitivity and uncertainty	Sensitivity and uncertainty analysis was not conducted	Sensitivity and uncertainty analysis was conducted for the main parameters.	Sensitivity and uncertainty analysis was conducted for all the parameters.	Low credibility	No sensitivity and uncertainty analysis was conducted.
Comparator experiment – Quantification of test samples	One sample was used.	Multiple samples were used but no statistical	Multiple samples were used but and statistical	High credibility	A total of 80 tests were conducted. Four medications were used, six needle gauges and

		significance was explored	significance was explored		four different syringe volumes.
Comparator experiment – range of properties of the test samples	One sample with the same set of properties was used	Multiple samples with a nominal range of properties	Multiples samples with the full range of properties	Medium credibility	Multiple medications were used for testing. Three low viscosity and one high viscosity medication was used. Needle gauge and volume were both tested.
Comparator experiment – measurement of test samples	No properties of test samples were measured.	Key properties of test samples were measured.	All the properties of test samples were measured.	High credibility	The properties of interest e.g. viscosity and volume were measured during the experiment.
Comparator experiment – Quantity of test conditions	One test conditions was used.	Two to four test conditions were used.	More than four test conditions were used	High credibility	Different test conditions were used such as injecting using different needle gauges or syringes.
Equivalency of input parameters	Some inputs were dissimilar	All input were similar but the range was dissimilar	All input and range were similar	Low credibility	The boundary condition at the injection site was different. Higher (atmospheric pressure) for the experiment and lower (muscle tissue back pressure) for the model.
Output comparison - Quantity	No outputs were compared	One output was compared.	Multiple outputs were compared.	Medium credibility	Only the dynamic pressure was compared.
Output comparison - Agreement of output comparison	The agreement of outputs comparison is not satisfactory for the main comparison.	The agreement of outputs comparison is satisfactory but not for all comparison.	The agreement of outputs comparison is satisfactory for all comparison.	Medium credibility	The trends of the changes in dynamic pressure are similar in both the model and experiment; just that the model results are higher than expected.

Table 8 summarises the results of the gradations scale for all the V&V activities. The computational model therefore has medium-to-high credibility due to the gradation system ranking. The COU risk is high and the credibility is medium-to-high. The model should be used to inform trends for new autoinjector designs, however no directly design decisions should be translated from the model without further testing and validation.

CHAPTER 6: CONCLUSION

A dynamic model combining a mathematical model that describes the kinematic properties of an autoinjector and a computational model that describe the fluid behaviour of different medications during the injection process was developed in this research. The latter was done by varying the fluid viscosity, needle diameter, needle length and medication volume.

The main observations from this research are:

- The motion of the plunger in an autoinjector is defined by an optimised model such that:

$$\frac{dx}{dt} = v$$

$$\frac{dv}{dt} = \frac{d^2x}{dt^2} = \frac{F_s - F_{fr} - F_{fl}}{m}$$

$$\frac{dP_{total}}{dt} = \frac{8\mu L}{4R^4}\frac{dx}{dt} + f_d\frac{L_s}{D_s}\frac{\rho {v_1}^2}{2} + f_d\frac{L_n}{D_n}\frac{\rho {v_2}^2}{2} + \frac{1}{2}\rho {v_1}^2 - \frac{1}{2}\rho {v_2}^2$$

- The plunger displacement increases linearly when the plunger motion is initiated until a maximum displacement is reached. The plunger accelerates until maximum velocity is reached.
- Medication viscosity below 20 cP, exhibit Newtonian characteristics while medications with viscosity between 20 – 80 cP show shear-thinning Non-Newtonian behaviour.
- Increasing viscosity results in a logistic increase in fluid dynamic pressure. The rate at which dynamic pressure increases, decreases until maximum dynamic pressure is reached.
- Fluid dynamic pressure is higher at the centre of the moving wall or plunger.
- Separation flow is observed in the syringe for viscosity between 15 - 80 cP. This means that flow slows down as pressure increase for medications with a viscosity in this range. This phenomenon increases the chances of needle deformation and injection pain due to tissue damage.
- Shear stress is negligible at the centre of the wall; then increases linearly to the highest value on the wall edges for Newtonian and shear-thinning medications at steady-state conditions.
- Wall shear stress is directly proportional to the medication viscosity.
- It is easier to inject low viscosity medications due to their low dynamic pressure, total pressure and wall shear stress. These medications have higher injectability and low syringeability.
- Needle gauges below 20 result in extremely slow fluid flow and are not recommended for intramuscular injections. This is due to large needle diameters.
- High gauge needles are more effective for injecting lower volumes and low viscosity medications, while low gauge needles work best for injecting larger volumes or highly-viscous medications.
- Decreasing needle diameter increases dynamic pressure for Newtonian fluids and decrease dynamic pressure for shear-thinning Non-Newtonian fluids.

- Increasing needle length or medication volume increases shear stress and dynamic pressure but decreases total pressure.
- Large doses or high viscous medications can be injected using autoinjectors at low pressures, however the bioavailability of the drug needs to be assessed and maintained.
- The developed CFD model risk is defined to be high. If the model results directly impact the autoinjector design without any further testing to inform the design process. Under this assumption, an incorrect model would result in poor performing autoinjectors that fail to deliver the desired dose of medication into the intramuscular layer at the required injection time.

Results from this research contribute to the conceptualisation of the injection process. The plunger motion is defined through a system of equations. This can be used to assess factors affecting the motion of the plunger such as actuation speed, siliconization and medication flow resistance. Medication viscosity and volume affects the injection process. The more viscous the medication, the higher the injectability. This is similar for high volume injections. Fluid behaviour is also influenced by the fluid domain e.g. the syringe and needle dimensions. Smaller syringes and low gauge needles work best for intramuscular injections. This research proves that it's possible to use spring-driven autoinjectors to inject high viscous drugs and large volumes if the right balance of injection force, injection time, needle dimensions is carefully selected to improve compliance and patient experience.

Assuming steady-state conditions meant that only a single point in time could be captured in the computational model. There is no certainty that the observations in the computational model are consistent at transient conditions. A vial was used in the computational model and it was replaced by a syringe in the validation experiment. Using vials for the validation experiment meant manufacturing of an injector system and this was outside the scope of this research. Most autoinjectors are equipped with a vial or cartridge that is reloadable to ensure sustainable use. This has influenced the choice of using a vial for the computational model.

Future Recommendation

A transient study to examine the fluid behaviour for the entire injection process is required. This study would mean that more trends and patterns can be identified including peak pressure zone during the injection process. The effects of needle length need to be further explored as not much evidence relating medication flow behaviour with needle length was deduced from this research. The effectiveness of an autoinjectors to deliver any drug should be evaluated via analysis of ultrasonographic depot localization, plasma levels and cardiovascular response.

REFERENCES

Adelman, J.U.,& Lewit EJ. (2001). Comparative aspects of triptans in treating migraine. Clin Cornerstone;4(3):53–64. Accessed on 20 February 2021.

Alldredge B.K., Gelb A.M., Isaacs S.M., Corry M.D., Allen F., Ulrich S., Gottwald M.D., O'Neil N., Neuhaus J.M., Segal M.R., & Lowenstein D.H. (2001). A comparison of lorazepam, diazepam, and placebo for the treatment of out-of-hospital status epilepticus. N Engl J Med. 2001 Aug 30;345(9):631-7. doi: 10.1056/NEJMoa002141. Erratum in: N Engl J Med 2001 Dec 20;345(25):1860. PMID: 11547716. Accessed on 28 March 2021.

Allmendinger A., Fischer S., Huwyler B., Mahler H.C., Schwarb E., Zarraga I.E., & Mueller R. (2014), Rheological characterization and injection forces of concentrated protein formulations: an alternative predictive model for non-Newtonian solutions. Eur. J. Pharm. Biopharm., 87 pp. 318-328.

Almutairi K, Nossent J, Preen D, Keen H, Inderjeeth C. The global prevalence of rheumatoid arthritis: a meta-analysis based on a systematic review. Rheumatol Int. 2021 May;41(5):863-877. doi: 10.1007/s00296-020-04731-0. Epub 2020 Nov 11. PMID: 33175207.

Andre A.D., Brand-Schieber E., Ramirez M., Munjal S., Kumar R. Subcutaneous sumatriptan delivery devices: comparative ease of use and preference among Migraineurs. Patient Preference and Adherence 2017:11 121–129

Badkar AV, Gandhi RB, Davis SP, LaBarre MJ. Subcutaneous Delivery of High-Dose/Volume Biologics: Current Status and Prospect for Future Advancements. Drug Des Devel Ther. 2021 Jan 13;15:159-170. doi: 10.2147/DDDT.S287323. PMID: 33469268; PMCID: PMC7812053

Beirne PV, Hennessy S, Cadogan SL, Shiely F, Fitzgerald T, MacLeod F. Needle size for vaccination procedures in children and adolescents. Cochrane Database Syst Rev. 2015 Jun 18;(6):CD010720. doi: 10.1002/14651858.CD010720.pub2. Update in: Cochrane Database Syst Rev. 2018 Aug 09;8:CD010720. PMID: 26086647.

Beyea S.C. & Nicoll L.H. (1995) Administration of medications viathe intramuscular route: an integrative review of the literature and research-based protocol for the procedure. Applied NursingResearch8, 23±33.

Brand-Schieber E, Munjal S, Kumar R, Andre AD, Valladao W, Ramirez M. Human factors validation study of 3 mg sumatriptan autoinjector, for migraine patients. Med Devices (Auckl). 2016 May 30;9:131-7. doi: 10.2147/MDER.S105899. PMID: 27313479; PMCID: PMC4892851.

Brown, S.G.A., Mullins, R.J., Gold, M., 2006. Anaphylaxis: diagnosis and management. The Medical journal of Australia. 185. 283-9. 10.5694/j.1326-5377.2006.tb00619.x.

Buysman E, Conner C, Aagren M, Bouchard J, Liu F. Adherence and persistence to a regimen of basal insulin in a pre-filled pen compared to vial/syringe in insulin-naïve patients with type 2 diabetes. Curr Med Res Opin 2011;27:1709-17

Chan H. 2011. Effects of injection duration on site-pain intensity and bruising associated with subcutaneous heparin. J adv Nurs; 35: 882 - 892

Chernikova NA. New classification of insulin needles. Diabetes Lifestyle 2011;4:55-6
ISO 11608-2: 2012. Needle-
Based Injection Systems for Medical Use - Requirements and Test Methods. Part 2 : Needles. Available from: https://www.iso.org/obp/ui/#iso: std:iso:11608:-2:ed-2:v1:en.

Cilurzo F., Selmin F., Minghetti P., 2011.Injectability evaluation: an open issue
AAPS PharmSciTech, 12 (2) (2011), pp. 604-609

Cook, I. F., & Murtagh, J. (2002). Comparative immunogenicity of hepatitis B vaccine administered into the ventrogluteal area and anterolateral thigh in infants. Journal of Paediatrics and Child Health, 38, 393–396. https://doi.org/10.1046/j.1440-1754.2002.00013.x

Diadiun T.V., Kovalenko S.M., Stepanenko S.V., 2016. Study of Key Commodity Aspects of Injection Pens for Insulin Administration and Needles for Them. Asian Journal of Pharmaceutics Oct-Dec 2016 (Suppl) • 10 (4), S717.

Doshi A, Chataway J. Multiple sclerosis, a treatable disease. Clin Med (Lond). 2016 Dec;16(Suppl 6):s53-s59. doi: 10.7861/clinmedicine.16-6-s53. PMID: 27956442; PMCID: PMC6329568. Multiple Sclerosis International Federation . London: MSIF; 2013. Atlas of MS mapping multiple sclerosis around the world. 2013.

Duffin K.C., Bukhalo M, Bobonich MA, Shrom D, Zhao F, Kershner JR, Gill A, Pangallo B, Shuler CL, Bagel J. Usability of a novel disposable autoinjector device for ixekizumab: results from a qualitative study and an open-label clinical trial, including patient-reported experience. Med Devices (Auckl). 2016 Oct 12;9:361-369. doi: 10.2147/MDER.S113752. PMID: 27785115; PMCID: PMC5067052

Farley F., Joyce N., Long B. & Roberts R. (1986) Will that IM needle reach the muscle? American Journal of Nursing86, 1327±1328

Fischer I, Schmidt A, Bryant A, Besheer A.,Calculation of injection forces for highly concentrated protein solutions,International Journal of Pharmaceutics,
Volume 493, Issues 1–2,2015,Pages 70-74,ISSN 0378-5173.

Fry A. 2014.Injecting Highly Viscous Drugs. Pharmaceutical Technology, Pharmaceutical Technology-11-02-2014, Volume 38, Issue 11

Food and Drug Administration (FDA), 2016. EVZIO, naloxone hydrochloride injection: highlights and prescribing information.

Gamble JAS, Dundee JW, Assaf RAE. Plasma diazepam levels after single dose oral and intramuscular administration. Anaesthesia. 1975; 30: 164– 169.

Ganesan K, Raza SK, Vijayaraghavan R. Chemical warfare agents. J Pharm Bioallied Sci 2010; 2: 166–178. [PMC free article] [PubMed] [Google Scholar] [Ref list]

Guerlain S, Hugine A, Wang L. A comparison of 4 epinephrine autoinjector delivery systems: usability and patient preference. Ann Allergy Asthma Immunol. 2010;104(2):172–177.

Güne¸s, Ü. Y., Ceylan, B., & Bayındır, P. (2016). Is the ventrogluteal site suitable for intramuscular injections in children under the age of three? Journal of Advanced Nursing, 72, 127–134. https://doi.org/
10.1111/jan.12813

Heise T., Nosek V, Dellweg V, Zijlstra E., Praestmark K.A., Kildegaard J., Nielsen G., Sparre T.. Impact of injection speed and volume on perceived pain during subcutaneous injections into the abdomen and thigh: a single center, randomised controlled trial Diabetes Obes. Metab. (2014), 10.1111/dom.12304

Hepp Z., Dodick DW., Varon SF, Gillard P, Hansen RN, Devine EB. Adherence to oral migraine-preventive medications among patients with chronic migraines, Cephalalgia. 2015; 35(6): 478 - 488.

Hey-Hadavi J, Pleil A, Deeb LC, et al. Ease of use and preference for a new disposable self-injection pen compared with a reusable pen for administering recombinant human growth hormone: A multicenter, 2-Month, single-arm, open-label clinical trial in patient-caregiver dyads. Clin Ther. 2010;32(12):2036–2047.

Hillestad L, Hansen T, Melsom H, Drivenes A. Diazepam metabolism in normal man: I. Serum concentrations and clinical effects after intravenous, intramuscular, and oral administration. Clin Pharmacol Ther. 1974; 16: 479– 484

Hoang, Phu & Carr, & Shepherd, Roberta. (2010). Multiple Sclerosis. Neurological Rehabilitation: Optimizing Motor Performance (pp.335-350)Edition: 2nd

Hsiao B, Fraenkel L. Patient preferences for rheumatoid arthritis treatment. Curr Opin Rheumatol. 2019 May;31(3):256-263. doi: 10.1097/BOR.0000000000000591. PMID: 30747733; PMCID: PMC6438722.

Hunter, J. 2008 Subcutaneous injection technique. Nursing Standard; 22: 21, 41-44.

Isojärvi JI, Tokola RA. Benzodiazepines in the treatment of epilepsy in people with intellectual disability. Journal of Intellectual Disability Research : JIDR. 1998 Dec;42 Suppl 1:80-92. PMID: 10030438.

Jackisch C, Hegg R, Stroyakovskiy D, Ahn JS, Melichar B, Chen SC, et al. HannaH phase III randomised study: association of total pathological complete response with event-free survival in HER2-positive early breast cancer treated with neoadjuvant-adjuvant trastuzumab after 2 years of treatment-free follow-up. Eur J Cancer (Oxford, England: 1990). 2016;62:62–75.

Kanto J. Plasma concentrations of diazepam and its metabolites after peroral, intramuscular, and rectal administration. Int J Clin Pharmacol. 1975; 12: 427– 432.

Kanto J. Plasma levels of diazepam after oral and intramuscular administration. Br J Anaesth. 1974; 46: 817.

Kanai S., Liu J., Patapoff T.W., Shire S.J.Reversible Self-Association of a Concentrated Monoclonal Antibody Solution Mediated by Fab–Fab Interaction That Impacts Solution Viscosity,Journal of Pharmaceutical Sciences, Volume 97, Issue 10,2008,Pages 4219-4227, ISSN 0022-3549. https://doi.org/10.1002/jps.21322.

Kirk A. 2018. Best practice technique in intramuscular injection. Journal of paramedic practice.

Krause RS, Moscati R, Filice M, Lerner EB, Hughes D. The effect of injection speed on the pain of lidocaine infiltration. Acad Emerg Med 1997; 4: 1032–1035.

Krayukhina E, Fukuhara A, Uchiyama S. Assessment of the Injection Performance of a Tapered Needle for Use in Prefilled Biopharmaceutical Products. J Pharm Sci. 2020 Jan;109(1):515-523. doi: 10.1016/j.xphs.2019.10.033. Epub 2019 Oct 22. PMID: 31654659.

Kyu HH, Mumford v, Stanaway JD, et al.
Mortality from tetanus between 1990 and 2015: findings from the global burden of disease study 2015
BMC Public Health, 17 (2017), p. 179

Landy SH, Tepper SJ, Wein T, Schweizer E, Ramos E. An open-label trial of a sumatriptan auto-injector for migraine in patients currently treated with subcutaneous sumatriptan. Headache. 2013 Jan;53(1):118-125. doi: 10.1111/j.1526-4610.2012.02295.x. Epub 2012 Nov 13. PMID: 23148799.

Leray E, Moreau T, Fromont A, Edan G. Epidemiology of multiple sclerosis. Rev Neurol (Paris). 2016 Jan;172(1):3-13. doi: 10.1016/j.neurol.2015.10.006. Epub 2015 Dec 21. PMID: 26718593.

Limmroth V, Reischl J, Mann B, Morosov X, Kokoschka A, Weller I, Schreiner T. Autoinjector preference among patients with multiple sclerosis: results from a national survey. Patient Prefer Adherence. 2017 Aug 3;11:1325-1334. doi: 10.2147/PPA.S137741. PMID: 28831243; PMCID: PMC5548304.

Lipton RB, Silbertstein SD, Episodic and chronic migraine headache: breaking down barriers to optimal treatment and prevention. Headache. 2015:55(suppl 2):103 - 122.

Loder E. Triptan therapy in migraine. N Engl J Med. 2010;363(1):63–70. [PubMed] [Google Scholar] [Ref list]

Lugaresi A. RebiSmart™ (version 1.5) device for multiple sclerosis treatment delivery and adherence. Expert Opin Drug Deliv. 2013 Feb;10(2):273-83. doi: 10.1517/17425247.2013.746311. Epub 2012 Dec 20. PMID: 23252744.

Magnussen I, Oxlund HRW, Alsbirk KE, Arnold E. Absorption of diazepam in man following rectal and parenteral administration. Acta Pharmacol Toxicol. 1979; 45: 87– 90.

Mahtab A. 2011. What is Migraine? What are the symptoms and treatments? What proportion of people does it affect in Australia? Is it more prevalent amongst young people or old, women or men?. 10.13140/2.1.3311.0081.

Mahetab A, Felicity R & Shakesheff K/ & Modo M. & White, L. (2017). Translational considerations in injectable cell-based therapeutics for neurological applications: concepts, progress and challenges. npj Regenerative Medicine. 2. 10.1038/s41536-017-0028-x.

Mallet J. & Bailey C. (1996)The Royal Marsden NHS Trust Manualof Clinical Nursing Procedures4th edn. Blackwell Science,London.

Mandrioli Roberto, Mercolini Laura and Raggi Augusta Maria, Benzodiazepine Metabolism: An Analytical Perspective, Current Drug Metabolism 2008; 9(8) . https://dx.doi.org/10.2174/138920008786049258

Markets and markets, 2020. The autoinjector market by therapy (rheumatoid arthitis, multiple sclerosis, anaphylaxis, cardiovascular diseases, diabetes), Types (disposable, reusable), route of administration (subcutaneous, intramuscular). End-user (hopsital) - global forecast to 2025.

Mathew NT, Dexter J, Couch J, et al. Dose Ranging Efficacy and Safety of Subcutaneous Sumatriptan in the Acute Treatment of Migraine. *Arch Neurol.* 1992;49(12):1271–1276. doi:10.1001/archneur.1992.00530360073020

Matucci A, Vultaggio A, Danesi R. The use of intravenous versus subcutaneous monoclonal antibodies in the treatment of severe asthma: a review. Respir Res. 2018;19(1):154.

Morandotti A, "Ompi Nexa Syringes: The Ideal Solution for the Most Demanding Drugs". ONdrugDelivery Magazine, Issue 55 (Feb 2015), pp 40-44.

Newmark J. Therapy for acute nerve agent poisoning: An update. Neurol Clin Pract. 2019 Aug;9(4):337-342. doi: 10.1212/CPJ.0000000000000641. PMID: 31583189; PMCID: PMC6745742.

Pati S, 2019. Designing a Drug-Delivery Device? Read This First. Medical device and diagnostic Industry

Radu A., Bungau S.G, 2021. Management of Rheumatoid Arthritis: An Overview. Cells 2021, 10, 2857. https://doi.org/10.3390/Cells10112857Simponi; Package insert, Hornsham, PA; Janssen Biotech, Inc, 2013.

Richter WF, Bhansali SG, Morris ME. Mechanistic determinants of biotherapeutics absorption following SC administration. AAPS J. 2012;14(3):559–70.

Roe MJ, "Challenges in High-Viscosity, High-Volume Drug Delivery". ONdrugDelivery, Issue 125 (Oct 2021), pp 40–43.

Roy, A., Geetha, R.V., Magesh, A., Vijayaraghavan, R., Ravichandran, V., 2021. Autoinjector - A smart device for emergency cum personal therapy. Saudi Pharmaceutical Journal 29 (2021) 1205 - 1215.

Sagent pharmaceuticals, 2018. AMIKACIN SULFATE- amikacin sulfate injection, solution.

Scarfone R.J., Jasani M., Gracely E.J. 1998. Pain of local anasthetics: rate of administration and buffering. Ann Emerg Med 1998; 36 - 40

Shin D, Kim Y, Go A, Velinova M. Comparison of the Pharmacokinetics, Safety, and Tolerability of the Autoinjector (AI) and Pre-Filled Syringe (PFS) of SB4 in Healthy Subjects. Drug Des Devel Ther. 2020 Jan 8;14:43-50. doi: 10.2147/DDDT.S224103. PMID: 32021090; PMCID: PMC6955637.https://clinicalinfo.hiv.gov/sites/default/files/glossaries/images/Pharmacokinetics-800.jpg

Shukla V.V., Shah R.C., 2017. Vaccinations in Primary Care. The Indian Journal of Pediatrics (December 2018) 85(12):1118–1127. https://doi.org/10.1007/s12098-017-2555-2

Sicherer, S.H., A.F., Simons, F.E.R., 2017. Epinephrine for First-aid
Management of Anaphylaxis. PEDIATRICS Volume 139 , number 3 , March 2017 :e 20164006

Sigurgeirsson B, Browning J, Tyring S, Szepietowski JC, Rivera-Díaz R, Effendy I, Keefe D, Bruin G, Paguet B, Fu R, Hampele I, Reinhardt M, Patekar M. Secukinumab demonstrates efficacy, safety, and tolerability upon administration by 2 ml autoinjector in adult patients with plaque psoriasis: 52-week results from MATURE, a randomized, placebo-controlled trial. Dermatol Ther. 2022 Mar;35(3):e15285. doi: 10.1111/dth.15285. Epub 2022 Jan 8. PMID: 34954841.

Simons, F.E.R., G, X., Simons, K.J., 2001. Epinephrine absorption in adults: Intramuscular vs subcutaneous injection. J. Allergy Clin. Immunology. 108, 871 - 873.

Simons, F.E.R., Ardusso, L.R., Bilo, M.B., Cardona, V., Ebisawa, M., El-Gamal, Y.M., Lieberman, P., Lockey, R.F., Muraro, A., Roberts, G., Sanchez-Borges, M., Sheikh, A, Shek, L.P., Wallace, D.V., Worm, M, 2014. International consesu on (ICON) anaphylaxis World Allergy Organisation Journal. 7, 9.5

Starkey ES, Sammons HM. Practical pharmacokinetics: what do you really need to know? Arch Dis Child Educ Pract Ed. 2015 Feb;100(1):37-43.

Tang L, Persky AM, Hochhaus G, Meibohm B. Pharmacokinetic aspects of biotechnology products. J Pharm Sci. 2004;93(9):2184–204.

Tejedor A. M.A, Moro Moro M, Múgica G.M.V. Epidemiology of anaphylaxis. Clin Exp Allergy 2015; 45(6): 1027-39.

Trinka E, Cock H, Hesdorffer D, Rossetti AO, Scheffer IE, Shinnar S, Shorvon S, Lowenstein DH. A definition and classification of status epilepticus--Report of the ILAE Task Force on Classification of Status Epilepticus. Epilepsia. 2015 Oct;56(10):1515-23. doi: 10.1111/epi.13121. Epub 2015 Sep 4. PMID: 26336950.

Turner PJ, Muraro A, Roberts G. Pharmacokinetics of adrenaline autoinjectors. Clin Exp Allergy. 2022 Jan;52(1):18-28. doi: 10.1111/cea.14055. Epub 2021 Dec 2. PMID: 34784074.

Umasunthar T, Leonardi-Bee J, Turner PJ, et al. Incidence of food anaphylaxis in people with food allergy: A systematic review and meta-analysis. Clin Exp Allergy 2015; 45(11): 1621-36.
Kase Tanno L., Demoly P. Action plan to reach the global availability of adrenaline auto-injectors. *J Investig Allergol Clin Immunol.* 2018;29 doi: 10.18176/jiaci.0346.

Vijayaraghavan, R.,2012. Autoinjector device for rapid administration of life saving drugs in emergency. Def. Sci, J. 62, 307-314.

Vijayaraghavan R. Autoinjector device for rapid administration of drugs and antidotes in emergency situations and in mass casualty management. J Int Med Res. 2020 May;48(5):300060520926019. doi: 10.1177/0300060520926019. PMID: 32436421; PMCID: PMC7243406.

Violan C, Foguet-Boreu Q, Flores-Mateo G, Salisbury C, Blom J, Freitag M, et al. Prevalence, determinants and patterns of multimorbidity in primary care: a systematic review of observational studies. *PLoS One.* 2014;9(7):e102149.

Wilkins, J., Simpson I.,2012. Mathematical Modelling for Faster Auto-Injector Design. Drug Dev, 41 - 45.

Winslow E.H. (1996) Research for practice.Journal of AdvancedNursing96, 53
Wilson M, Brumwell A, Stowe MJ, Shelly S, Scheibe A. Personal experience and awareness of opioid overdose occurrence among peers and willingness to administer naloxone in South Africa: findings from a three-city pilot survey of homeless people who use drugs. Harm Reduct J. 2022 Feb 11;19(1):17. doi: 10.1186/s12954-021-00561-w. PMID: 35148779; PMCID: PMC8832761.

Wysham C.H., Rosenstock J., Vetter M.L., Dong F., Öhman, P., Iqbal N. Efficacy and tolerability of the new autoinjected suspension of exenatide once weekly versus exenatide twice daily in patients with type 2 diabetes.Diabetes Obes. Metab., 20 (2018), pp. 165-172

Yeung KHT, Duclos P, Nelson EAS, Hutubessy RCW. An update of the global burden of pertussis in children younger than 5 years: a modelling study. Lancet Infect Dis. 2017 Sep;17(9):974-980. doi: 10.1016/S1473-3099(17)30390-0. Epub 2017 Jun 13. PMID: 28623146.

Xu Z, Marciniak S.J., Frederick B., Kim L., Zhuang Y., Davis H.M., Zhou H. Pharmacokinetic Bridging Approach for Developing Biologics-delivery Devices: A Case Study With a Golimumab Autoinjector. Clinical Therapeutics/Volume 37, Number 2, 2015.

Ziemssen, T., Sylvester, L., Rametta, M., Ross, A.P., 2015. Patient satisfaction with new interferon beta-1b autoinjector (BETACONNECT). Neurol. Ther. 4, 125-136.

Zuckerman JN. The importance of injecting vaccines into muscle. Different patients need different needle sizes. BMJ. 2000 Nov 18;321(7271):1237-8. doi: 10.1136/bmj.321.7271.1237. PMID: 11082069; PMCID: PMC1118997.